universität wien

MASTERARBEIT / MASTER'S THESIS

Titel der Masterarbeit / Title of the Master's Thesis

„Multi-omics analysis for the characterization of inflammatory signatures in patients with active ulcerative colitis (UC)"

verfasst von / submitted by

Dina Schuster BSc

angestrebter akademischer Grad / in partial fulfilment of the requirements for the degree of

Master of Science (MSc)

Wien, 2019 / Vienna 2019

Studienkennzahl lt. Studienblatt / degree programme code as it appears on the student record sheet:	A 066 862
Studienrichtung lt. Studienblatt / degree programme as it appears on the student record sheet:	Chemie
Betreut von / Supervisor:	Univ.-Prof. Dr. Christopher Gerner
Mitbetreut von / Co-Supervisor:	Dr. Astrid Slany

TABLE OF CONTENTS

ABSTRACT **4**

ZUSAMMENFASSUNG **5**

ABBREVIATIONS **6**

1. THEORETICAL BACKGROUND **8**

1.1. Inflammatory bowel disease 8
1.2. Ulcerative colitis 10
1.3. Fatty acids and eicosanoids 23
1.4. Proteomics 24
1.5. Mass spectrometry 25

2. OBJECTIVES **29**

3. MATERIALS AND METHODS **30**

3.1. Patient sample collection and ethical considerations 30
3.2. Plasma preparation 30
3.3. UC patient colon biopsy sample preparation 30
3.4. Cell culture 31
3.5. Proteomics methods 33
3.6. Eicosanoid analysis methods 45

4. RESULTS AND DISCUSSION **49**

4.1. Digestion protocol optimization 49
4.2. Ulcerative colitis patient data and heterogeneity 51
4.3. Proteomic analysis of UC patient colonic biopsies 53
4.4. Proteomic analysis of UC patient plasma samples 63
4.5. Eicosanoid analysis of patient plasma samples 67
4.6. Proteomic analysis of differentially stimulated CCD-18Co cells 69

5. CONCLUSIONS AND OUTLOOK **88**

6. SUPPLEMENTARY INFORMATION **91**

ACKNOWLEDGEMENT **96**

REFERENCES **97**

LIST OF FIGURES **109**

LIST OF TABLES **112**

Abstract

Ulcerative colitis (UC) is – alongside Crohn's disease – one of the most common forms of inflammatory bowel diseases. The disease is characterized by a chronic and recurring inflammation of the colon mucosa, starting in the rectum and continuing upwards to more proximal colonic regions. While the incidence and prevalence of the disease are on the rise and extensive research has been conducted over the recent years, the etiology and pathology of UC remain unresolved. A complex interplay of the microbiome, a possible genetic predisposition, as well as an exaggerated immune response is currently regarded as the reason for disease development.

In order to increase the current understanding of underlying disease mechanisms a proteomic analysis of colonic biopsy specimen excised from different colonic regions as well as eicosanoid and proteomic analyses of respective patient plasma samples were performed. A complementing *in vitro* analysis of inflammatorily stimulated CCD-18Co cells was conducted to gain insight into the contribution of colonic (myo-)fibroblasts to the disease phenotype as well as the persistence of the inflammation in patients suffering from UC.

The results of the abovementioned analyses support the hypothesis that (myo-)fibroblasts contribute to the chronicity and the phenotype of UC.

Zusammenfassung

Colitis ulcerosa ist – neben Morbus Crohn – eine der häufigsten chronisch entzündlichen Darmerkrankungen. Die Krankheit ist charakterisiert durch eine chronische und wiederkehrende Entzündung der Dickdarm Mukosa, welche im Rektum beginnt und kontinuierlich in proximalere Regionen des Dickdarms fortschreitet. Trotz steigender Inzidenz- und Prävalenzraten, sowie ausführlicher wissenschaftlicher Studien, welche in den vergangenen Jahren durchgeführt wurden, bleiben die Ätiologie und Pathologie der Erkrankung ungeklärt. Derzeit wird ein komplexes Zusammenspiel des Mikrobioms, einer etwaigen genetischen Prädisposition und einer gesteigerten Immunantwort für die Entstehung der Erkrankung verantwortlich gemacht.

Um einen tieferen Einblick in die Erkrankung und die zugrundeliegenden Erkrankungsmechanismen zu gewinnen, wurde eine proteomische Analyse von Dickdarmbiopsaten unterschiedlicher Darmregionen betroffener Patienten, sowie eine Proteom- und Eicosanoidanalyse von Patientenplasmaproben durchgeführt. Zusätzlich wurde eine *in vitro* Analyse entzündlich stimulierter CCD-18Co Zellen durchgeführt, um den Einfluss von Dickdarm(myo-)fibroblasten auf den Phänotyp der Erkrankung, sowie ihren etwaigen Beitrag zur Chronizität und der Aufrechterhaltung der Entzündung in Patienten mit Colitis ulcerosa zu untersuchen.

Die Resultate der durchgeführten Analysen unterstützen die Hypothese, dass Myofibroblasten/Fibroblasten sowohl zur Chronizität als auch zum typischen Phänotyp von Colitis ulcerosa beitragen.

Abbreviations

AA	Acrylamide
ABC	Ammonium bicarbonate
ACN	Acentonitrile
AGC	Automatic gain control
APS	Ammonium persulfate
Asc	Colon ascendens
AUC	Area under curve
BCA	Bicinchoninic acid
BSA	Bovine serum albumin
CD	Crohn's disease
CHAPS	3-[(3-Chloramidopropyl)dimethylammonium]-1-propanesulfonate hydrate
DC	Direct current
Desc	Colon descendens
DNA	Deoxyribonucleic acid
DTT	Dithiothreitol
EDTA	Ethylenediaminetetraacetic acid
EMEM	Eagle's minimum essential medium
ESI	Electrospray ionization
EtOH	Ethanol
MeOH	Methanol
FA	Formic acid
FASP	Filter-aided sample preparation
FCS	Fetal calf serum
FDR	False discovery rate
FT-ICR	Fourier-transform ion cyclotron resonance
Gd-HCl	Guanidinium hydrochloride
GO	Gene ontology
GWAS	Genome wide association studies
H&E	Hematoxylin and eosin
HCD	Higher energy collisional dissociation
HEPES	2-[4-(2-hydroxyethyl)piperazin-1-yl]ethansulfonic acid
IAA	Iodoacetamide
IBD	Inflammatory bowel disease
IPA	Isopropyl alcohol
LC	Liquid chromatography
LC-MS	Liquid chromatography-mass spectrometry
LFQ	Label free quantification

LPS	Lipopolysaccharide
MALDI	Matrix-assisted laser desorption ionization
MS	Mass spectrometry
MS/MS	Tandem mass spectrometry
MWCO	Molecular weight cut-off
nLC	Nano-flow liquid chromatography
PAGE	Polyacrylamide gel electrophoresis
PBS	Phosphate buffered saline
PCA	Principal component analysis
PMSF	Phenylmethylsulfonyl fluoride
PSM	Peptide spectrum match
PUFA	Polyunsaturated fatty acid
QQ	Quantile-quantile
Rec	Rectum
RF	Radio frequency
ROS	Reactive oxygen species
rpm	Revolutions per minute
RT	Room temperature
SCFA	Short-chain fatty acid
SDC	Sodium deoxycholate
SDS	Sodium dodecyl sulfate
SFA	Saturated fatty acids
Sig	Colon sigmoideum
SPE	Solid phase extraction
SRB	Sulfate reducing bacteria
TCEP	Tris(2-carboxyethyl)phosphine
TEAB	Triethylammonium bicarbonate
TEMED	Tetramethylethylenediamine
TFA	Trifluoroacetic acid
TOF	Time-of-flight
Trans	Colon transversum
Tris	2-Amino-2-(hydroxymethyl)propane-1,3-diol
UC	Ulcerative colitis

1. Theoretical background

1.1. Inflammatory bowel disease

The group of inflammatory bowel diseases (IBDs) is mainly comprised of Crohn's disease (CD) and ulcerative colitis (UC), both of which are chronic inflammatory conditions of parts of the gastrointestinal tract. IBD has, in recent years, grown to be a worldwide challenge due to its rising incidence and prevalence, especially in western civilizations. Currently, in North America more than 1.2 and in Europe more than 2 million people suffer from one form of IBD, respectively. Crohn's disease and UC are recognized as "Western diseases" with the highest estimated incidence rates of 29.3 in 100,000 people in Oceania (Geelong, Australia) in the case of CD and 57.9 people in 100,000 in Northern Europe (Faroe Islands) in the case of UC. The highest estimated prevalence rates of IBD are to be found in North America with 318.5 people affected in 100,000 (Nova Scotia, Canada) in the case of CD and 505 in 100,000 in the case of UC in Northern Europe (Southeast Norway). In newly industrialized regions such as Africa, South America and Asia, incidence rates are accelerating as well, despite still being low in comparison to the abovementioned countries.[1, 2] Disease onset is usually between the second and forth life decade with some studies suggesting a second peak onset between the sixth and seventh life decade. Pediatric IBD, with a disease onset in childhood, is estimated to account for 7 to 20% of IBD cases [3, 4].

Crohn's disease and UC, even though they are often times being treated as one disease, differ quite significantly in their phenotypes. While CD can involve parts of the whole gastrointestinal tract – in most cases, however, affecting the perianal region or the terminal ileum -, UC is to be found only in the large intestine. CD is characterized by a discontinuous inflammation, whereas UC spreads from the terminal

to more proximal regions of the colon in a continuous fashion. The inflammatory phenotype as observed during histo-pathological evaluation of excised tissue specimen shows different features: CD induces a thickened submucosa, fissuring ulcerations, as well as transmural inflammation, whereas UC is confined to the mucosa and submucosa, characterized by cryptitis and crypt abscesses.[5]

The etiology and pathogenesis of both diseases are still not understood; however, studies have shown a strong contribution of genetic background. Genome wide association studies (GWAS) suggest the involvement of several gene loci and twin studies have led to the conclusion that genetics play a more important role in the development of the diseases than environmental factors [6]. A substantial overlap of risk loci is to be found between CD and UC. Genes that are distinct for one or the other disease are likely to involve the response to environmental triggers or tissue specific stimuli [7]. The microbiome seems to be of undeniable importance in the development of IBD, as studies have shown that mice kept in germ-free conditions do not develop colitis [8]. A normal gut microflora might be required for the development of IBD in a host that is genetically susceptible to develop the disease. It would be obvious to suspect specific microorganism derived pathogens to be the root of disease development; however, so far no specific organism has been identified as being the cause for IBD [9].

1.2. Ulcerative colitis

Ulcerative colitis is characterized by a chronic and recurring inflammation limited to the colonic mucosa and submucosa. The inflammation usually starts in the rectum or colon sigmoideum (distal parts of the colon) and continues upwards to more proximal regions of the colon. In 95.6% of patients the rectum is affected, in 80.1% the colon sigmoideum, in 46.6% the colon descendens, in 33.1% the colon transversum and in 27.1% the colon ascendens.[10]

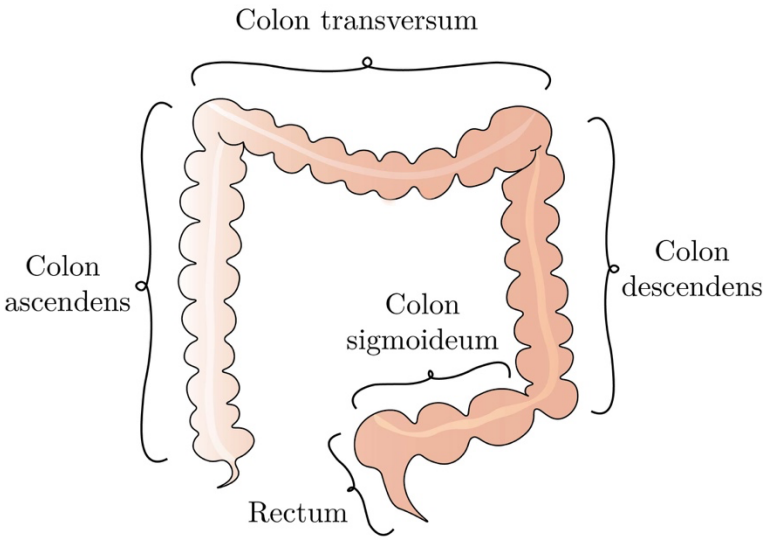

Figure 1 Colonic regions affected by ulcerative colitis

1.2.1. Symptoms

Symptoms of ulcerative colitis include bloody diarrhea, urgency, incontinence, abdominal cramps, mucus discharge and in more severe cases extreme weight loss and high fever. Patients suffering from left-sided colitis or proctitis also report constipation. The extent of inflammation strongly depends on the disease severity. While milder forms can show involvement of only the distal parts of the colon, more severe cases can affect the whole colon (pancolitis) with eventual spread of the inflammation to the terminal ileum.[11] Patients affected by UC often times suffer not only from symptoms directly induced by the colonic inflammation, extraintestinal manifestations affecting the joints (peripheral and axial arthropathies) or the skin (pyoderma gangraenosum, erythema nodosum) are also very common and are an indicator of disease activity [12].

Badly and untreated disease can lead to toxic megacolon and also colorectal cancer [13, 14].

1.2.2. Pathogenesis

Despite the exact pathogenesis not being understood, recent studies suggest an interplay of epithelial barrier defects, microbial dysbiosis and a deregulated immune response to be the reason for disease development [15]. A study, examining colonic tissue samples from patients suffering from UC, showed that PPARγ (peroxisome proliferator-activated receptor gamma) – an important inhibitor of NF-κB (nuclear factor kappa-light-chain-enhancer of activated B cells) – mRNA expression, as well as PPARγ protein expression are impaired. These observations were made in patients with active inflammation as well as in patients without signs of active disease. The same study showed that bacteria and TLR4 (Toll-like receptor 4) levels affect the expression of PPARγ, thereby suggesting that elevated levels of TLR4 in UC, as well as a down-regulation of PPARγ in epithelial cells of UC patients, could lead to a decreased tolerance of bacteria derived LPS (lipopolysaccharide), leading to inflammation [16, 17]. It has also been observed that butyrate – a major energy source for the colonic epithelium – uptake and oxidation are decreased in patients with UC due to decreased levels of the butyrate transporter SLC16A1, as well as enzymes involved the oxidation of butyrate (ACSM3, ACADS, ACAT2, ECHS1, HSD17B10).[18, 19] PPARγ dependent transcription activity has been shown to be linked to butyrate and propionate levels in a dose-dependent manner [20]. Altogether, an increased activation of NF-κB, leading to increased inflammatory cytokine production, and simultaneously reduced levels of inhibitory factors such as butyrate and PPARγ could lead to an increased immune response to bacteria and bacteria derived pathogens, thereby inducing the phenotype of UC.

1.2.3. Healthy colon structure

The human colon is organized in different membranes, namely the mucosa (composed of an epithelial layer, the lamina propria and the muscularis mucosae), the submucosa, the muscularis propria and the serosa (Figure 2). As ulcerative colitis is confined to the mucosa and the submucosa, focus will be laid on these two membrane structures. The normal colonic epithelium is constituted in a specific pattern, forming structures called "crypts". Located underneath the epithelium is the lamina propria, which is inhabited by different cell populations, such as fibroblasts, myofibroblasts, T and B cells, macrophages and dendritic cells. Below the lamina propria is a thin muscle layer, the muscularis mucosae, separating it from the mucosa. The submucosa, which is to be found underneath the muscularis mucosae, includes nerves and vasculature.[21]

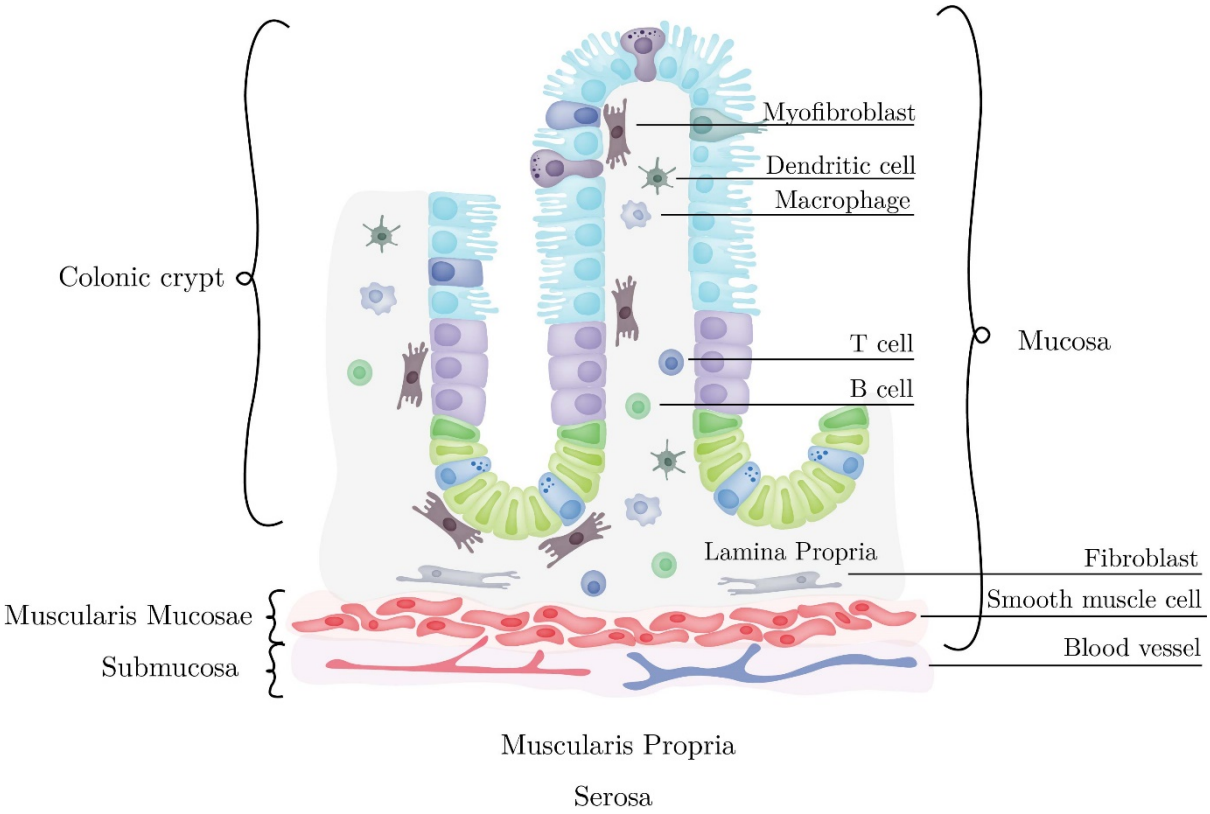

Figure 2 Colonic membrane structure

The epithelial layer of the colonic crypt is inhabited by different cells (Figure 3), separated into three different regions: the differentiated cells on top, followed by transit amplifying cells and the stem cells underneath on the crypt base. The differentiated cells consist mainly of epithelial cells (colonocytes), goblet cells, tuft cells and enterocytes. While Paneth cells are usually only found in the right colon and the small intestine, in ulcerative colitis they can also be observed in the left colon (Paneth cell metaplasia) as a consequence of epithelial injury.[22, 23]

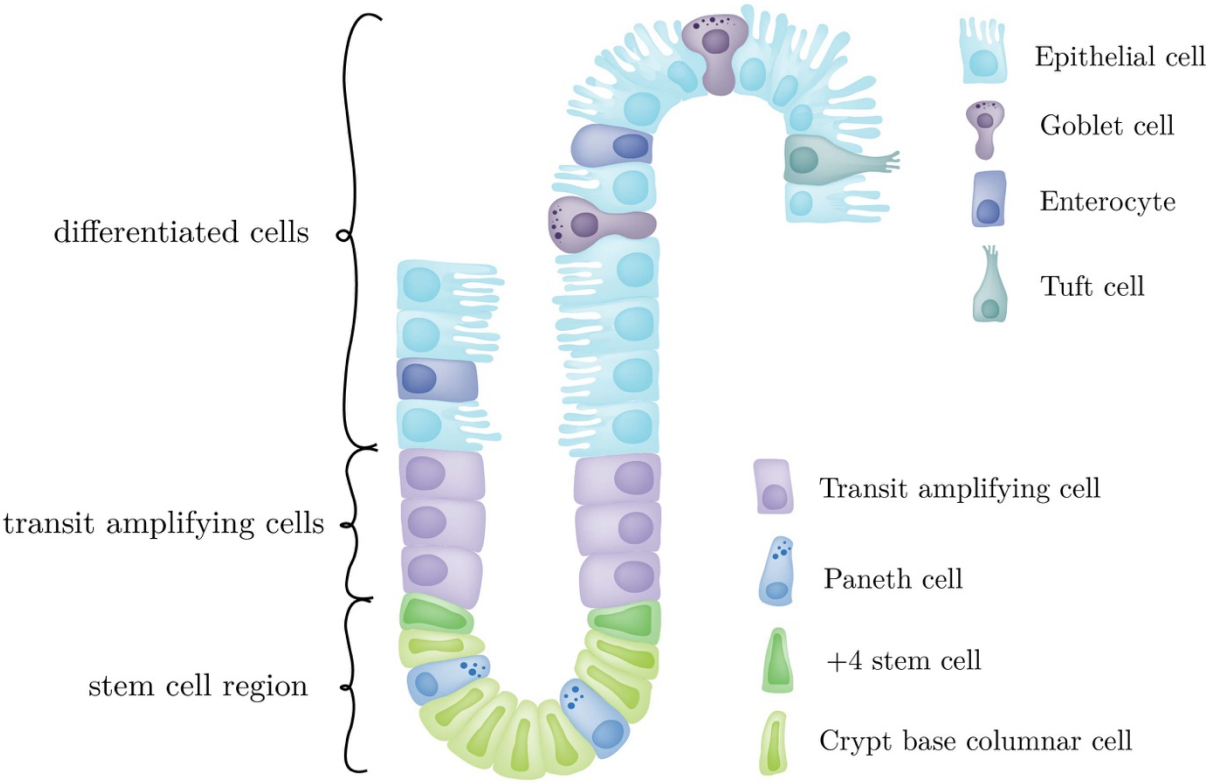

Figure 3 Colonic crypt structure and cellular composition in ulcerative colitis

The epithelial layer of the colon is protected against bacterial pathogens and invading microorganisms by two layers of mucus of varying densities (Figure 4). The inner layer which is attached to the epithelial lining has a higher density and does not harbor any bacteria. The outer mucus layer, on the other hand, is of looser consistency, movable and colonized by different bacteria. Both layers consist in great parts of Muc2, which is a mucin secreted by goblet cells.[24, 25]

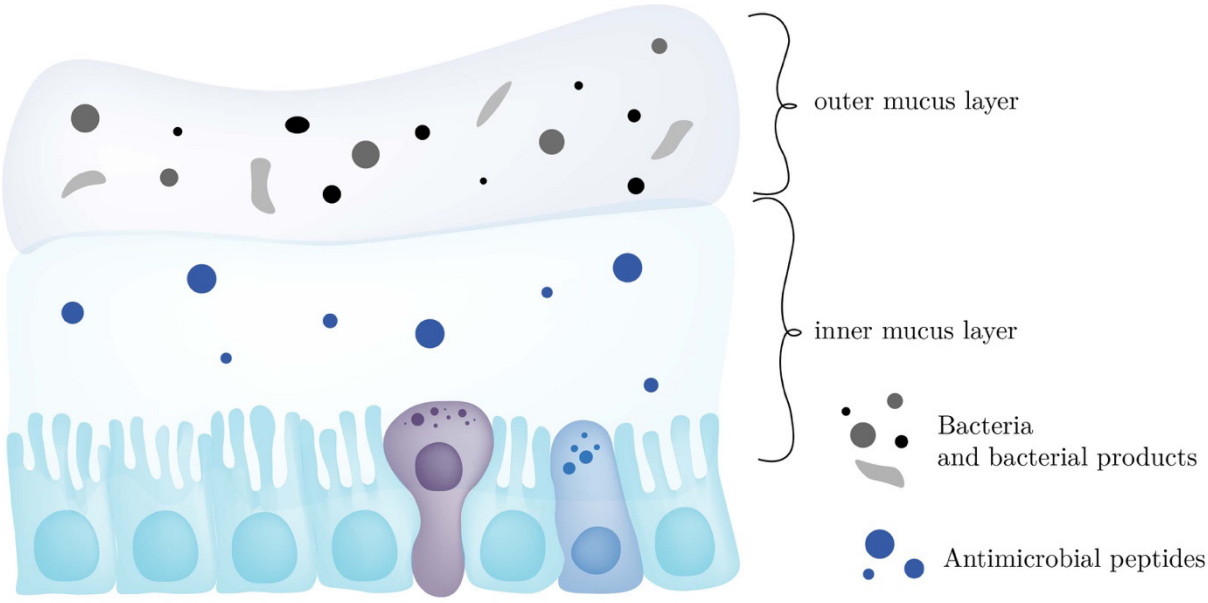

Figure 4 Mucus structures acting as a physical barrier and protection for the colonic epithelium

1.2.4. Microbiome in ulcerative colitis

The large intestine is a habitat for different organisms such as bacteria, viruses and micro-eukaryotes supporting the host in various processes involved in digestion and detoxification [26]. Even in healthy individuals, the gut microbiome is highly diverse mainly populated by *Bacteriodetes* and *Firmicutes*, as well as a small percentage of *Proteobacteria* and *Actinobacteria* [27, 28]. Many studies have reported a change in microbiome diversity in IBD, with some alterations in abundance of bacterial species being specific to either CD or CU and some being attributed to IBD in general [29, 30]. In most studies, a decrease in microbiome diversity has been reported alongside increases of *Proteobacteria*, *Bacteroidetes* and *Firmicutes* [31]. Over the recent years, the research focus for the understanding of disease pathogenesis has increasingly been laid on the study of sulfate reducing bacteria (SRB) [19, 32, 33]. The rationale behind this being that the disease spread of UC is very specific with its start in the more distal colonic regions and continuous spread to the proximal regions. This fact led to the notion that a toxin, present in higher concentrations in the rectum or colon sigmoideum, might be the reason for disease initiation. Indeed, H_2S – a

metabolite, produced by SRB – has proven to be an interesting candidate to study. The human colon forms a pH gradient, with lower pH in the proximal regions and higher pH in the more distal regions, due to the decreasing ability to digest carbohydrate structures [34]. Fermentation of carbohydrates is crucial for the nutrition of the colonic epithelium, as it leads to the production of short-chain fatty acids (SCFA), such as butyrate – one of the main energy sources of colonocytes. The more alkaline pH in the distal colon favors the growth of SRB and thereby the production of H_2S [35]. Total viable counts of SRB have also been shown to be elevated in UC patients, correlating with disease severity [36]. H_2S is known to have an inhibitory effect on butyrate oxidation, thereby depriving colonocytes of their major energy source [37]. A recent article by Ijsenagger *et al.* [38] suggests that in the case of UC elevated levels of H_2S play a role in mucus breakdown, thus making the epithelial layer more accessible for bacteria and bacterial antigens and products, such as H_2S itself.

1.2.5. Diagnosis of ulcerative colitis

Diagnosis of UC can be challenging, as it involves distinguishing between UC, CD and other diseases of the gastrointestinal tract, such as irritable bowel syndrome or food intolerances which all can display similar symptoms. Often times, proper diagnosis of UC can take several years.[39] Furthermore, infections can lead to similar clinical presentations as the abovementioned diseases, complicating the disease diagnosis even further. For example symptoms of tuberculosis, sexually transmitted diseases or *Entamoeba histolytica* infections can include abdominal pain, weight loss, fever and bloody diarrhea, similar to the symptoms presented in UC and CD [40, 41]. Most commonly, the diagnosis of UC involves the analysis of serum markers, indicative of an acute phase reaction, such as C-reactive protein and the erythrocyte sedimentation rate. Other markers commonly used for clinical evaluation of UC are an increased platelet count, an increased white blood cell count, increased levels of serum

amyloid A and ferritin, as well as decreased levels of serum albumin and transferrin. C1s, C2, C3, C4 – members of the complement system – are also indicative of active disease, as well as increased concentrations of haptoglobin, ceruloplasmin, alpha-1 antitrypsin, fibrinogen, prothrombin, plasminogen and several cytokines, such as IL-6, IL-8, IL-10, IL-1β, TNF-α and interferon-β. Anti-neutrophil cytoplasmic antibodies (ANCAs) are also indicative of IBD.[42] Additionally, fecal biomarkers for the diagnosis of IBD also exist, with the most important one being fecal calprotectin (neutrophil derived heterodimer of proteins S100A8 and S100A9) [43-45]. Other than serum and fecal analyses, colonoscopic examination still remains one of the most powerful tools to diagnose UC and to differentiate it from CD. Endoscopic indicators of UC include edema, erythema, friability, spontaneous bleeding, erosions, ulcerations, as well as an observable loss of vasculature [46]. Colonoscopy for UC diagnosis usually involves the excision of biopsy samples from different colonic regions for histological evaluation and analysis. Commonly, tissue biopsies will be fixated in formalin and paraffin, then cut into thin slices, de-waxed and further stained using a hematoxylin and eosin stain (H&E stain) [47]. Active disease can be recognized by crypt infiltrating neutrophils (cryptitis) and collection of neutrophils in the crypts (crypt abscess). Chronicity is to be identified by distorted crypt architectures, the invasion and collection of large numbers of lymphocytes and plasma cells (lymphoplasmacytosis) and Paneth cell metaplasia in the left colon.[22] The overall severity of the disease can be assessed by different scores, such as the Mayo-score (Table 1) and the Disease Activity Index (DAI). These scores take into account the stool frequency, bleeding, as well as physician assessment and endoscopic appearance of the colonic mucosa during colonoscopy.[48]

Table 1 Mayo-score components and disease severity grading

Points	Stool frequency
0	Normal
1	1-2 stools per day more than normal
2	3-4 stools per day more than normal
3	>4 stools per day more than normal
Points	**Rectal bleeding**
0	None
1	Visible blood with stool less than half of the time
2	Visible blood with stool half of the time or more
3	Passing blood alone
Points	**Endoscopic appearance**
0	Normal
1	Mild disease (erythema, decreased vascular pattern, mild friability)
2	Moderate disease (marked erythema, absent vascular pattern, friability, erosions)
3	Severe disease (spontaneous bleeding, ulceration)
Points	**Physician rating**
0	Normal
1	Mild
2	Moderate
3	Severe

1.2.6. Treatment of ulcerative colitis

The main therapies currently applied in the treatment of UC can be divided into four main groups: steroids, aminosalicylates, immunosuppressants and biologics [49]. Depending on disease severity, extension, current treatment and drug history, the appropriate drug or drug combination is chosen, following a treatment scheme (Figure 5). As for the assessment of disease severity, in the case of patients having less than four stools daily, with or without blood and normal erythrocyte sedimentation rate the disease severity is classified as “mild”.[50] Mild forms of UC – often times limited to the rectum are commonly treated with topical application of mesalazine (5-ASA) [51]. A moderate disease course is classified by patients with more than four stools daily,

including signs of toxicity, such as fever, tachycardia (increased heart rate), anemia or elevated erythrocyte sedimentation rate. Patients suffering from mild-to-moderate disease forms are treated with mesalazine both orally and topically. More severe forms, characterized by more than six stools with blood, as well as fever and signs of toxicity, require the patient to be hospitalized and receive steroid infusions, as this condition can be life-threatening.[52] Patients who do not respond to 5-ASA treatment are treated with corticosteroids. Patients not tolerating mesalazine as well as corticosteroids, are treated with immunosuppressive thiopurine agents or cyclosporine (calcineurin inhibitor).[53, 54] Biologics, such as anti-TNF-α therapies are considered as a treatment for patients who do not respond to immunosuppressive therapy. Combinations of biologics with immunosuppressants are also common treatment options.[55] Biologics applied in clinics today are anti-TNF-α antibodies (infliximab, certolizumab, golimumab and adalimumab), anti-integrin antibodies (natalizumab and vedolizumab), as well as interleukin-12 and interleukin-23 agonists.[56] Up to 15% of

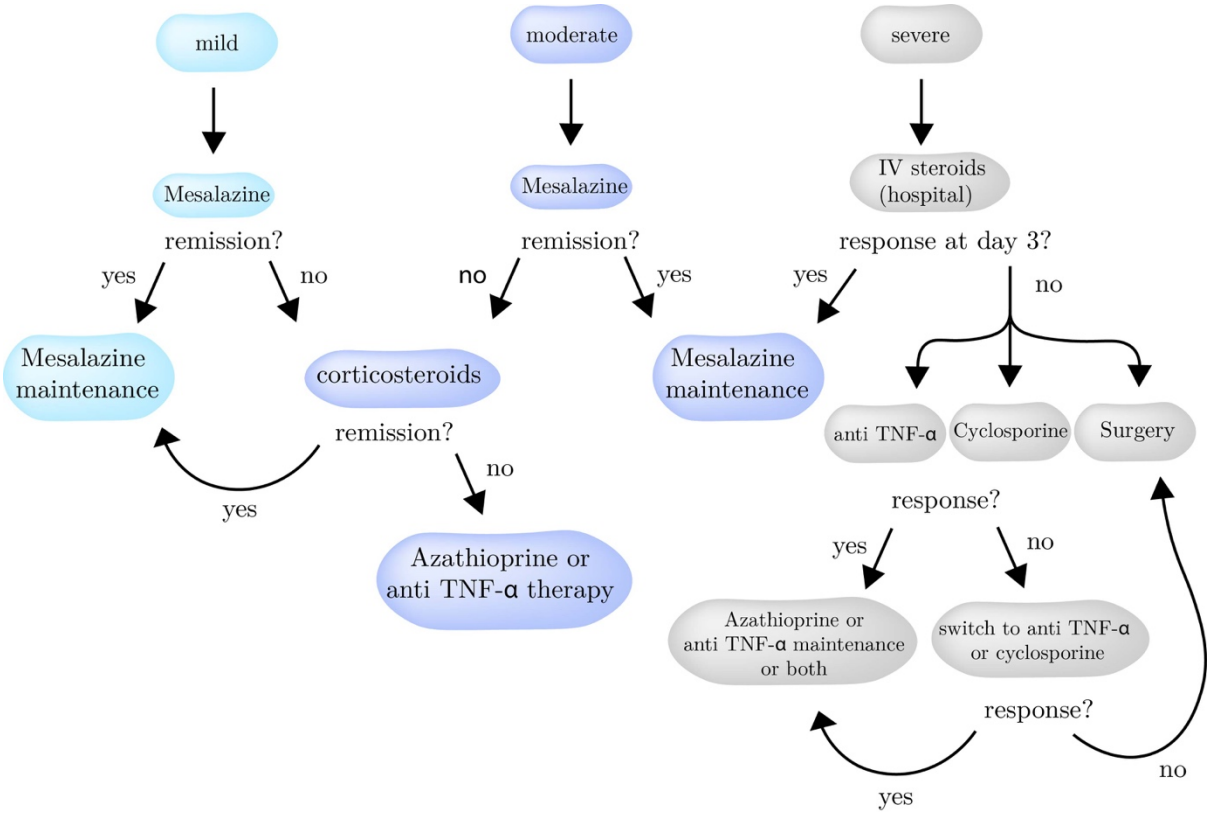

Figure 5 Ulcerative colitis treatment scheme, modified after Panés et al. (2017)

patients do not respond to any of the abovementioned therapy options and therefore require colectomy.[57]

1.2.7. Inflammation and inflammasome in ulcerative colitis

Inflammation is a process induced by tissues and cells used as a defense mechanism against invading pathogens or as a response to damaged cells. The inflammatory process usually results in tissue repair or pathology, if not tightly regulated and controlled properly.[58] Inflammasomes are receptors of the innate immune system that regulate caspase-1 activation, induced by invasion of infectious microbes [59]. Pattern recognition receptors, such as Toll-like receptors (TLRs) and NOD-like receptors (NLRs) recognize danger-associated patterns (DAMPs) and pathogen-associated patterns (PAMPs) and are part of the innate immune system's first line defense against microbes [60]. The production of proinflammatory cytokines, such as IL-1β and IL-18 is crucial for inflammation, which starts with the activation of NF-κB, inducing the production of pro-IL-1β and pro-IL-18, which will then be cleaved into the active forms by caspase-1 in the inflammasome. Several studies on IBD have addressed the importance and role of NLRP3 – a component of the inflammasome – in the pathogenesis, however, yielding conflicting results. IL-1β levels have been shown to be increased in active ulcerative colitis and correlating with disease severity [61]. Zaki *et al.* [62] have reported that the inflammasome – more importantly IL-18 itself – is crucial for the repair of the epithelial gut layer. Perera *et al.* [63], on the other hand, reported that inhibiting NLRP3 in a mouse model is mitigating colitis. Ranson *et al.* [64] reported a reduced colocalization of NLRP3 and IL-1β in active UC, thereby suggesting an NLRP3 independent mechanism of IL-1β production during active disease. This process has also been shown to occur during other pathological conditions, such as *Candida albicans* infections, acute arthritis and osteomyelitis and is dependent on IL-1β activation by neutrophil-derived proteinase 3.[65-67] As the

phenotype of UC is largely characterized by invading neutrophils and increased amounts of neutrophils localized in the lamina propria, neutrophil-mediated cleavage of pro-IL-1β to mature IL-1β is an important topic to study.

1.2.8. Neutrophils in inflammation and ulcerative colitis

Neutrophil recruitment is one of the first defense mechanisms and responses to tissue damage. These cells are the most prominent leukocytes in the blood and are very effective in the resolution of damage and fight against infectious threats through several processes, such as phagocytosis, generation of reactive oxygen species (ROS), degranulation and the formation of neutrophil extracellular traps.[68, 69] Increased neutrophil invasion can lead to signs of chronic inflammation and is limiting tissue repair [70]. Neutrophil migration is mainly mediated by pathogen-associated molecular patterns (PAMPs), released by microorganisms, or damage-associated molecular patterns (DAMPs), derived from dead cells or as a stress response [71]. Leukocyte extravasation from vasculature is a multi-step process and involves the sensing of proinflammatory cytokines by neutrophils and vascular cells, triggering a cascade of neutrophil adhesion and motility processes (Figure 6). The first step during neutrophil migration is the interaction between neutrophils and vascular cells, close to the site of inflammation. This interaction induces the production of chemoattractants on the luminal side of the blood vessel, thereby facilitating leukocyte arrest, adhesion, crawling and migration into the tissue.[71, 72] The multi-step cascade requires several proteins, such as selectins (P-, E-, L-selectin), integrins, MADCAM1, VCAM1, and

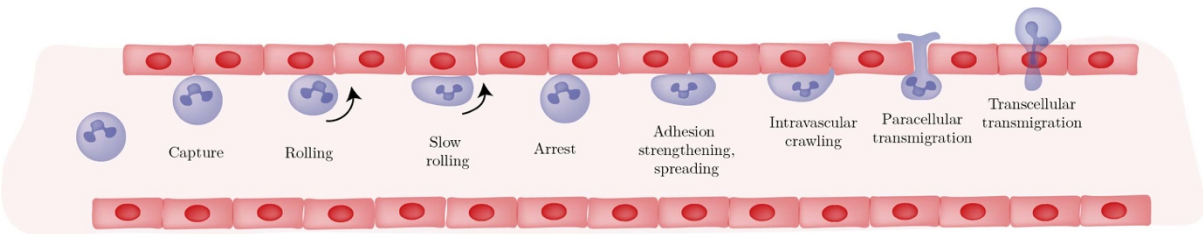

Figure 6 Different steps of the neutrophil extravasation cascade, modified after Ley *et al.* (2007)

VLA4 for neutrophil rolling and ICAM1 and VCAM1 (expressed on endothelial cells) for the arrest of neutrophils. Chemoattractants, such as CXCL4 and CXCL5 proteins, as well as integrins can also mediate neutrophil arrest. ICAM1, VCAM1, PECAM1 and junctional adhesion molecules mediate neutrophil crawling and transmigration through the endothelium.[72] In ulcerative colitis, the rate and extent of neutrophil extravasation correlates with disease severity and is also actively used to assess disease severity [73]. Neutrophils form different granules during the process of maturation:

- **azurophilic granules**: containing myeloperoxidase (MPO), neutrophil elastase (ELANE), cathepsin G and lysozyme
- **secondary granules:** containing lactoferrin and collagenase (MMP8)
- **tertiary granules:** containing MMP9

The release of said granules can either help fight infections or, if the activation occurs in a prolonged fashion, it can lead to tissue damage. Released ROS damage DNA, proteins and lipids, released proteases lead to tissue damage and an aggravated inflammation. 5-lipoxygenase produced by neutrophils is an important enzyme, involved in the formation of proinflammatory lipids and fatty acids.[74] Matrix metalloproteinases (MMPs) and ELANE released by neutrophils are able to degrade extracellular matrix proteins, such as collagen, elastin and fibronectin, facilitating the release of cells trapped in the extracellular matrix.

1.2.9. Myofibroblasts and fibroblasts in inflammation

Myofibroblasts are activated fibroblasts, also known as smooth-muscle like fibroblasts. There exist many different definitions for the cell type, they are, however, best described as α-SMA, vimentin and CD90 expressing cells, negative for desmin – a smooth muscle cell marker [75]. Myofibroblasts contribute to the formation of the extracellular matrix by their secretion of collagens, fibronectin, tenascin, laminin and matrix metalloproteinases. They are crucial for wound healing and the resolution of inflammatory processes as they secrete a plethora of cytokines, chemokines and growth factors.[76, 77] Typical for the phenotype of myofibroblasts is the production of smooth muscle actin (ACTA2) and vimentin. Fibroblasts can be differentiated into myofibroblasts through the treatment with TGF-β and oxidative stress [78, 79]. Neutrophil elastase [80] and cell density have been shown to have an impact on the differentiation process as well. Masur *et al.* reported that fibroblasts, seeded at a density of 5 cells per mm^2 yielded in cell populations of 70-80% myofibroblasts at 5-7 days post seeding.[81] Fibroblasts are the most abundant cell type in the stroma and are important for the production and remodeling of extracellular matrix components in tissues. Their ability to survive for a prolonged period of time, as well as their capability to alter their phenotypes - especially during inflammation - indicates, that these cells contribute in large parts to the inflammatory process and also to the persistence of chronic inflammation. Recent studies of our working group have also suggested a contribution of fibroblasts to chronic inflammation [82, 83]. In the healthy colon, subepithelial myofibroblasts are located directly underneath the epithelium, where they contribute to mucosal repair. In active IBD, increased numbers of myofibroblasts have been detected, possibly contributing to processes of tissue repair and fibrosis.[84]

1.3. Fatty acids and eicosanoids

Fatty acids are composed of hydrocarbon chains and carboxylic acid as a functional group. Their nomenclature takes into account the hydrocarbon chain length, as well as the number and position of double bonds. Fatty acids can be further divided into subgroups, depending on their number of double bonds: Polyunsaturated fatty acids (PUFAs) possess more than one double bond, whereas saturated fatty acids (SFAs) have no double bonds, monounsaturated fatty acids have one double bond. PUFAs are derived from phospholipids making up membrane bilayer structures. Enzymes (phospholipases) hydrolyze phospholipids and form fatty acids. Eicosanoids are enzymatic or non-enzymatic products of arachidonic acid (AA) or other PUFAs (Figure 7) [85]. They are involved in inflammatory, as well as homeostatic processes [86, 87]. The mode-of-action of prostaglandins and leukotrienes is strongly dependent on their interaction with GPCRs, however also PPARs are thought to be able to be activated by and bind different eicosanoids, such as LTB_4 and 8(S)-HETE, for example [86, 88]. The 5-LOX pathway, through which leukotrienes are formed, is an important

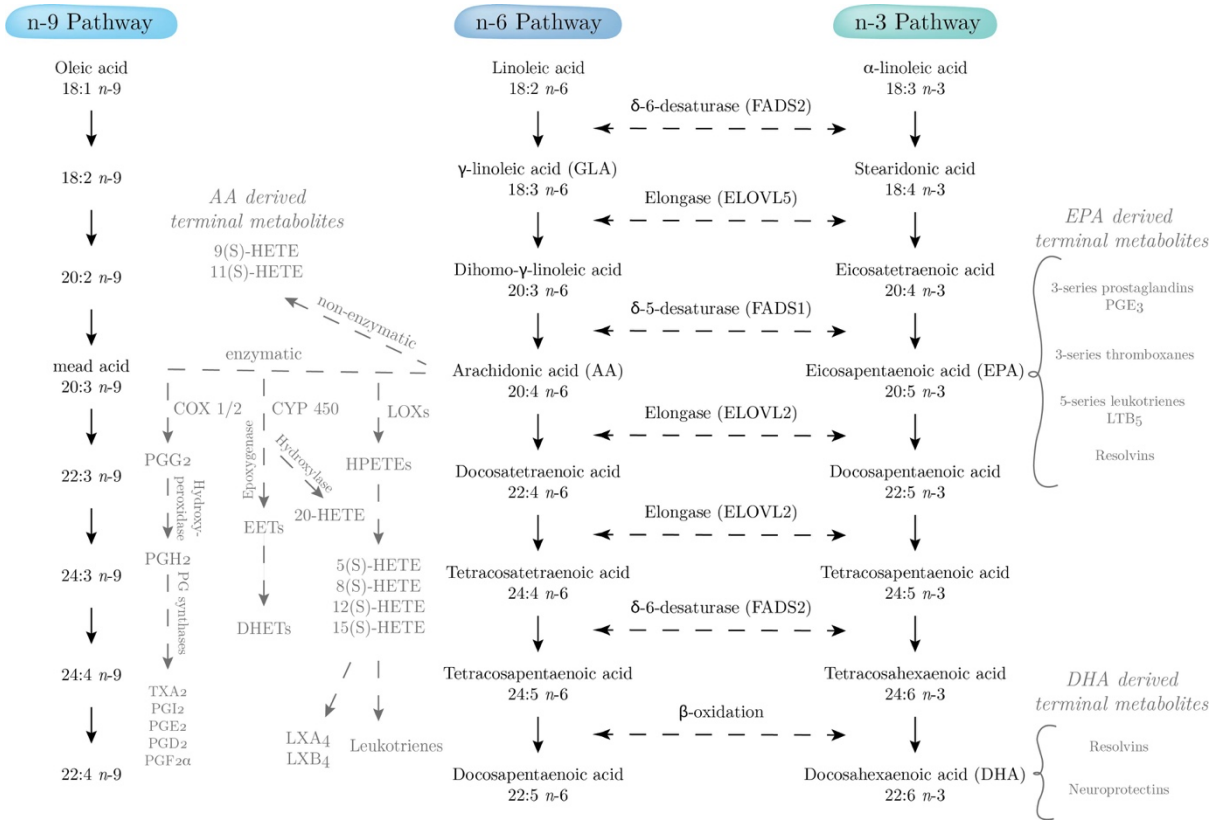

Figure 7 Fatty acid and eicosanoid metabolism and synthesis pathways; modified from Martin C.R. (2015)

proinflammatory cascade. LTD_4 and LTB_4, emerging from this pathway, are important chemoattractants for eosinophils and neutrophils, respectively. Prostaglandins have also been recognized to be acting on peripheral sensory neurons, thereby inducing the sensation of pain [86]. Several studies, conducted on IBD patients, have revealed that the PUFA profile in these patients is altered [89-92]. In plasma analyses of patients with active ulcerative colitis, an increase in n3-PUFAs, as well as alterations in n6-PUFA levels were noted. Palmitic acid levels were increased and stearic acid concentrations were lower in patients with active disease.[89] In patients with non-active disease, plasma levels of C22:6n3 were found to be elevated, as well as plasma levels of arachidonic acid [90]. In mucosal preparations of patients with active disease, levels of PGE_2, PGD_2, TXB_2, 5-HETE, 11-HETE, 12-HETE and 15-HETE have been reported to be significantly elevated and correlating with inflammation severity [91].

1.4. Proteomics

The term "proteome" was introduced in 1995, in order to describe the *total protein complement of the genome* [93]. Today, the term "proteomics" encompasses a whole range of different analyses, such as the identification and quantification of whole proteomes, as well as the analysis of protein structures, conformational changes, posttranslational modifications (PTMs), isoforms, protein localization and turnover rates in different matrices. Proteomics includes top-down, bottom-up and middle-down techniques. Top-down techniques are suited for the analysis of isoforms and PTMs, bottom-up, also termed "shotgun", approaches – the term having been established by John R. Yates in 2013 [94] – describes the analysis of peptides derived from enzymatic protein digests by tandem mass-spectrometry. Middle-down proteomics analyses use peptides generated by limited proteolytic digests, in order to identify proteins. [95] More than 30 years ago, when proteomics was still in its developing stages, proteins were hard to analyze using mass-spectrometry, as these molecules could not be ionized

in their intact forms. This changed rapidly, when J. B. Fenn and co-workers developed electrospray ionization (ESI) [96]. It was only until soft ionization methods, such as MALDI and ESI, were introduced that proteomics could replace peptide sequencing techniques, such as Edman degradation [97]. In the early times of proteomics analyses, SDS-PAGE and 2DE methods were used to reduce sample complexity and obtain protein fractions that could be excised and analyzed using mass-spectrometry. Identifications were performed using peptide-mass-fingerprinting, as well as uninterpreted mass spectra [98]. Proteome analyses today are performed on time-of-flight (TOF), as well as Orbitrap, Fourier-transform ion cyclotron resonance (FT-ICR), quadrupole and ion trap instruments. Extensive protein databases, including sequence information, as well as bioinformatic tools are available nowadays, facilitating protein identification.

1.5. Mass spectrometry

Nowadays, various mass spectrometric setups are available for the analysis of different samples and analytes. However, as the mass spectrometer of choice for the protein analysis described in this thesis was a Q Exactive™ Hybrid Quadrupole-Orbitrap™ mass spectrometer, focus will be laid on this instrument (Figure 8). Protein analyses, which are a major part of this project, were carried out in positive ionization mode, hence this process will be described in more detail. A typical untargeted, shotgun protein analysis performed on a Q Exactive™ mass spectrometer requires, first of all, a tryptic digestion of proteins resulting in a mixture of peptides with known cleavage sites (C-terminus of lysine and arginine). These peptides are further separated on a nanoflow HPLC system, resulting in a reduction of sample complexity. The separated peptides are ionized using a nanospray source. In detail, the analyte solution is transferred through a capillary under high-voltage, thereby producing charged droplets. These charged droplets are deprived of solvent by successive solvent

evaporation until very small and highly charged droplets are remaining. The droplets are repelled by each other by Coulombic repulsion and transported along the electric field. As the droplets reach a point where surface tension is weaker than the Coulomb repulsion inside the droplet, Coulomb explosion or Coulomb fission occurs. The droplets are broken apart into smaller droplets which possess a higher mass-to-charge ratio. Further solvent evaporation and Coulomb fission processes lead to only the charged analyte ion, which will be transported into the mass spectrometer through the transfer capillary.[99] Nanospray sources are commonly used for peptide analyses, as they create much smaller initial droplets, leading to faster evaporation, as well as faster

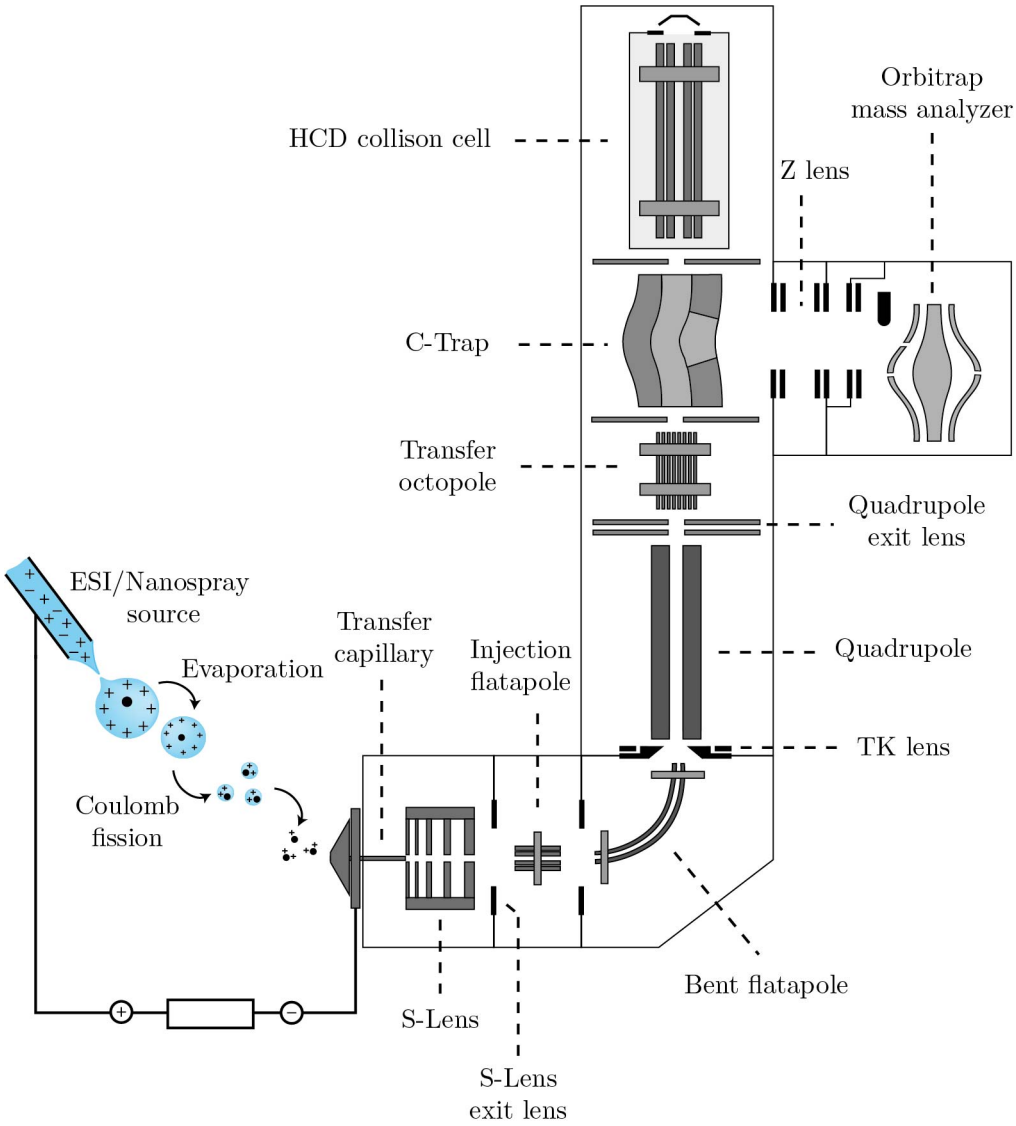

Figure 8 Q Exactive™ mass spectrometer and ESI-process leading to ion generation, modified after Exactive Series, Operating Manual

creation of charged analytes. The small nanospray capillary can be positioned very closely to the sampling cone of the mass spectrometer, leading to increased sensitivity and improved electrospray stability. Another advantage of nanospray ionization are the prolonged analysis times due to the low flow rate, leading to higher analyte coverage, resulting in more in-depth proteome analyses.[100, 101] The ion source interface of Q Exactive™ instruments is composed of an ion transfer capillary, two cartridge heaters, a heater block, a vent preventing ball, an ion sweep cone, an S-lens and an exit lens. Desolvation of ions is supported by the ion transfer capillary, which is surrounded by a heater block, reaching temperatures of up to 400°C. The decreasing pressure in the instrument, due to vacuum creation inside of the instrument, draws ions from the API (atmospheric pressure ionization) source to the S-lens region, where RF is applied to the spaced electrodes, focusing and guiding the ions to the exit lens. The S-lens and the exit lens are both evacuated by the source vacuum pump. Ions exiting the S-lens exit lens are further transported to the injection flatapole in a lower pressure region. The injection flatapole is an ion focusing device, consisting of four electrodes. The ions inside the flatapole are focused though an RF voltage applied to the electrodes, creating an electric field alongside the electrode-axis. The ions are further transported to the bent flatapole, which is used as a transmission device, guiding ions in a 90° angle into the quadrupole. Neutral molecules, as well as remaining solvent droplets are removed in the flatapole, as these are not able to pass the 90° bend of the flatapole. The TK (Turner-Kruger) lens focuses ions into the quadrupole and acts as a vacuum shield between the quadrupole and the bent flatapole. The quadrupole is a mass filtering device, consisting of four round rods, arranged in a square symmetry. Rods, which are opposite to each other are connected electrically, making it feasible to apply different RF and DC voltages to the different pairs of electrodes. During injections, the voltages on the different rod-pairs are set to fixed voltages of opposite signs, so that only ions of specific m/z ratios are able to pass the

quadrupole. Ions which cannot pass the quadrupole, will hit the rods, become neutralized and are removed by the vacuum pump. Passing the quadrupole, ions will enter the gas-filled curved-linear trap (C-trap) and lose their kinetic energy as they collide with nitrogen gas. Ions are further collected in the C-trap and a collector behind the C-trap assesses the Automatic Gain Control (AGC) accuracy. Ions collected in the C-trap will be extracted by increasing the RF on the C-trap rods, pushing the ions through a small slot, creating an ion beam which will enter the Orbitrap analyzer. Ion packets injected into the Orbitrap analyzer will be squeezed and transported closer to the inner electrode, as the electric field strength of the outer electrode is increased. When all ions have entered the analyzer, image current detection is performed, as the voltage on the central electrode is kept constant.

$$\omega = \sqrt{\frac{z}{m} * k} \qquad \text{(Eq.1)}$$

The oscillation frequencies along the inner electrode are dependent on the m/z ratio of the injected ions and an instrument constant k (Eq. 1). The image current created by the oscillating ions is detected through the slits in the outer electrode, amplified and the analog signal is converted into a digital signal. The digital signal is processed by Fast Fourier Transformation (FFT) and m/z ratios are obtained. An HCD (Higher Energy Collisional Dissociation) cell, consisting of a multipole, facilitates ion fragmentation through ion collision with gas. As the C-trap and the HCD are connected to each other, this gas is shared between the two instrument parts. In this way, ions collected in the C-trap can be transferred to the HCD-cell, where they are fragmented. The ion fragments can be transferred back to the C-trap, collected and ejected into the Orbitrap analyzer. Combining this process with the filtering capability of the quadrupole MS/MS analyses can be performed. [102, 103]

2. Objectives

The aim of this master's project was to characterize the inflammatory process occurring in patients suffering from an acute inflammation of the colon mucosa and submucosa induced by ulcerative colitis. As the pathogenesis of ulcerative colitis remains unclear, a study of colon biopsy specimen, as well as plasma samples on the protein level with the addition of the collection of eicosanoid composition information of plasma samples, is a suitable approach to gain a better and more comprehensive understanding of the inflammatory process taking place during a disease flare up. The specific phenotype of a UC induced inflammation makes it feasible to compare colonic regions of the same patients, thereby limiting interpatient variation due to the avoidance of control samples of unrelated, healthy patients. Plasma samples of patients suffering from an active inflammation were compared to healthy control samples. Combining this multi-omics approach for the analysis of patient samples with an *in-vitro* analysis of inflammatorily stimulated colonic fibroblasts/myofibroblasts, the role of these cells in the chronicity and persistence of the disease should be assessed.

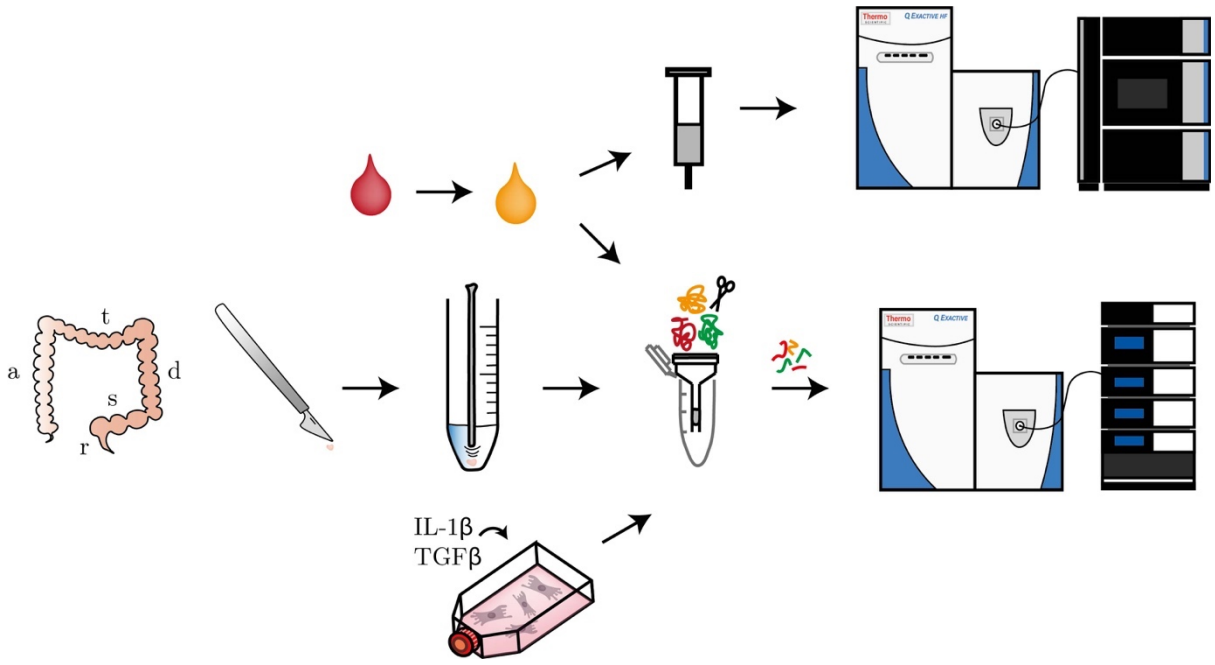

Figure 9 Master's thesis workflow; including the proteomic analyses of colon tissue specimen, plasma samples, inflammatorily stimulated (myo-)fibroblasts, as well as eicosanoid analyses of plasma samples

3. Materials and Methods

3.1. Patient sample collection and ethical considerations

All patient samples were obtained in agreement with the ethics committee "Ethikkommission der Stadt Wien" as part of the study "Multi-omics Analyse zur Charakterisierung entzündlicher Signaturen in PatientInnen mit aktiver Colitis ulcerosa (CU)" (EK 18-193-0918).

3.2. Plasma preparation

Patient blood samples were collected and plasma was prepared directly at the hospital Rudolfstiftung. Control plasma samples were collected and plasma was prepared at the University of Vienna, Faculty of Chemistry, Department of Analytical Chemistry. Briefly, approximately 10 mL of blood were collected in EDTA coated tubes (Vacuette® 4 and 6 mL K3EDTA coated tubes, Greiner Bio-One) and centrifuged for 10 minutes at 1,500 x g and 4°C. Plasma was aliquoted to 1 mL plasma per 1.5 mL Eppendorf microcentrifuge tube and stored at -80°C until further processed. For protein digestion, plasma samples were thawed, diluted 1:10 in Protifi® lysis buffer (8 M urea, 50 mM TEAB, 5% SDS, pH 7.55) and left at 4°C overnight. The next day, protein concentration was determined, using BCA assay and the sample was diluted to a final protein amount of 1 µg/µL. 20 µg (equal to 20 µL of sample) were used for the protein digestion, following Protifi® digestion protocol. Unless indicated otherwise, all solvents used were LC-MS grade.

3.3. UC patient colon biopsy sample preparation

Colonic biopsies from the rectum, colon sigmoideum, colon descendens, colon transversum and colon ascendens were excised at the hospital Rudolfstiftung during surveillance colonoscopy, using biopsy forceps. Samples were washed with 0.9% NaCl

solution and transferred to cryotubes. Samples were stored at -80°C until further processed.

For protein digestion, samples were thawed and transferred to 15 mL Falcon tubes. Depending on the biopsy sample size, 75 or 100 µL of Protifi® lysis buffer were added to the sample and stored at 4°C overnight. The next day, the sample was sonicated (2-4 impulses per sample, depending on sample size) and centrifuged at 4,000 x g for 5 minutes. The sample was transferred to a 1.5 mL Eppendorf microcentrifuge tube and centrifuged again at 15,000 x g for 5 minutes. The supernatant was used for further processing. Protein concentration was determined using BCA assay, 20 µg of protein per sample were used for protein digestion, following Protifi® digestion protocol.

3.4. Cell culture

The normal human colonic fibroblast/myofibroblast cell line CCD-18Co (ATCC) was cultivated in EMEM cell culture medium with 10% heat inactivated FCS (Sigma Aldrich, 56°C, 10 min in water bath) and penicillium/streptomycin. In detail, the cells were thawed, pipetted into a 15 mL Falcon tube with 5 mL cell culture medium and centrifuged at 1,100 rpm for 5 minutes at room temperature. The resulting supernatant was discarded, the cell pellet resuspended in 1 mL cell culture medium, then suspended in additional 10 mL cell culture medium in a T75 cell culture flask. Cells were incubated at 37°C, 5% CO_2 (Heracell 150i CO_2 Incubator, Thermo Scientific). Two days later, the cells were split: the culture medium was aspirated, cells were washed two times with 5 mL preheated PBS (37°C) and consequently treated with 3 mL preheated trypsin (37°C). After 4 minutes incubation at 37°C with 5% CO_2 the cells were analyzed under the microscope to ensure they had detached from the bottom of the flask. 4 mL of cell culture medium were added, the cell suspension transferred to a 15 mL Falcon tube and centrifuged at 1,100 rpm for 5 minutes at

room temperature. Supernatant was removed and the cell pellet resuspended in 1 mL preheated cell culture medium (37°C). 10 mL of preheated cell culture medium were transferred to the previously used T75 cell culture flask and another 10 mL were added to a new one. 0.5 mL of cell suspension were suspended in the cell culture flasks and the cells incubated at 37°C, 5% CO_2. Five days later, when the cells had reached 65% confluency, they were split once more, suspended in six T75 cell culture flasks and incubated for another five days. The cells were now split and separated into 18 different T25 cell culture flasks (4.5 mL cell culture medium and 0.5 mL cell suspension). Three days later the cell culture medium was aspirated from all 18 flasks and replaced with 6 x 5 mL cell culture medium and 10 ng/mL IL-1β, 6 x 5 mL cell culture medium and 2 ng/mL TGF-β and 6 x cell culture medium without any additives. The cells were once more incubated at 37°C, 5% CO_2. Cells were treated at passage 4, cells treated for one day were harvested and fractionated at passage 4, whereas cells treated for one week were harvested and fractionated at passage 5.

3.4.1. Cell fractionation

Cell culture medium was removed, cells were washed with 4 mL PBS, followed by washing with 4 mL serum-free cell culture medium. 3 mL serum-free EMEM were added and cells were incubated for 6 h at 37°C, 5% CO_2. After incubation, the cell culture medium was removed and centrifuged at 3,500 rpm for 5 minutes. All further fractionation steps were performed on ice. The supernatant was transferred to a clean Falcon tube and proteins were precipitated by adding 12 mL ice-cold EtOH and storage at -20°C for at least 14 hours. In order to obtain the cytoplasmic fraction, 1 mL of isotonic lysis buffer (10 mM HEPES/NaOH, pH 7.4, 0.25 M sucrose, 10 mM NaCl, 3 mM $MgCl_2$, 0.5% Triton X-100, 1 µg/mL pepstatin, 1 µg/mL leupeptin, 1 µg/mL aprotinin) were added to the cells and cells were removed from the flask, using a cell scraper. Cells were then exposed to mechanical shear stress, using a syringe and needle.

Briefly, the cell suspension was pressed out of the syringe, pressing the needle against the wall of a Falcon tube. This step was repeated until when examined under the microscope cells appeared to be lyzed. The suspension was centrifuged at 3,500 rpm for 5 minutes. The supernatant was precipitated in 4 mL ice-cold EtOH for at least 14 hours. The remaining liquid above the residual pellet, containing cell nuclei, was removed using paper towels. 100 µL of extraction buffer (500 mM NaCl) was added to the pellet and the pellet let to swell on ice for 10 minutes. 900 µL of NP40 buffer was added to the suspension and let to swell for another 15 minutes on ice, followed by centrifugation at 3,500 rpm for 5 minutes. The supernatant was precipitated in 4 mL ice-cold EtOH for at least 14 hours.

3.5. Proteomics methods

3.5.1. Protein digestion protocol optimization

In order to find a suitable protein digestion protocol for colon tissue analysis, different approaches to a FASP protocol were tested. Three lysis conditions were compared, as well as two reduction and two alkylation method. The different methods were tested in triplicates using colon tissue. After identification of the most suitable FASP method using Microcon® 10 kDa MWCO filters, the best method was compared to a different spin column protocol (Protifi®).

3.5.1.1. Colon tissue method optimization

Colon tissue was thawed and a slice (approximately 0.5 x 0.5 x 0.5 cm min size) was cut off using a scalpel, the remaining tissue was stored at -196°C in liquid nitrogen. The cut off tissue piece was homogenized in 100 µL sample buffer (7.5 M urea, 1.5 M Thiourea, 0.1 M DTT, 65 mM CHAPS, 0.05 % (w/v) SDS) using sonication (7 impulses, 100% intensity). Protein concentration of the tissue sample was determined and SDS-PAGE was performed to assess the intactness of the tissue. The remaining tissue was stored at -196°C. After intactness was ensured using SDS-PAGE, the tissue was thawed again and a slice (approximately 0.5 x 0.5 x 0.5 cm min size) was cut off. The tissue piece was homogenized in 400 µL 7.5 M urea using sonication. After protein concentration determination according to the Bradford protocol, 40 µL of tissue suspension were added to 150 µL of lysis buffer. The three lysis buffers used were **sample buffer** (7.5 M urea, 1.5 M thiourea, 0.1 M DTT, 65 mM CHAPS, 0.05 % (w/v) SDS), **sample buffer + SDC** (7.5 M urea, 1.5 M thiourea, 0.1 M DTT,

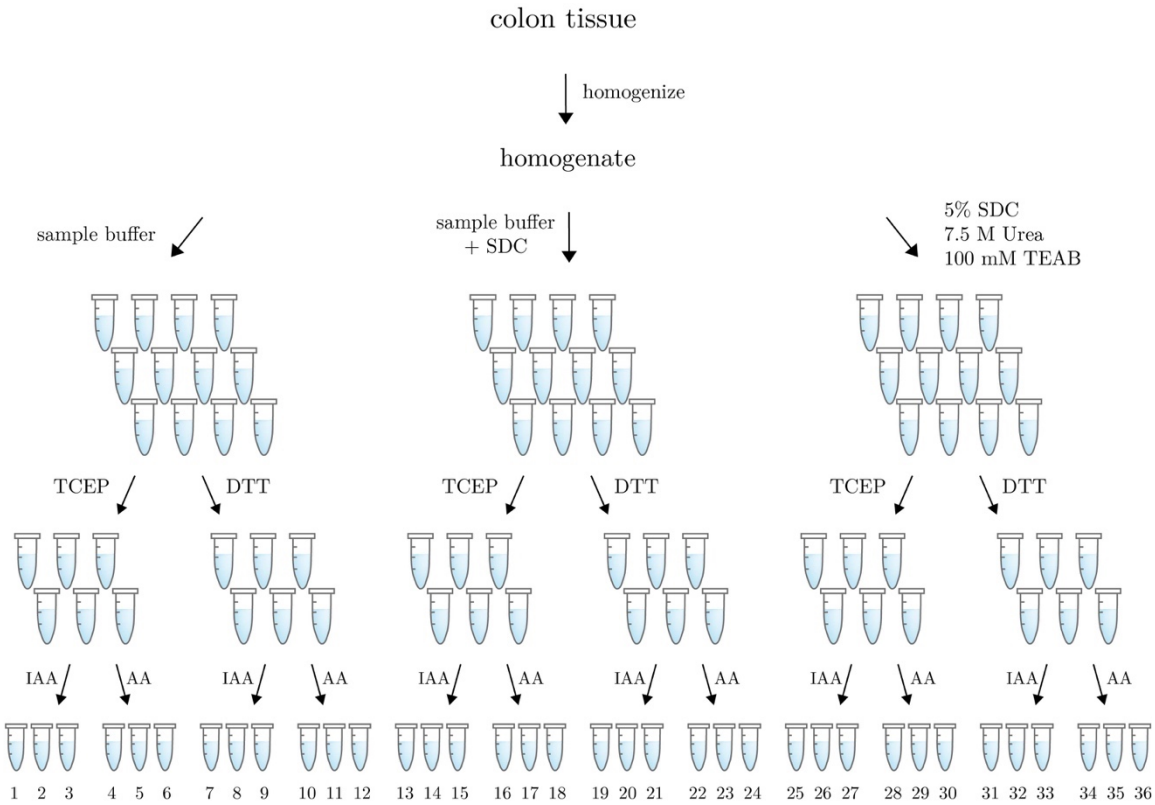

Figure 10 Digestion protocol optimization using colon tissue

65 mM CHAPS, 0.05 % (w/v) SDS, 0.05 % SDC (w/v)) and a modified **5% (w/v) SDC** lysis buffer, containing 5% (w/v) SDC and additionally 7.5 M Urea and 100 mM TEAB. The samples were stored overnight at 4°C. Protein concentrations were determined again, using Bradford assay for samples lyzed in sample buffer, sample buffer + SDC and BCA assay for the one sample lyzed in 5% (w/v) SDC. 20 µg of protein were digested, following the FASP protocol using Merck Microcon® 10 kDa MWCO filters and applying different reduction and alkylation methods.

3.5.2. Protein-concentration determination

Depending on the lysis buffer used for protein solubilization, different colorimetric methods were used to determine protein concentrations.

3.5.2.1. Bradford assay

For samples and proteins solubilized in lysis buffers containing low amounts of SDS and SDC, Bradford assay [104] was used to determine the protein concentration. A calibration curve was prepared by adding different amounts of a 1 µg/µL BSA standard ranging from 0 to 5 µg to a mixture of 50 µL of Bradford reagent, 1 µL of the corresponding lysis buffer in which the sample protein had been solubilized and LC-MS grade water. The resulting volume was equivalent to 250 µL. To determine the concentration of samples, 1 µL of sample was mixed with 50 µL of Bradford reagent and 199 µL of LC-MS grade water, again resulting in a volume of 250 µL. Dilution and mixing steps were performed in 0.5 mL Eppendorf microcentrifuge tubes, following a vortexing step and a short spin-down step on a mini centrifuge. 200 µL of the solutions were pipetted onto 96 well plates and absorbance was measured at a wavelength of 595 nm.

3.5.2.2. Bicinchoninic acid assay (BCA)

Protein concentrations of samples containing higher amounts of SDS and/or DTT or thiourea were determined with BCA assay [105]. BCA reagent A (26 mM bicinchoninic acid disodium salt hydrate, 186 mM sodium carbonate, 8 mM sodium tartrate, 113 mM sodium bicarbonate, pH 11.25) was mixed with reagent B (200 mM copper sulfate pentahydrate) in a 50:1 ratio (5 mL A + 0.1 mL B) to obtain the BCA working reagent. The working reagent was prepared freshly directly before usage. Calibration standards were prepared in 1.5 mL Eppendorf microcentrifuge tubes by

mixing 200 µL of working reagent with 0 to 5 µL of 1 µg/µL BSA standard and 1 µL of lysis buffer and adding the respective amount of LC-MS grade water to obtain a volume of 210 µL. For sample protein concentration determination 1 µL of sample was added to 200 µL of working reagent and 9 µL of LC-MS grade water. The calibration and sample solutions were incubated for 30 minutes at 60°C in the dark with slight agitation (1100 rpm) on an Eppendorf ThermoMixer®. After incubation, the samples were cooled down to room temperature, spun down on a mini centrifuge and 200 µL of sample and calibration solutions were transferred onto a 96 well plate. Absorptions were measured at a wavelength of 562 nm.

3.5.3. SDS-PAGE (Lämmli)

3.5.3.1. Gel preparation

A separation (12% AA) and a stacking (4% AA) gel were prepared. Firstly, the separation gel (12 mL in total) was prepared by mixing 4.8 mL 30% AA (29.2 % AA, 0.8 % PDA) with 2.25 mL 2 M Tris-HCl (pH 8.8) and 4.83 mL LC-MS grade water. 2 mL of this solution were separated and mixed with 20 µL 10% (w/v) APS and 5 µL TEMED in order to prepare a denser gel for the bottom layer to avoid leakage. 1 mL of this solution were pipetted into the gel chamber (Mini-Protean-Cell, BIO-RAD, 1 mm spacer) immediately. The remaining separation gel solution was degassed for 10 minutes in a desiccator, *in vacuo*. Meanwhile the stacking gel was prepared by mixing 1.066 mL 30% AA (29.2 % AA, 0.8 % PDA) with 1 M Tris-HCl (pH 6.8) and 5.86 mL LC-MS grade water. The solution was degassed for 10 minutes. To induce polymerization, 50 µL 20% SDS (w/v), 45 µL 10% APS (w/v) and 7.5 µL TEMED were added to the remaining separation gel solution. The solution was mixed and pipetted into the gel chamber. 1 mL of 90% IPA was added to the gel chamber to cover the separation gel. After 30 minutes the IPA was removed using filter paper. Subsequently, the stacking gel was prepared for polymerization by adding 40 µL 20%

SDS (w/v), 40 µL 10% APS (w/v) and 8 µL TEMED to the degassed stacking gel solution. After mixing, 3 mL of the solution were pipetted onto the separation gel and a 10 well comb (Mini-Protean comb, 10-well, 1.0 mm, 44 µL) was inserted. As soon as the gel was completely polymerized, the gel chamber was lowered into the electrophoresis chamber, filled with electrode buffer (25 mM Tris, 192 mM glycine, 0.1% (w/v) SDS). The comb was removed and 20 µL of sample, premixed with 5 µL loading buffer (5x Lämmli buffer, preheated to 95°C + β-mercaptoethanol) were pipetted into the gel pockets. The protein amount loaded onto the gel was approximately 20 µg. To one of the outer pockets of the gel a molecular-weight size marker was added. Electrophoresis was performed at 20 mA current (constant) and a maximum of 200 V voltage. After completed electrophoresis, the gel was removed from the gel chamber and proteins were fixated by washing the gel in a mixture of 50% (v/v) methanol and 10% (v/v) acetic acid for 30 minutes under slight agitation.

3.5.3.2. Silver staining

Following the protein fixation, the gel was washed three times 10 minutes in 50% (v/v) methanol under slight agitation and two times 5 minutes each in LC-MS grade water under slight agitation. Before staining, the gel was treated with 0.02% (w/v) sodium thiosulfate pentahydrate for 1 minute under slight agitation and washed two times with LC-MS grade water. Silver staining was achieved by slightly agitating the gel in a 0.1% (w/v) silver nitrate solution for 10 minutes, washing the gel in LC-MS grade water and developing in 3% (w/v) sodium carbonate, 0.05% (w/v) formaldehyde until dark enough. The reaction was stopped by incubating the gel in 1% (v/v) acetic acid.

3.5.4. Protein digestion protocols

3.5.4.1. Filter assisted sample preparation (FASP) - protein digestion using Merck Microcon®-10 kDa MWCO filters

Protein samples containing only small amounts of SDS were processed on Microcon® 10 kDa MWCO filters. The filters were placed in microcentrifuge tubes provided by the manufacturer and 500 µL LC-MS grade water were loaded onto the filter. After 30 minutes centrifugation at RT and 14,000 x g the filters were inspected, if there was remaining liquid on the filters, they were centrifuged again. Every centrifugation step was followed by manual inspection of all filters and removal of the flow-through. 200 µL of reduction buffer (32 mM DTT or TCEP, 8 M guanidinium hydrochloride, 50 mM ABC) were added to the filter and the sample was spiked directly into the DTT solution on the filter. The overall loaded sample amount was equivalent to 20 µg protein. The filters carrying DTT reduction buffer and the sample were then incubated at 37°C for 30 minutes with slight agitation (1100 rpm) on a ThermoMixer®. Following the incubation, the filters were centrifuged for 60 minutes at 14,000 x g. 100 µL 50 mM ABC were added onto the filters and centrifuged for 15 minutes at 14,000 x g. The previous step was repeated with 30 minutes of centrifugation. Alkylation buffers (54 mM IAA or AA, 8 M guanidinium hydrochloride, 50 mM ABC) were loaded onto the filters. The filters were incubated at 30°C for 30 minutes in the dark, while having been slightly agitated (1100 rpm). After 60 minutes centrifugation at 14,000 x g, the filters were washed twice by adding 100 µL ABC each time and centrifuging for 20-30 minutes. Subsequently, filters were placed in clean microcentrifuge tubes. 20 µg of protease (Trypsin/Lys-C mix, Promega) were dissolved in 200 µL resuspension buffer (50 mM acetic acid) and kept on ice. 95 µL of 50 mM ABC cooled to 4°C were placed on the filters and 5 µL of protease were spiked into the solution. The filters were placed on a ThermoMixer® set to 4°C and slightly agitated (1100 rpm) for 10 minutes. After incubation, the filters were placed in a rack

and kept in an incubator set to 37°C overnight. The next morning, 45 µL cold ABC were placed on top of the solution and 5 µL of protease were spiked into the solution. The filters were slightly agitated on a ThermoMixer® set to 4°C and incubated for 4 h at 37°C. Peptides were eluted by centrifuging for 20 minutes at 14,000 x g, adding 50 µL LC-MS grade water to the filters, centrifuging for 20 minutes and adding 50 µL of 0.5% TFA to the filter followed by another centrifugation step. Samples were stored at -20°C until further processed.

3.5.4.2. C-18 peptide clean up

Tissue and serum samples digested using Merck Microcon® 10 kDa MWCO filters required C-18 peptide clean-up. C-18 columns were placed in 2 mL Eppendorf microcentrifuge tubes and washed twice, by adding 400 µL 50% ACN directly onto the column, each step followed by centrifugation at 1,500 x g for 1 minute. The flow-through was discarded. Column washing was followed by an equilibration step, loading the columns two times with 200 µL 5% ACN, 0.5% TFA each, followed by centrifugation at 1,500 x g for 1 minute. Flow-through was discarded. Sample was acidified by adding 10% TFA, to obtain a final concentration approximately 1% TFA (e.g. sample volume 250 µL + 25 µL 10% TFA). Sample was loaded onto the column, followed by centrifugation at 1,500 x g for 1 minute. Flow-through was loaded onto the column to increase sample binding, followed by centrifugation at 1,500 x g for 1 minute. The flow-through obtained after this step was discarded. Column washing was performed by adding 200 µL 5% ACN, 0.5% TFA directly onto the column and centrifugation at 1,500 x g for 1 minute, flow-though was discarded. This washing step was repeated. Columns were put into a clean 1.5 mL Eppendorf microcentrifuge tube and peptides were eluted twice by adding 40 µL 50% ACN, 0.1% TFA each time, followed by centrifugation at 1,500 x g for 1 minute. Samples were dried in a vacuum centrifuge and stored at -20°C until used.

3.5.4.3. Protifi® S-Trap™ digestion protocol

Samples which contained any precipitate were centrifuged for 8 minutes at 13,000 x g to remove insoluble matter. Protein concentration was determined according to BCA protocol. All samples were diluted to a final protein amount of 1 µg/µL in lysis buffer (8 M urea, 50 mM TEAB, 5% SDS). 20 µL of diluted sample (equal to 20 µg protein) were pipetted into a 1.5 mL Eppendorf microcentrifuge tube and disulfide bonds were reduced by adding 20 µL 64 mM DTT and incubating the solution at 95°C for 10 minutes, under slight agitation (300 rpm). The sample was cooled to room temperature and 5 µL 486 mM IAA were added for the alkylation of cysteine residues. Under slight agitation (300 rpm) the sample was incubated in the dark at 30°C for 30 minutes. 4.5 µL of 12% phosphoric acid were added to acidify the sample. 297 µL S-Trap buffer (90% MeOH (v/v), 0.1 M TEAB) were added to the sample. 175 µL of solution were added to the Protifi® digestion column, the column was placed in a 2 mL Eppendorf microcentrifuge tube. The column was centrifuged at 4,000 x g for 1 minute. Remaining sample solution was transferred to the column, the column was rotated by 180° and centrifuged again. The column was washed by adding 150 µL S-Trap buffer, followed by centrifugation at 4,000 x g for 1 minute. This step was repeated three times. Digestion column was transferred to a clean 2 mL Eppendorf microcentrifuge tube. Trypsin/Lys-C was dissolved in 400 µL 50 mM TEAB and 20 µL of the protease solution were added directly onto the column. The column was incubated for 1 hour at 47°C. Peptides were eluted in three steps: adding 40 µL TEAB, followed by centrifugation at 4,000 x g for 1 minute, adding 40 µL 0.2% FA, followed by centrifugation and lastly adding 35 µL 50% ACN, 0.2% ACN, followed by a centrifugation step. The peptides were dried in a vacuum concentrator and stored at -20°C until further processed.

3.5.5. nLC-MS/MS

3.5.5.1. Nanoflow Liquid Chromatography

Previously dried peptide samples were reconstituted in 5 µL of a mixture of synthetically produced standard peptides (10 fmol/µL in 30% FA) and diluted with 40 µL eluent A (97.9% LC-MS grade water, 2% ACN, 0.1% FA). The sample solution was transferred to a 96-well plate and placed in the autosampler of the chromatograph (Dionex UltiMate® 3000 RSLCnano), which was kept at 4°C. In order to concentrate and desalt the sample, it was transferred to a pre-column (Acclaim™ Pepmap™ 100; 100 µm x 2 cm, nanoViper; C18, 5 µm, 100 Å) at a flow-rate of 10 µL per minute, 100% eluent A. The sample was further transferred onto the separation column at a flow rate of 300 nL/min. Depending on the sample, the analytes were eluted applying different gradient elution profiles. For the analysis of plasma and CCD-18Co supernatant samples, 1 µL of sample was injected and eluted by increasing the percentage of eluent B (79.9% ACN, 20% LC-MS grade water, 0.1% FA): 1% B for 10 minutes, increase from 0-1% B over the time course of 10 minutes, 1-7% B for 1 minute, 7-35% B for 38 min, 35-40% B for 3 minutes, hold at 40% B for 2 minutes. The stepped gradient elution was followed by a washing step, increasing the percentage of eluent B from 40-80% B over a time course of 2 minutes, then decreasing the percentage to 1% for 7 minutes, followed by equilibration at 1% B for 22 minutes. The total LC method time was 85 minutes. CCD18-Co cytoplasmic fractions, as well as colon tissue samples were eluted following a different stepped gradient: 1% B for 9 minutes, 1-8% B for 1 minute, 8-30% B for 80 minutes, 30-40% B for 15 minutes, followed by washing by increasing the percentage of eluent B from 40-80% for 5 minutes, 5 minutes hold at 80% B, then decreasing the percentage to 1% B for 3 minutes, followed by 17 minutes equilibration at 1% B. The total LC method time was 135 minutes.

3.5.5.2. Mass spectrometry

After nLC separation, the eluted peptides were further transferred to a Q Exactive™ Orbitrap mass spectrometer, where they were ionized applying nano-electrospray ionization, further fragmented in a Top8 method and analyzed in an Orbitrap mass analyzer. The mass spectrometry analysis of all sampled followed an established data-dependent acquisition (DDA) workflow (Table 2). Again, as with the LC-methods, the MS-methods differed for the different samples. Colon tissue samples, as well as cell culture samples were measured once, plasma samples were measured in duplicates.

Table 2 Mass spectrometric parameters used for the analysis of proteins

Parameters	Plasma, CCD-18Co supernatant	Tissue samples, CCD-18Co cytoplasm
Method duration [min]	65	115
MS1 resolution	70,000	70,000
MS1 AGC target	3e6	3e6
MS1 max IT [ms]	100	50
MS1 scan range	400-1400	400-1400
MS2 resolution	17,500	17,500
MS2 AGC target	2e4	2e4
MS2 max IT [ms]	100	100
TopN	8	8
MS2 scan range	200-2000	200-2000
Charge exclusion	unassigned, 1, 5-8, > 8	unassigned, 1, 5-8, > 8
Dynamic exclusion [s]	30	30
Lock mass	445.12003 m/z	445.12003 m/z
Chromatographic peak width [s]	10	15

3.5.5.3. Data analysis

.raw files obtained after mass spectrometric analysis were further processed in MaxQuant [106] version 1.6.3.4 in order to obtain LFQ values. Measurements of similar experiments (same mass spectrometric methods) were processed in the same workflow.

For method optimization of the colon tissue digestion protocol one single workflow was prepared, comparing the Protifi® protocol to all other tested methods. Similar alkylation methods were grouped in one MaxQuant workflow. All colon tissue measurements of tissue samples (30 measurements) obtained from patients suffering from ulcerative colitis were processed in the same workflow. Plasma sample measurements obtained from patients suffering from ulcerative colitis and the control cohort were also analyzed in one single workflow. Cell culture samples were searched according to cellular fractions (two different searches; CYT 1d, CYT 1w and SN 1d, SN 1w). All measurements were searched against a Uniprot derived .fasta file (downloaded on 14.03.2018, 20,316 entries) of human proteins (Taxonomy ID 9606). Variable modifications included in the analyses were oxidation of methionine and acetylation of the protein N-terminus. Fixed modification included in the analysis was either carbamidomethylation of cysteine or propionamide modification of cysteine, depending on the alkylation method applied. Digestion mode was set to specific and "Trypsin/P" set as the digestion enzyme. A maximum of two missed cleavages was accepted. The peptide spectrum match FDR, as well as the protein FDR were set to 0.01. The minimum number of identified peptides was set to two peptides, the minimum number of unique peptides was set to one peptide.

3.5.5.4. Statistical analysis

The proteinGroups.txt files – as well as the peptides.txt file for the method comparison - obtained by the analysis in MaxQuant were used for statistical analyses, using Perseus software [107], version 1.6.5.0. Proteins only identified by site, as well as reverse identifications and potential contaminants were filtered out. All LFQ values were log2 transformed. For the preparation of profile plots from colonic tissue samples, the matrix obtained in this way was used as is. For the preparation of volcano plots, as well as PCA analyses, missing values had to be replaced from normal distribution.

For plasma, as well as colon samples this was done separately for each column. Cell culture samples were grouped according to their replicates and the minimum number of valid values was set to two in at least one group. Using the significantly regulated proteins, defined by the volcano plots prepared using Perseus software, the Cytoscape plugin ClueGO was used to prepare gene ontology (GO term biological process) based network analyses.

3.6. Eicosanoid analysis methods

3.6.1. Sample preparation

Eicosanoid-standard 1:

Reagents	Volume [µL/500 µL]
15-S-HETE-d8	4
12S-HETE-d8	4
5-Oxo-ETE-d7	12
11,12-DiHETrE-d11	4
PGE2-d4	8
2D-HETE-d	4
ACN	464

Eicosanoid-standard 2:

Reagents	Volume [µL/500 µL]
5-S-HETE-d8	4
14,15-DiHETrE-d11	4
8-iso-PGF2alpha-d4	8
ACN	484

200 µL of plasma were used per patient, mixed with 800 µL of ice-cold EtOH and 5 µL of eicosanoid-standard 1 (all standard compounds were purchased from Sanova Pharma GesmbH), then left at 4°C overnight in order to precipitate proteins. The sample was centrifuged at 5,000 rpm for 30 minutes at 4°C. The supernatant was transferred to a 15 mL Falcon tube, concentrated in a vacuum concentrator and

reconstituted in LC-MS grade water to obtain a final volume of 1 mL. All reagents used in the sample processing, as well as all samples were kept on ice. SPE-columns (Strata™ X 33 µm Polymeric Reversed Phase Tubes) were conditioned two times with 1 mL MeOH each, followed by two times 1 mL LC-MS grade water. The sample is loaded in two steps and the Falcon tube was rinsed twice with 1 mL LC-MS grade water each time, the rinsing solutions are loaded onto the SPE columns. Columns are flushed with 1 mL LC-MS grade water and eicosanoids are eluted with 250 µL ice-cold MeOH, 2% FA. The solution was stored at -80°C until processed further.

Before LC-MS analysis samples were dried under a N_2-gas stream and reconstituted in 145 µL 35% eluent B (10% MeOH, 90% ACN, 0.2% FA), with the addition of 5 µL of eicosanoid-standard 2.

3.6.2. LC-MS/MS

3.6.2.1. Liquid chromatography

The sample was transferred to a 200 µL V-shaped glass inlet, placed in a glass vial, the glass vial placed in the autosampler of the UHPLC (Vanquish UHPLC, Thermo Fisher Scientific™) and kept at 4°C. 20 µL of sample were injected and separated on a reversed-phase separation column (Kinetex™ 2.1 mm x 150 mm, 2.6 µm C_{18}, 100 Å) equipped with a Viper Inline Filter (Thermo Fisher Scientific™, article nr.: 6036.1045). The flow rate was set to 200 µL/min and a 20-minute method, with a gradient elution profile was executed. Eluent A consisted of 99.8% LC-MS grade water with 0.2% FA and eluent B of 89.8% ACN, 10% MeOH and 0.2% FA). The elution was performed as follows: 0-1 min 35% eluent B, 1-10 min 35-90% B, 10-10.5 min 90-99% B, 10.5-15.5 min 99% B, 15.5-16 min 99-35% B, followed by equilibration at 35% B from 16-20 min.

3.6.2.2. Mass spectrometry

Following the LC-separation, the analytes were transferred to a Q Exactive™ HF Hybrid Quadrupole Orbitrap™ mass spectrometer (Thermo Fisher Scientific™) via electrospray ionization using an ESI-source, operating in negative ionization mode (Table 3). All samples were measured in duplicates.

Table 3 Mass spectrometric parameters used for the analysis of eicosanoids

Parameters	Eicosanoids
Method duration [min]	20
MS1 resolution	60,000
MS1 AGC target	3e6
MS1 max IT [ms]	50
MS1 scan range	250-700 m/z
MS2 resolution	15,000
MS2 AGC target	2e4
MS2 max IT [ms]	250
TopN	2
Charge exclusion	unassigned, 2-8, > 8
Dynamic exclusion [s]	2
Chromatographic peak width [s]	3

3.6.3. Data analysis

Measurements were searched against a manually curated compound database of 223 compounds, using TraceFinder™ Software (Thermo Fisher Scientific™) version 4.1, using retention times and m/z values for identification. A mass shift of up to 7 ppm, as well as a retention time shift of up to 7 seconds was accepted for identification. For the detection of compounds, ICIS detection algorithm was used, the peak threshold was set to 1e4. Peaks were integrated, manually checked and reintegrated if necessary.

3.6.4. Statistical analysis

AUC values were further normalized, using the mean of the AUC values of the eicosanoid standard compounds. The average of the duplicates was calculated,

compounds without clear identification were removed, as well as compounds with less than 3 valid values for the 3 controls (except for 13-HpODE) after average calculation. A PCA was prepared using Perseus software, version 1.6.5.0 – for that purpose, values were log2 transformed and missing values replaced from normal distribution. In GraphPad Prism 8, the original, normalized AUC values were tested for normal distribution (Shapiro-Wilk-test) and unpaired t-tests of normally distributed values were performed, p-values below 0.05 were considered significant.

4. Results and Discussion

4.1. Digestion protocol optimization

4.1.1. Assessment of tissue protein intactness

Before testing the different digestion protocols, it was necessary to assess the intactness of the tissue samples used for the optimization, as the tissue samples used for the analysis had been stored for longer periods of time. Colon tissue protein intactness was evaluated through SDS-PAGE analysis of both tissue specimen (Figure 11).

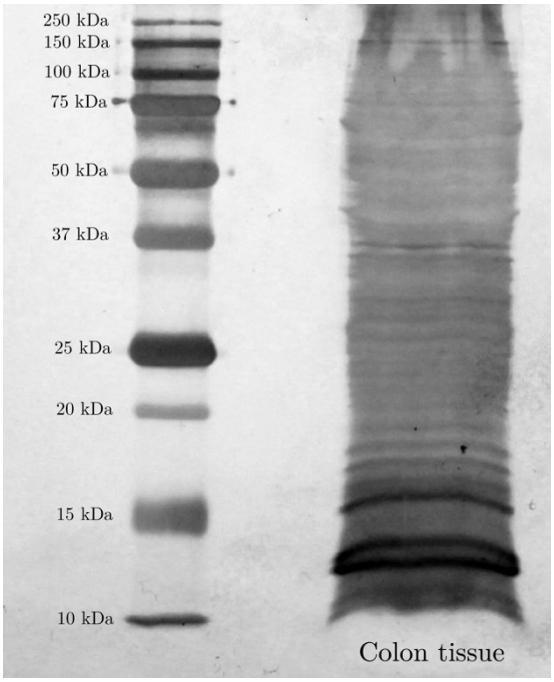

Figure 11 SDS-PAGE for the assessment of tissue intactness

SDS-PAGE preparation and analysis of colon tissue proteins showed that the proteins contained in the tissue could be considered intact. Therefore, the colon tissue was used for method evaluation.

4.1.2. Colon – protein digestion protocol evaluation

For the comparison of different lysis conditions, as well as reduction and alkylation methods, the number of identified peptides was considered to be the most relevant parameter. All replicates (two for the Protifi® protocol and three for the Microcon® protocols) were grouped in Perseus and all peptides with less than three values for each condition were excluded. Generally, the Protifi® protocol yielded in the most identified peptides (16,477) followed by the Microcon® protocol using the lysis buffer containing 5% SDC, as well as urea and TEAB, TCEP as the reduction agent and AA for the alkylation (Figure 12). AA as an alkylation method typically yielded in more peptide identifications than IAA when applying the Microcon® protocol. As the Protifi® protocol showed the best results and required overall less time for sample preparation, this method was used for the analysis of patient colon tissue specimen, patient plasma samples and cell culture samples.

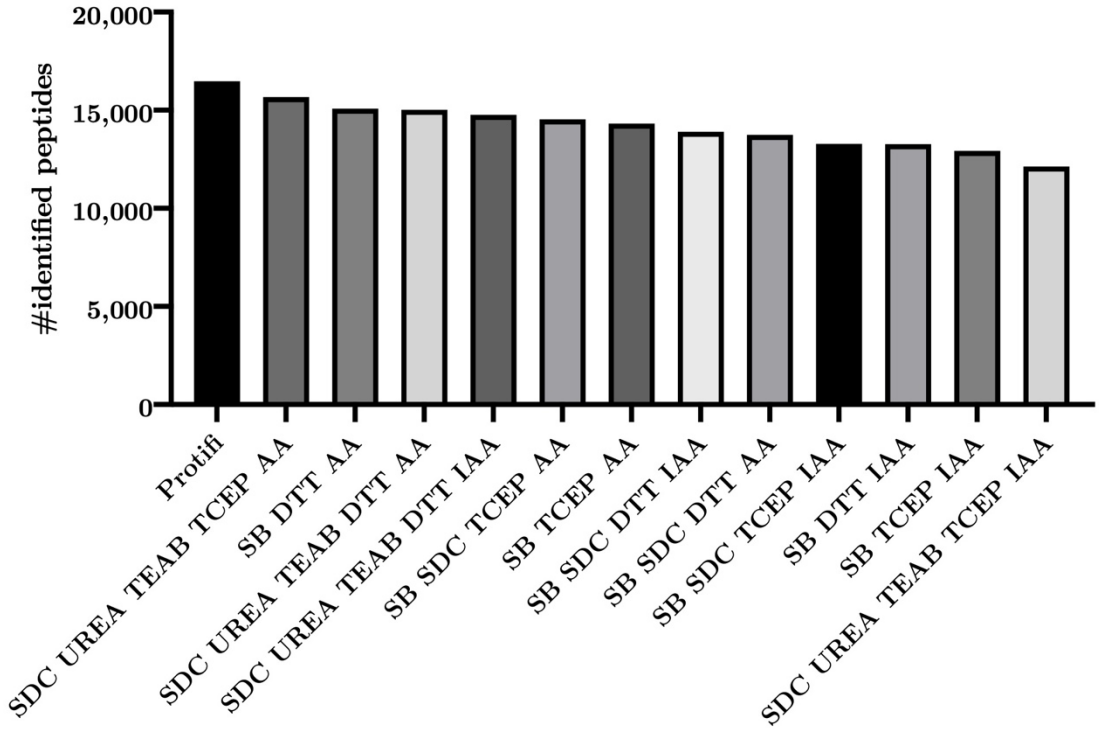

Figure 12 Method comparison results showing the numbers of identified peptides for each digestion protocol

4.2. Ulcerative colitis patient data and heterogeneity

Patient data, as assessed by clinicians at the hospital Rudolfstiftung, showed high variability in the patients' symptoms, as well as patient data itself (Table 4). Mayo-scores were varying among the patients, as were CRP levels. Unfortunately, not all fecal calprotectin levels were assessed in close timely proximity to the determination of CRP levels and Mayo-scores. Therefore, only calprotectin levels determined in timeframe of ± 10 days were found to correlate with Mayo-scores and CRP blood levels. Calprotectin levels are listed in the supplementary information. Included in the study were patients number 0, 1, 3, 4, 6 and 7, the other patients had to be excluded due to either suffering from pancolitis or showing no visible signs of inflammation during colonoscopy. Areas of most severe inflammation were assessed during colonoscopy, as well as during histo-pathological evaluation of excised biopsy-specimen. Patients number 4, 1 and 0 showed the most severe signs of inflammation, whereas patients number 6 and 7 only showed signs of inflammation in the rectum. Patient number 3 showed only minor inflammation in the rectum during colonoscopy, however, upon histo-pathological evaluation signs of inflammation were also detected in the other colonic areas.

Table 4 Patient data sorted by highest Mayo-score, areas of most severe inflammation are highlighted in orange

					inflamed areas					
Patient nr.	**Gender**	**Age [years]**	**Disease duration [years]**	**Mayo-score**	**Rec**	**Sig**	**Desc**	**Trans**	**Asc**	**CRP [mg/L]**
4	f	43	1	10	x	x	x			63.2
1	f	48	18	9	x	x	x			8.9
0	m	39	23	5	x	x	x	(x)		4.9
7	f	56	30	5	x					0.3
3	f	28	15	4	x	x	x	x	x	1.2
6	m	37	12	4	x					1

The histo-pathological evaluation of patients showed varying degrees of crypt architectural distortions, including branching, as well as elongation of crypts depending on inflammation severity. A decrease in goblet cell count, as well as the invasion of neutrophils into the crypts was noted during active inflammation. Invasion of lymphocytes was seen in some patients, indicating a chronic disease course. Areas of dense inflammatory cell population were seen in some patients, as well as the presence of high numbers of eosinophils in patients being treated with anti-TNF-α therapies. A more detailed description of the histo-pathological findings is included in the supplementary material. Some exemplary photos of the histo-pathological evaluation of the colonic biopsies are shown in Figure 13. Figure 13A, a cross section of the crypts of the colon sigmoideum of patient 0, shows areas of higher density of inflammatory cells (upper arrow), as well as some distorted crypts and minimal invasion of neutrophils into the crypts (lower arrow), as well as some reduction in goblet cell count. Figure 13B, a cross section of colonic crypts of the rectum in patient 1 shows elongated crypts, as well as crypt abscesses (arrow), a high density of inflammatory cells in the lamina propria and a decrease in goblet cell count. Figure 13C shows a cross section of crypts in the colon descendens of patient 1. The crypts are severely distorted, crypt-invading neutrophils, as well as lymphocytes can be seen and crypt abscesses are present in many of the depicted crypts. Goblet cell count is drastically decreased and the cell population surrounding the crypts in the lamina propria is very dense. Figure 13D shows a cross section of the crypts in the colon sigmoideum of patient 3. Generally, many of the crypts shown in the photo have a normal, round architecture, some of them are branched. In the right corner of the photo, some neutrophils invading the crypts can be seen, in the center of the photo, there is a spot of high inflammatory cell density including eosinophils in red. The goblet cell count appears to be normal in most of the crypts in the photo.

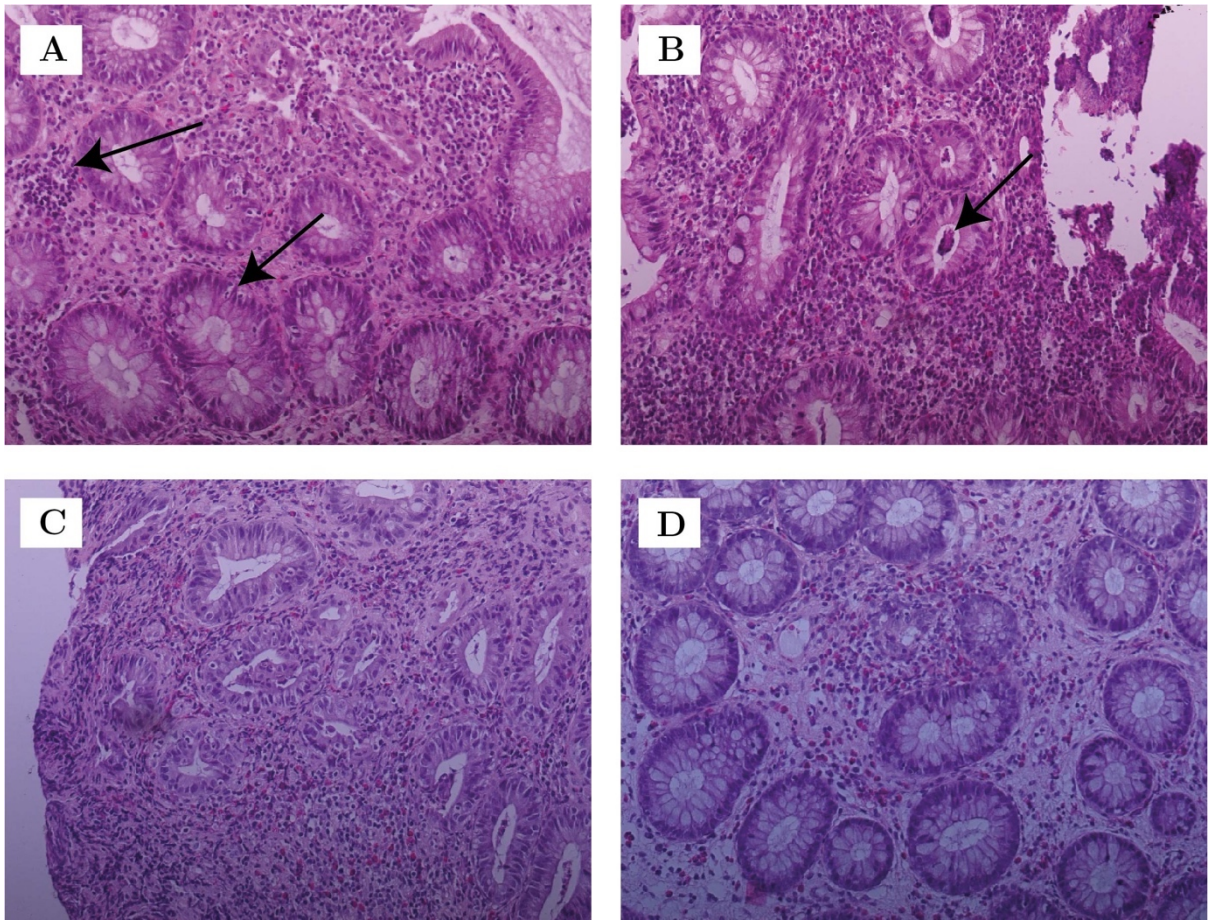

Figure 13 H&E stained cross sections of colonic crypts showing signs of acute inflammation; **A**: Patient 0, colon sigmoideum; **B**: Patient 1, rectum; **C**: Patient 1, colon descendens; **D**: Patient 3, colon sigmoideum

4.3. Proteomic analysis of UC patient colonic biopsies

Overall, the patient heterogeneity observed in the patient data, is also reflected in the proteome profiles of the different colonic regions analyzed as part of this project. Proteomic analysis of colonic biopsies yielded in a total number of 4,533 identified proteins. A PCA of all analyzed colonic biopsy samples (Figure 14) shows a separation of the samples by the respective degree of inflammation (component 1) and a separation of samples according to the patients themselves (component 2). Areas of most severe inflammation are to be found on the far right, whereas non-inflamed areas are concentrated on the left side.

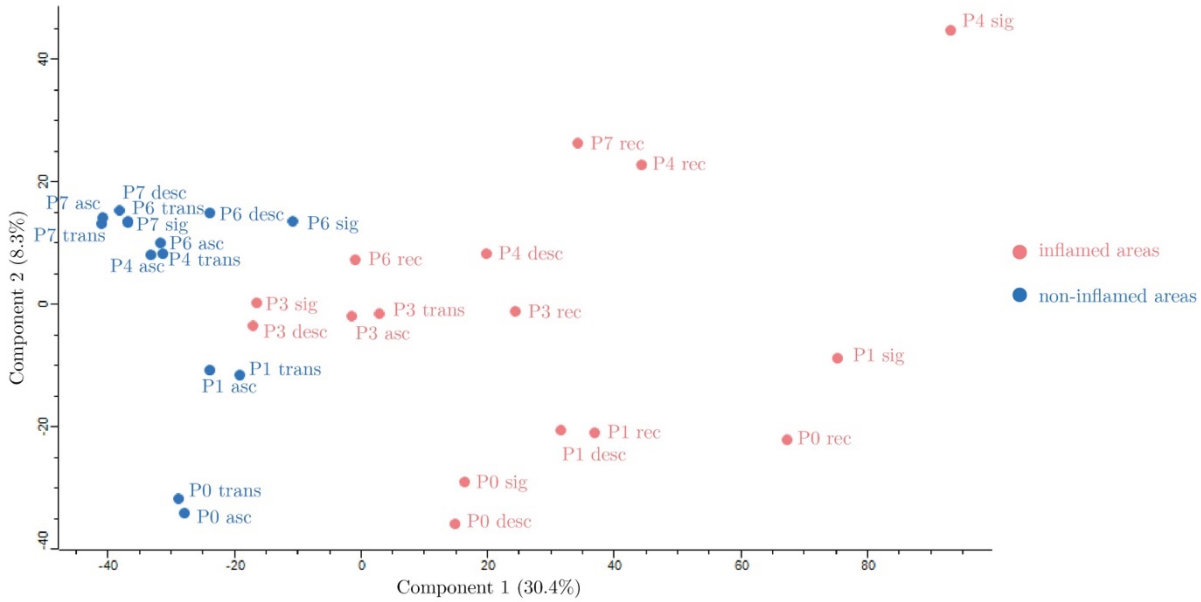

Figure 14 Principal component analysis of proteomic analysis of colonic biopsy samples

Generally, the analysis of inflamed and non-inflamed areas showed a severe reduction of membrane integrity, as well as barrier function in more severely inflamed areas. A reorganization of the extracellular matrix, as well as neutrophil invasion into the lamina propria was noticeable and correlating with the degree of inflammation. The H_2S metabolism was also found to be impaired in areas of more severe inflammation.

4.3.1. General alterations in the proteome profile during inflammation

In order to assess impaired processes between inflamed and non-inflamed areas, the least inflamed areas of all patients (colon ascendens) were compared to the most inflamed areas (rectum or colon sigmoideum) (Figure 15). Downregulated proteins (Figure 16) were mostly involved in different metabolic processes, as well as biological oxidations and degradation of cysteine and homocysteine. Upregulated proteins (Figure 17) were involved in neutrophil degranulation, extracellular matrix organization, integrin cell surface interactions, antimicrobial and other processes.

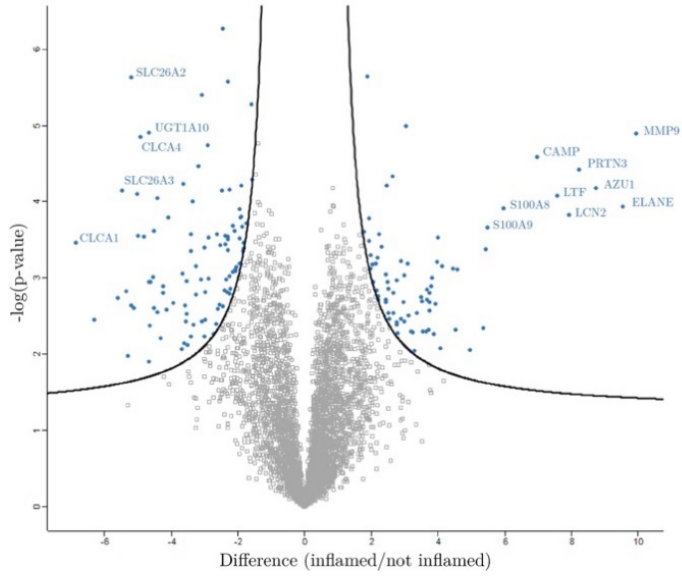

Figure 15 Volcano plot showing alterations in relative protein abundance between inflamed and non-inflamed colonic areas; FDR=0.01, S0=0.5

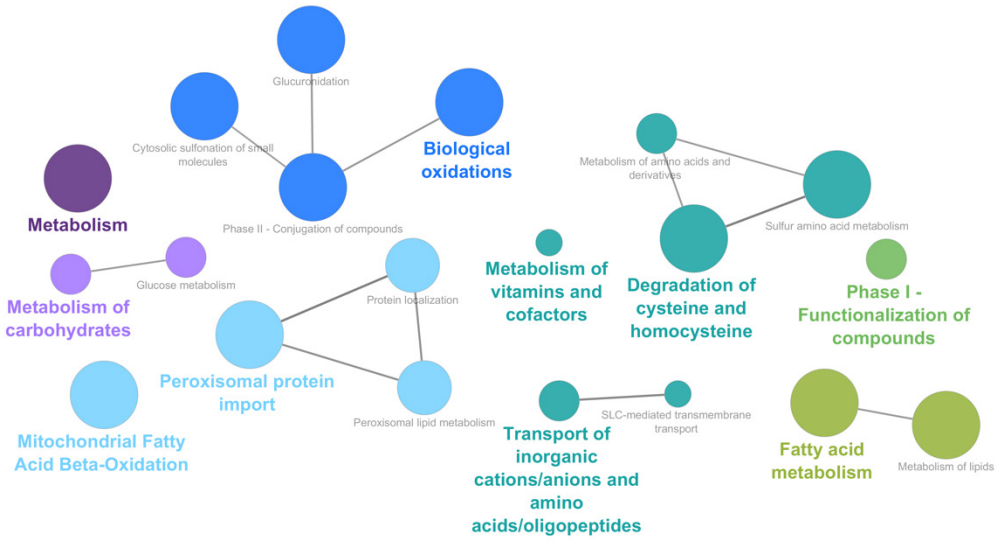

Figure 16 Biological processes downregulated during UC induced inflammation

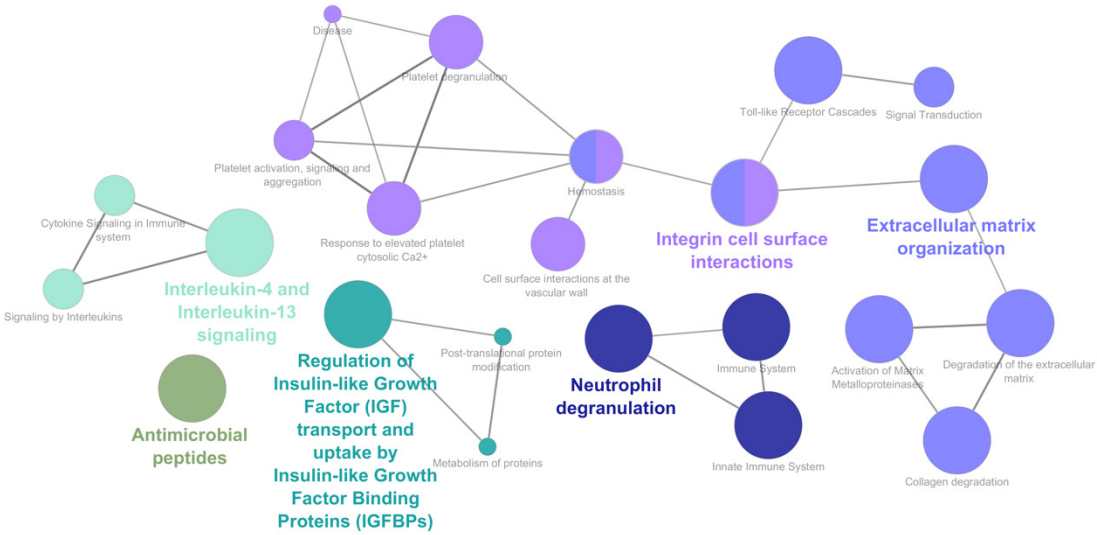

Figure 17 Biological processes upregulated during UC induced inflammation

4.3.2. Membrane integrity

The epithelial layer of the crypt region is usually held together by different connecting proteins, such as tight junction proteins, adherens junction proteins, desmosomes and integrins, which ensures the integrity of the membrane (Figure 18). Disturbances in the structure and integrity of the intestinal epithelium has been reported to occur in ulcerative colitis and has detrimental consequences for the intestinal health [108]. A disturbed membrane structure makes the lamina propria more accessible for bacteria and bacterial products and leads to an increased immune response.

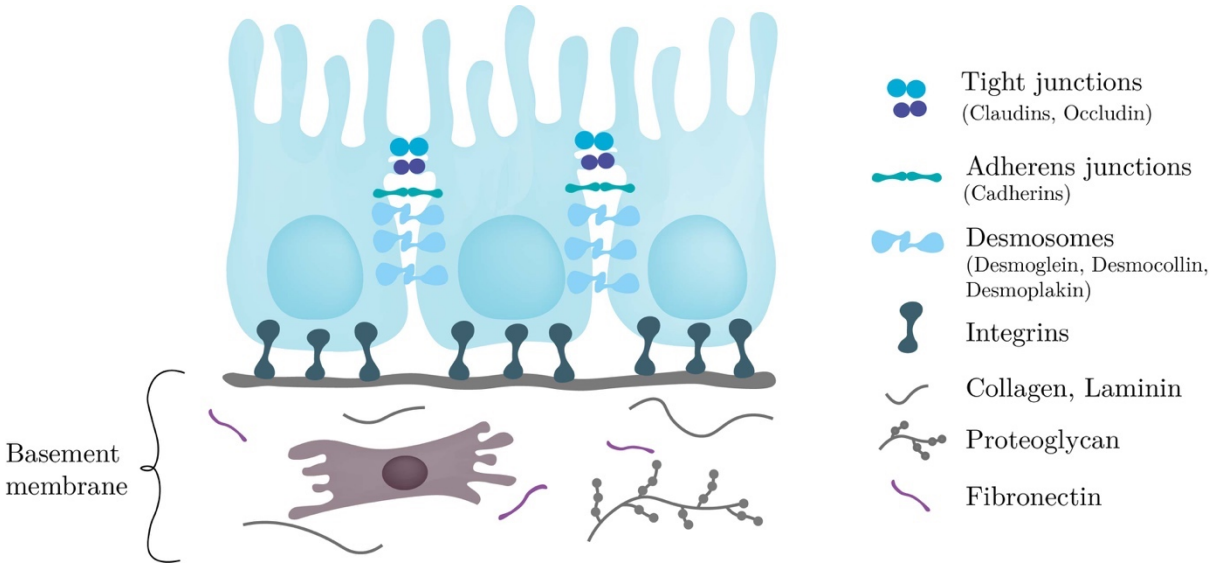

Figure 18 Structure and components of the intestinal epithelial layer

The proteomic analysis of the different inflamed and non-inflamed colonic regions showed that a reduction in proteins important for the epithelial integrity occurs during inflammation. A correlation between degree of inflammation and decrease in abundance of claudins (CLDN3, CLDN7), cadherins (CDH1, CDH17), desmosome proteins (DSG2, DSC2), as well as integrins (ITGA6, ITGB4) was noticeable (Figure 19).

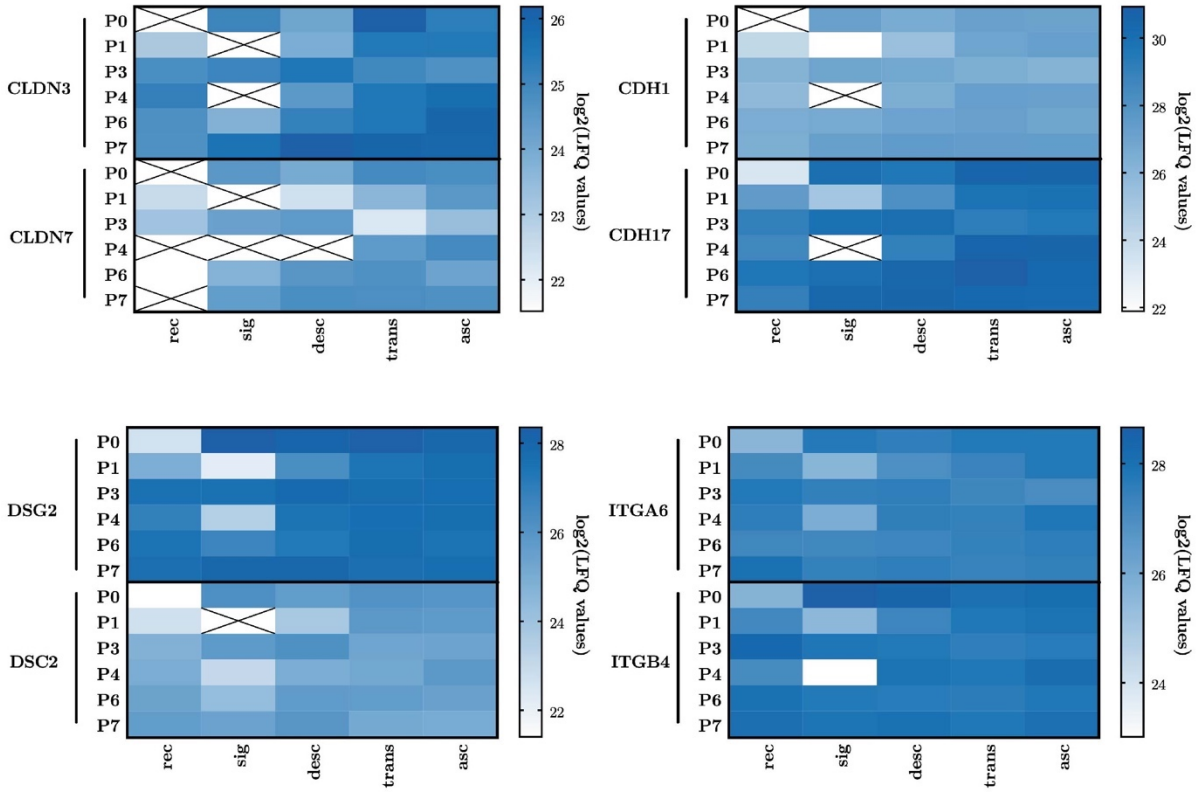

Figure 19 Heatmaps showing the relative abundance of proteins involved in the epithelial membrane integrity during inflammation

4.3.3. Extracellular matrix reorganization

Proteins indicative of the degradation of extracellular matrix (Figure 20) were found to be upregulated during inflammation (Figure 21). These proteins are commonly secreted by neutrophils, they are able to cleave collagens and thereby facilitate neutrophil migration [109, 110].

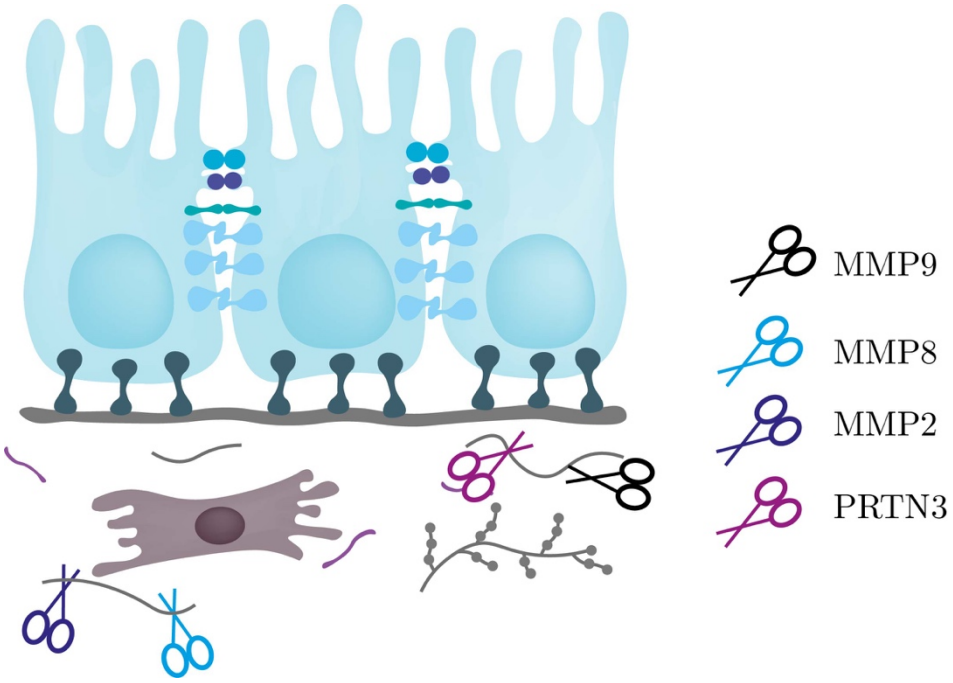

Figure 20 Role of matrix metalloproteinases in the degradation of the extracellular matrix

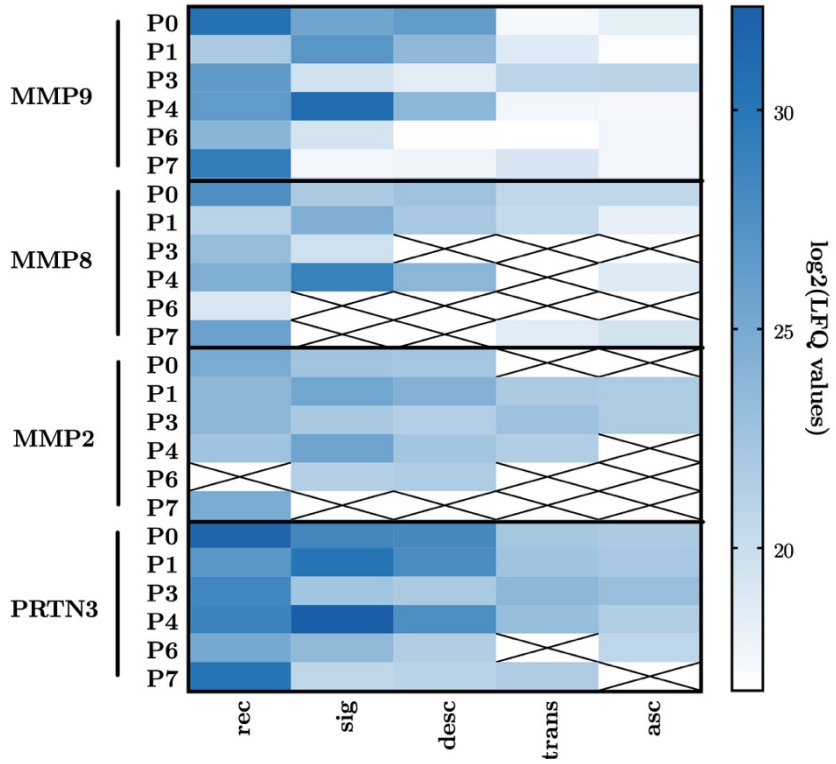

Figure 21 Heatmap showing the relative abundance of proteins involved in the degradation of the extracellular matrix during inflammation

4.3.4. Intestinal barrier

The analysis of proteins involved in the protection of the intestinal epithelium (Figure 22) showed an increase in the abundance of antimicrobial peptides and proteins (LYZ, CAMP) during inflammation (Figure 23). Proteins involved in the formation and the stability of the intestinal barrier [111] and mucus layers derived from goblet cells were decreased in an inflammation correlating manner. The decrease in goblet cells as observed during histo-pathological evaluation of colonic biopsy specimen is, therefore, also reflected in the proteome of biopsies. The presence of cathelicidin (CAMP), a protein commonly secreted by Paneth cells only in inflamed areas might be an indicator of Paneth cell metaplasia, occurring during CU induced inflammation.

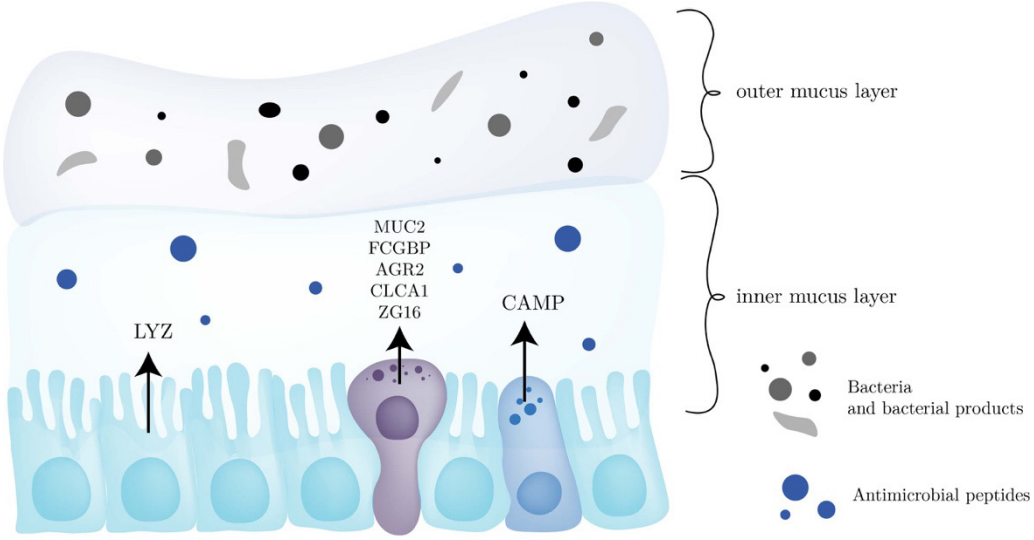

Figure 22 Intestinal barrier and protein secretion by epithelial cells, goblet cells and Paneth cells

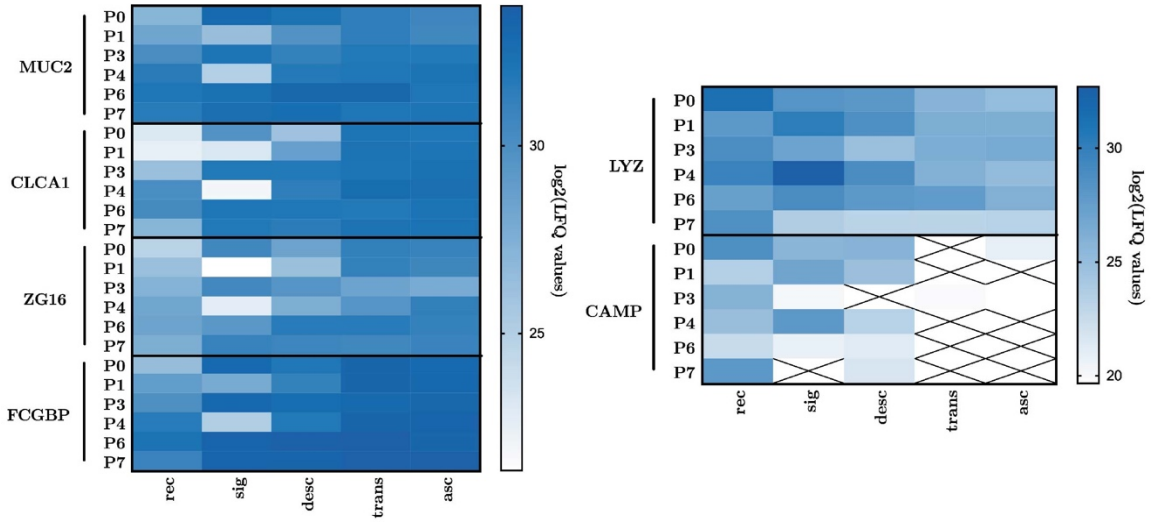

Figure 23 Heatmaps showing the relative abundance of goblet cell derived proteins (left) and antimicrobial proteins/peptides (right)

4.3.5. Neutrophil extravasation

An increased abundance of neutrophil derived proteins was detected in areas of more severe inflammation, in accordance with results of the histo-pathological evaluations (Figure 25). The invasion of neutrophils into the lamina propria and crypts (cryptitis) (Figure 24), as well as the formation of crypt abscesses is a key feature of the phenotype of ulcerative colitis.

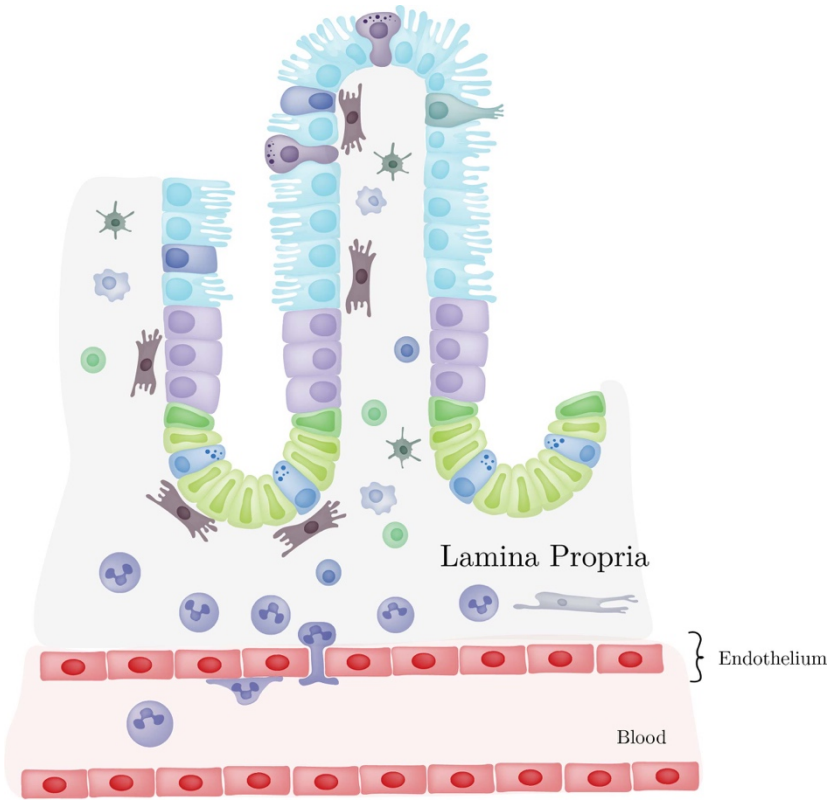

Figure 24 Schematic of the process of neutrophil extravasation

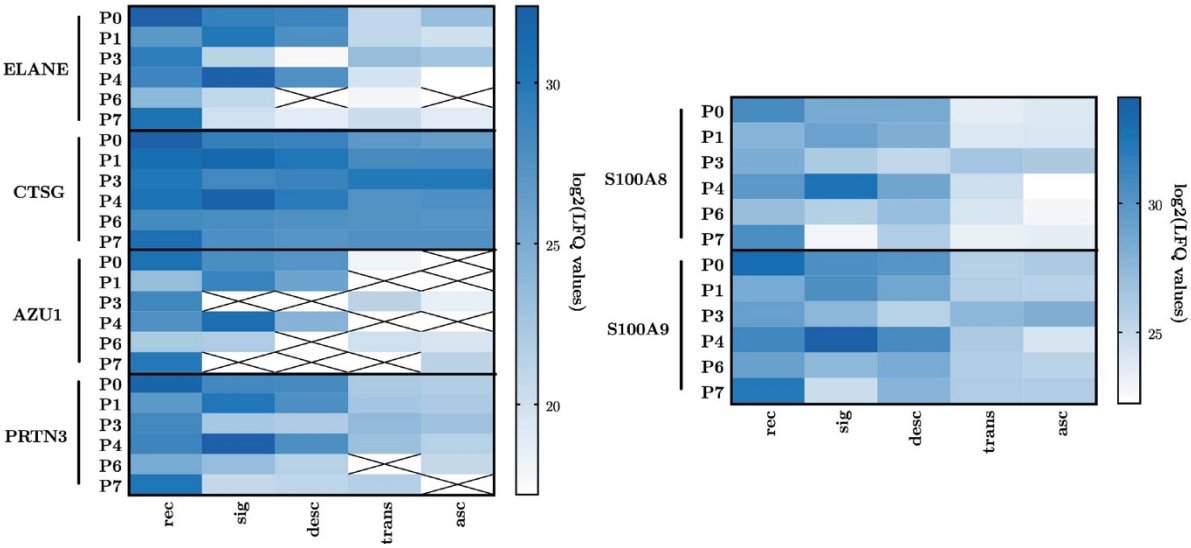

Figure 25 Heatmaps showing the relative abundance of neutrophil-derived proteins in inflamed and non-inflamed areas

4.3.6. H_2S metabolism

The relative abundance of proteins involved in the mitochondrial metabolism of H_2S (Figure 26), a major bacterial product, was found to be slightly decreased in areas of higher-grade inflammation (Figure 27). As mentioned before, an accumulation and decreased ability to detoxify H_2S can have detrimental effects on the intestinal health and the mucus barrier. MPST, a protein involved in the formation of H_2S was also found to be downregulated in cases of more severe inflammation, showing that the H_2S metabolism seems to be overall dysregulated in active UC.

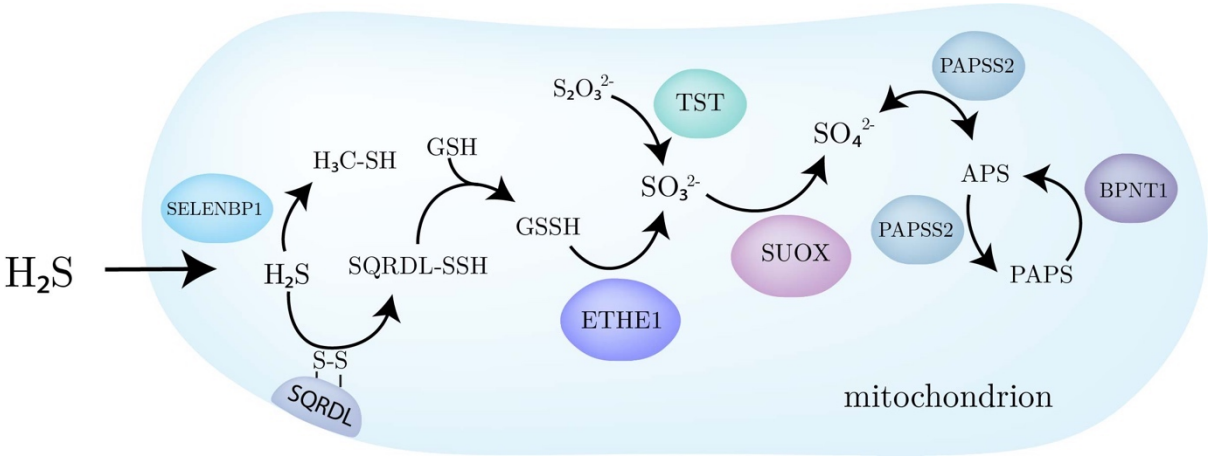

Figure 26 Schematic of the mitochondrial H_2S metabolism

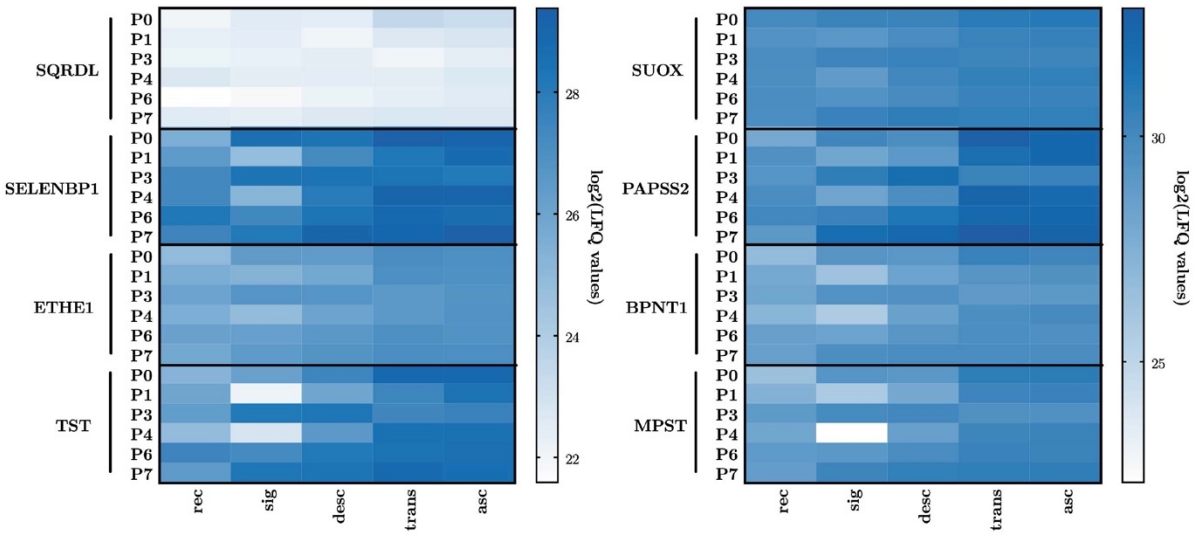

Figure 27 Heatmaps showing relative abundances of proteins involved in the H_2S metabolism

4.3.7. Myofibroblast proteins

Proteins found to be prominently secreted by CCD-18Co cells were also present in the different colonic regions of patients suffering from acute UC induced inflammation. The levels of VIM, FN1 and LAMB2 were slightly elevated in regions of more severe inflammation, indicative of higher presence of myofibroblasts/fibroblasts during acute inflammation (Figure 28).

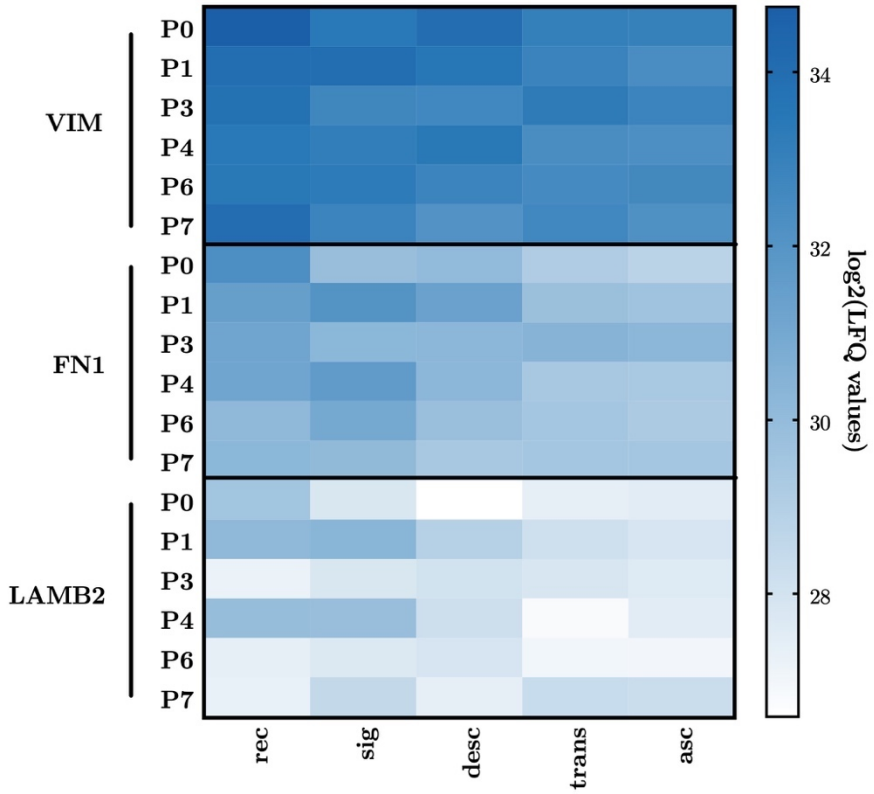

Figure 28 Heatmap showing the relative abundance of myofibroblast-/fibroblast-derived proteins in inflamed and non-inflamed regions

4.4. Proteomic analysis of UC patient plasma samples

Generally, a high degree of heterogeneity was observable during the analysis of plasma samples from patients. A PCA analysis of the 304 identified proteins showed no separation of patient and control cohort when considering only the first and second component of the PCA (Figure 29). Separation of the two sample cohorts was only obtained when plotting the first and third component of the PCA (Figure 30). The preparation of Volcano plots taking into account all patient samples did not reveal any significant differences when comparing patients and healthy controls. Therefore, in order to find proteins indicative of the disease patient 4 – showing the most severe symptoms and signs of inflammation – was analyzed in more detail (Figure 31).

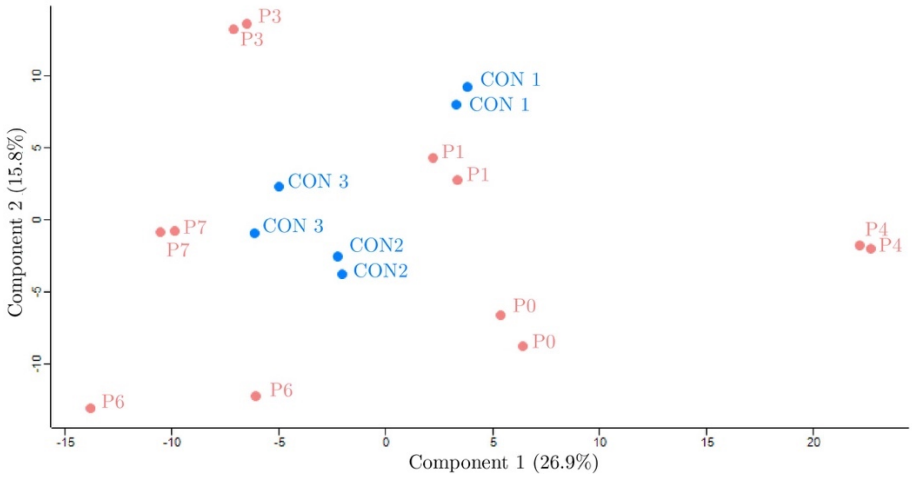

Figure 29 Principal component analysis of CU patient and control plasma samples - component 1 and 2

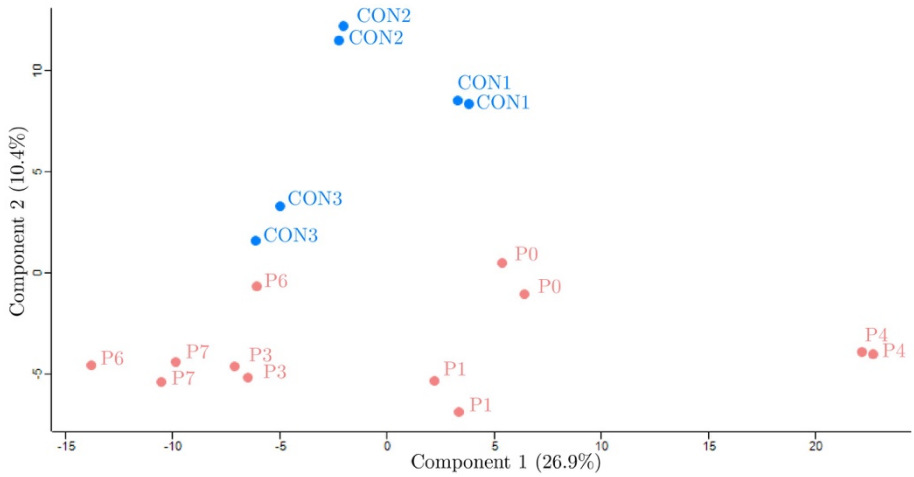

Figure 30 Principal component analysis of patient and control plasma samples - component 1 and 3

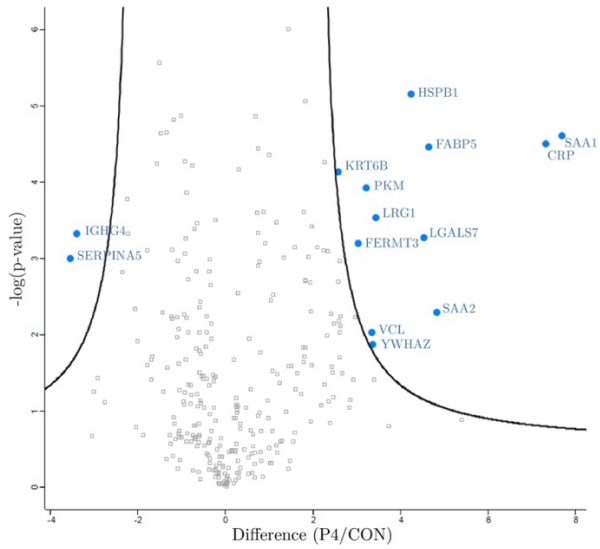

Figure 31 Volcano plot showing differentially regulated proteins between plasma of P4 and control samples; FDR=0.01, S0=2

Downregulated proteins included SERPINA5 and IGHG4. **SERPINA5** was not identified in the plasma samples of patient 3 and 4. The plasma levels of the other patients appeared to be normal. **IGHG4** was decreased in all patients, except for patients 6 and 7 who exhibited the least severe symptoms of all patients. **KRT6B** was increased in all patients, except for patient 7. **FERMT3** (kindlin-3) levels were elevated only in patient 4. Kindlin-3 is involved in the regulation of integrin function and as it has been shown that in mice, higher levels of kindlin-3 are required during stress situations, as well as infections and injuries for proper integrin functions in platelets and neutrophils [112]. The elevation of kindlin-3 might, therefore, be an indicator of increased injury and stress response in patient 4 due to the severe inflammation in the colon. **PKM** levels were only elevated in patient 4. This protein has, however, been suggested to be used as a new biomarker for IBD [113]. **VCL** was only found to be increased in patient 4; the protein has been proposed to be involved in neutrophil adhesion processes [114]. **YWHAZ** levels were elevated only in patient 4, the protein was not detected in patient 6 and 7. The protein YWHAZ is part of the 14-3-3 protein family, a group of proteins, which interact with phosphosites and regulate various cellular functions, such as apoptosis, cell motility, cell cycle

progression, autophagy and others. The response of 14-3-3 proteins is stress-associated.[115] **LRG1** levels were the highest in patient 4 and also found to be slightly elevated in the most severely inflamed colonic regions. LRG1 has been reported to be expressed by neutrophils and has also been proposed as a new biomarker for ulcerative colitis activity[116]. **HSPB1** – a protein involved in the cellular protection against oxidative stress [117] – abundance was the highest in patient 4 and patient 0. **LGALS7** was only identified in patient 4, the expression of the protein was highly heterogeneous in the colon biopsy specimen without any apparent correlation between the different regulation levels. **FABP5** was found to be elevated only in patient 4. Abundance levels of FABP5 are decreasing from the proximal to distal colonic regions. FABP5 has been associated with anti-inflammatory effects [118]. **SAA1** and **SAA2** are proteins associated with the acute phase response to inflammatory disturbances which activate cells of the adaptive and innate immune system [119]. SAA1 levels correlate with the inflammation severity in patients with the highest abundance levels to be detected in patients 0, 1 and 4. **CRP** is another acute phase protein and probably the most commonly known marker for inflammation in patients with IBD or any other inflammatory disease. CRP levels are the highest in patient 4, followed by patient 1 and then patient 0. The protein was not detected in patient 3, 6 or 7 (Table 5).

Table 5 List of differentially regulated proteins between P4 and control cohort

Gene names	p-value	Difference	Protein names
SERPINA5	$1{,}00*10^{-3}$	-3.55	Plasma serine protease inhibitor
IGHG4	$0{,}47*10^{-3}$	-3.40	Ig gamma-4 chain C region
KRT6B	$0{,}07*10^{-3}$	2.58	Keratin, type II cytoskeletal 6B
FERMT3	$0{,}64*10^{-3}$	3.03	Fermitin family homolog 3
PKM	$0{,}12*10^{-3}$	3.22	Pyruvate kinase PKM
VCL	$9{,}30*10^{-3}$	3.34	Vinculin
YWHAZ	$13{,}49*10^{-3}$	3.36	14-3-3 protein zeta/delta
LRG1	$0{,}29*10^{-3}$	3.44	Leucine-rich alpha-2-glycoprotein
HSPB1	$0{,}01*10^{-3}$	4.25	Heat shock protein beta-1
LGALS7	$0{,}54*10^{-3}$	4.53	Galectin-7
FABP5	$0{,}03*10^{-3}$	4.64	Fatty acid-binding protein, epidermal
SAA2	$5{,}08*10^{-3}$	4.82	Serum amyloid A-2 protein
CRP	$0{,}03*10^{-3}$	7.32	C-reactive protein
SAA1	$0{,}02*10^{-3}$	7.70	Serum amyloid A-1 protein

4.5. Eicosanoid analysis of patient plasma samples

Eicosanoid analysis of plasma samples yielded a total of 22 eicosanoids which were identified in at least all 3 controls (except for 13-HpODE, which was still included to indicate the regulation differences between control and patient samples). Three of the identified eicosanoids showed significant differences in their abundance (eicosanoids which were not significantly differentially regulated, as well as the corresponding QQ plots, are depicted in the supplementary information). Shapiro-Wilk-tests were performed to test for normal distribution, even though normal distribution might not occur in this data set as the inflammation severity distribution might not equal a normal distribution. The PCA analysis showed a separation between control and patient samples, however, no separation according to disease severity could be achieved (Figure 32).

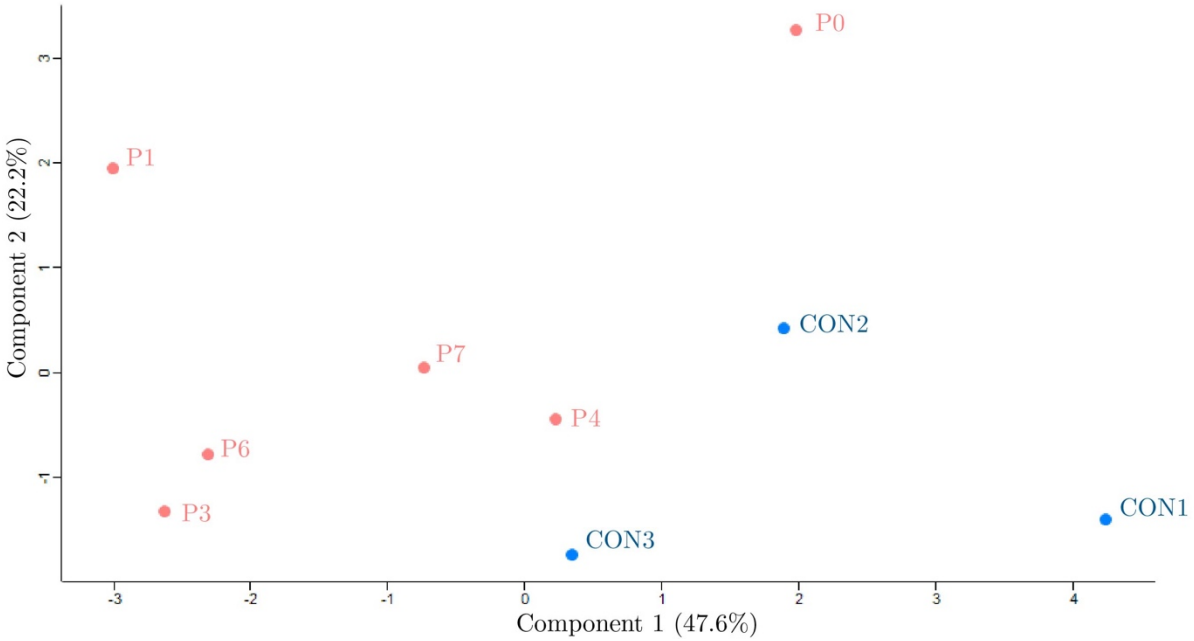

Figure 32 Principal component analysis of eicosanoids in patient and control plasma samples

The three eicosanoids of differential abundance were 13-HpODE, 20-HDoHE and DHA (Figure 33). **13-HpODE** (13-hydroperoxyoctadecadienoic acid) is a pro-inflammatory eicosanoid, reported to be involved in different inflammatory diseases [120]. **DHA** (docosahexaenoic acid), as well as other omega-3 polyunsaturated fatty acids have

been proposed to show anti-inflammatory activity and are considered to be used as a treatment for IBD [121].

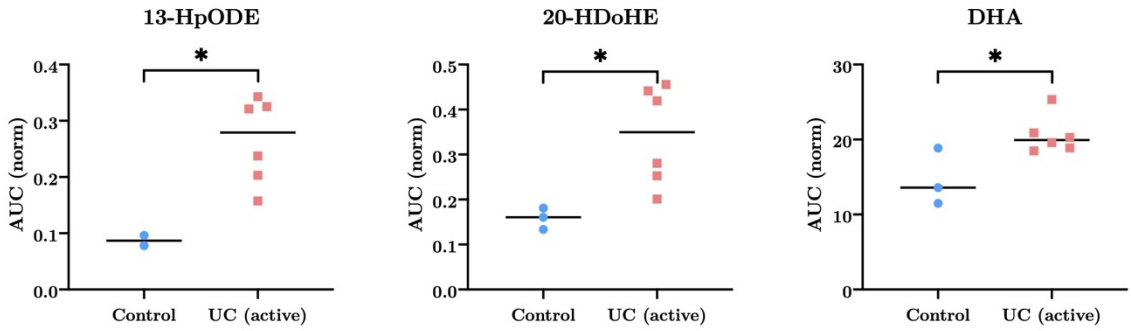

Figure 33 Significantly regulated eicosanoids between patient and control plasma samples; eicosanoids labelled with " * " showed significant differences in their abundance (p-value<0.05)

4.6. Proteomic analysis of differentially stimulated CCD-18Co cells

4.6.1. CCD-18Co general protein expression

In total, 3,735 proteins were identified in the cytoplasmic and 1,170 in the supernatant fractions. All CCD-18Co replicates expressed a more-or-less typical myofibroblast proteome profile, including the expression of paxillin in all cytoplasmic replicates and tenascin in all replicates. Alpha-smooth muscle actin – a marker for myofibroblasts - was not present in any cytoplasmic fractions, however, previous studies have shown that the expression of alpha-smooth muscle actin is dependent on the dose and duration of TGF-β treatment. To induce alpha-smooth muscle actin expression, Simmons *et al.* [122] treated CCD-18Co cells with 1 ng/mL cell culture medium for 7 days, including medium change every 24 h. In our case, treatment was only performed once, including one medium change without the addition of TGF-β in the exchanged medium. Myofibroblast markers also include vinculin, paxillin and tensin [123]. Vincullin was not identified in any of the cell fractions analyzed, whereas paxillin was present in all cytoplasmic fractions. Tensin was identified in all cytoplasmic fractions one week after treatment. All fractions showed the expression of different collagens, notable differences were observed with COL11A1, which was secreted in all cells one day after treatment, one week after treatment, however, only by one of the TGF-β treated replicates. COL6A2 was only secreted by TGF-β treated cells one day post treatment. One week post treatment it was expressed by all replicates. Vimentin, fibronectin and laminin subunit beta-2 were expressed and secreted by all replicates (Figure 34). The classification of CCD-18Co cells and the determination whether these cells are fibroblasts or myofibroblasts is difficult, as these cells possess fibroblast and myofibroblast-like properties and their proteome profiles are a mixture of fibroblast and myofibroblast profiles. In research, CCD-18Co cells are used as a myofibroblast and fibroblast cell line, depending on the research question.

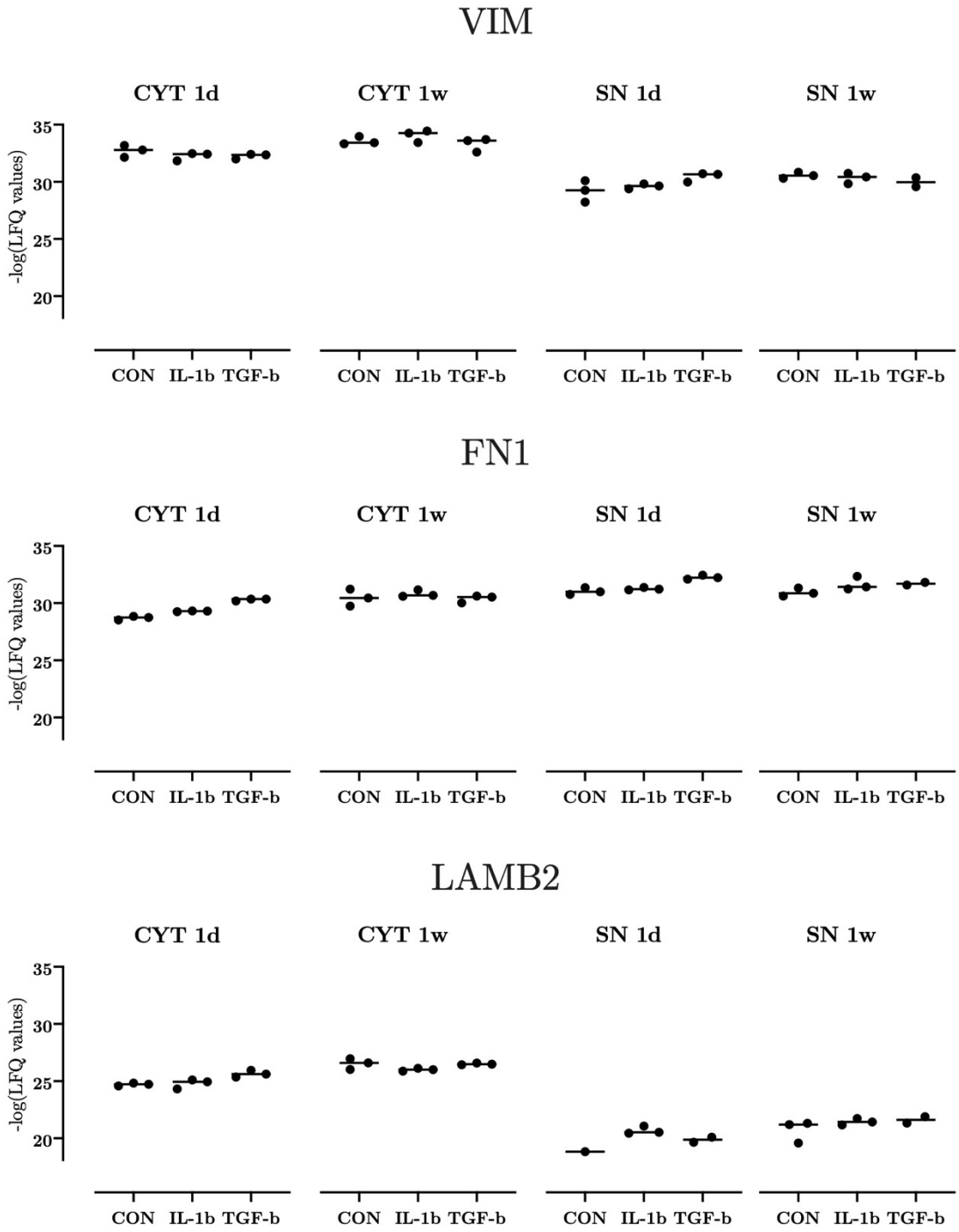

Figure 34 Protein expression of vimentin, fibronectin and laminin subunit beta-2 in CCD-18Co cells

4.6.2. CCD-18Co proteome changes upon stimulation with IL-1β and TGF-β

4.6.2.1. CCD-18Co cytoplasmic changes

Overall, only minor alterations in the cytoplasmic fractions upon treatment could be observed one day, as well as one week after treatment, respectively (Figure 36). The only significantly regulated protein to be identified during the analysis is S100A7 in the cytoplasmic fraction one day after TGF-β treatment. S100A7 was identified in all cytoplasmic fractions obtained one day after treatment, with the highest abundance levels present in the control samples. One week post treatment S100A7 levels were comparable among the different treatment conditions, while still being slightly higher in the control samples and one of the TGF-β treated samples (Figure 35). Overall, the expression of S100A7 is fluctuating and highly individual even in between the replicates. S100A7 could also be identified in all of the supernatant fractions. S100A7 – also known as Psoriasin - is a member of the S100 proteins, which are a group of calcium binding signaling proteins. Psoriasin is reported to be involved in wound healing, possessing antibacterial properties [124]. S100A7 levels have been reported to be elevated during inflammatory diseases, also in the case of IBD [125]. Our data show that S100A7 derived from fibroblasts/myofibroblasts is slightly downregulated in an inflammatory environment, showing that these cells might not contribute to elevated S100A7 levels in IBD.

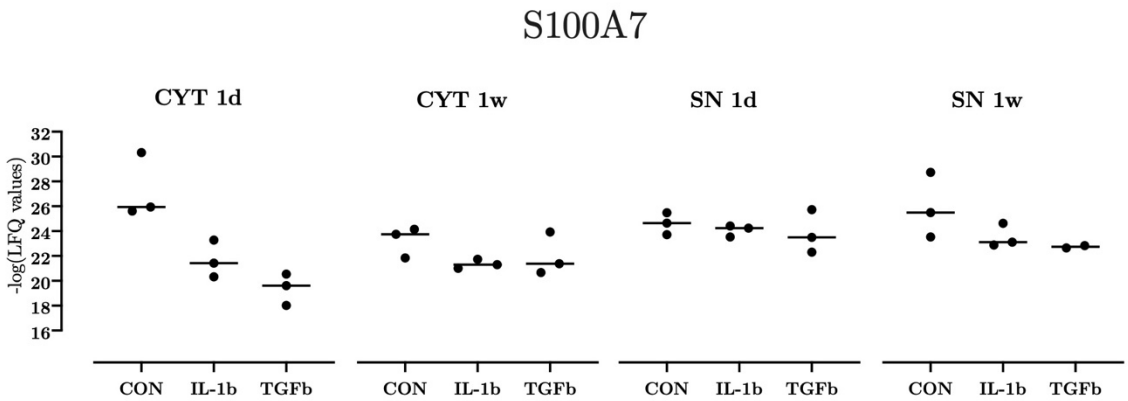

Figure 35 S100A7 abundance comparison in the different cellular fractions and treatment conditions

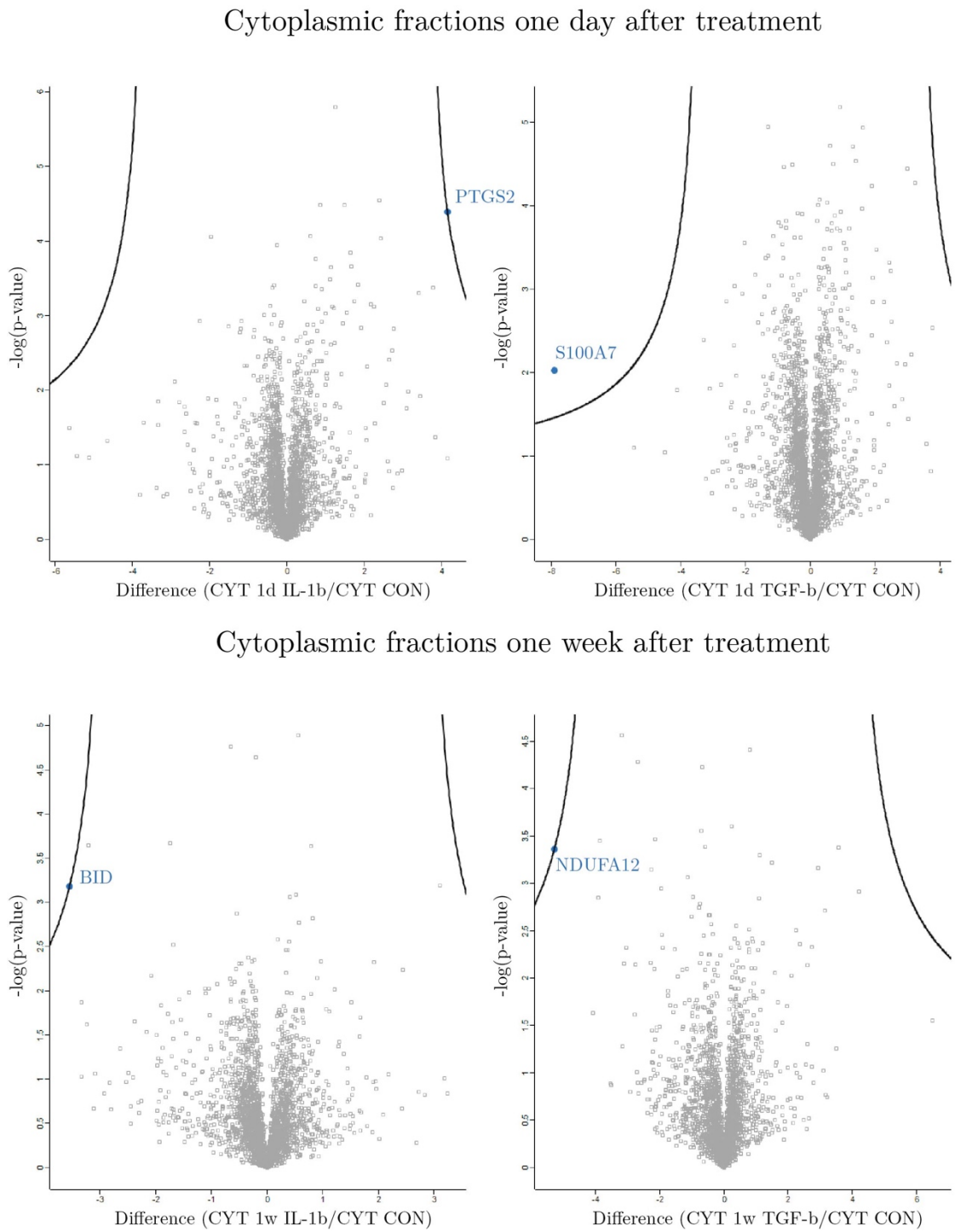

Figure 36 Volcano plots showing differentially regulated proteins in the cytoplasmic fractions one day and one week post treatment with IL-1b and TGF-b; FDR=0.01, S_0=2

An increase in **PTGS2** (prostaglandin G/H synthase 2) levels is noticeable in IL-1β treated cells one day post treatment. The protein COX-2, encoded by the PTGS2 gene, is relevant in inflammation and has, in several studies, been reported to be elevated during active inflammation [126]. Through the production of prostaglandins, it mediates pain and triggers inflammation processes in the host. Seeing that the levels

of PTGS2 are slightly elevated in IL-1β treated CCD-18Co cells, this might indicate, that fibroblasts/myofibroblasts in the inflammatory environment contribute to the release of prostaglandins and thereby support an ongoing inflammation. However, to verify this hypothesis, levels of prostaglandins in the secretome post IL-1β treatment would have to be assessed. **BID** was noted to be differentially regulated, one week after treatment with IL-1β. When evaluating the data in more detail, it could be assessed, that BID was not identified in any of the cytoplasmic fractions treated with IL-1β one day post treatment (Figure 37). BID is a pro-apoptotic protein, activated by caspase 8, which can form pores in mitochondrial membranes, upon interaction with BAX (apoptosis regulator BAX), leading to the release of cytochrome c. For the survival of myofibroblasts, the ratio between pro- and antiapoptotic proteins, as well

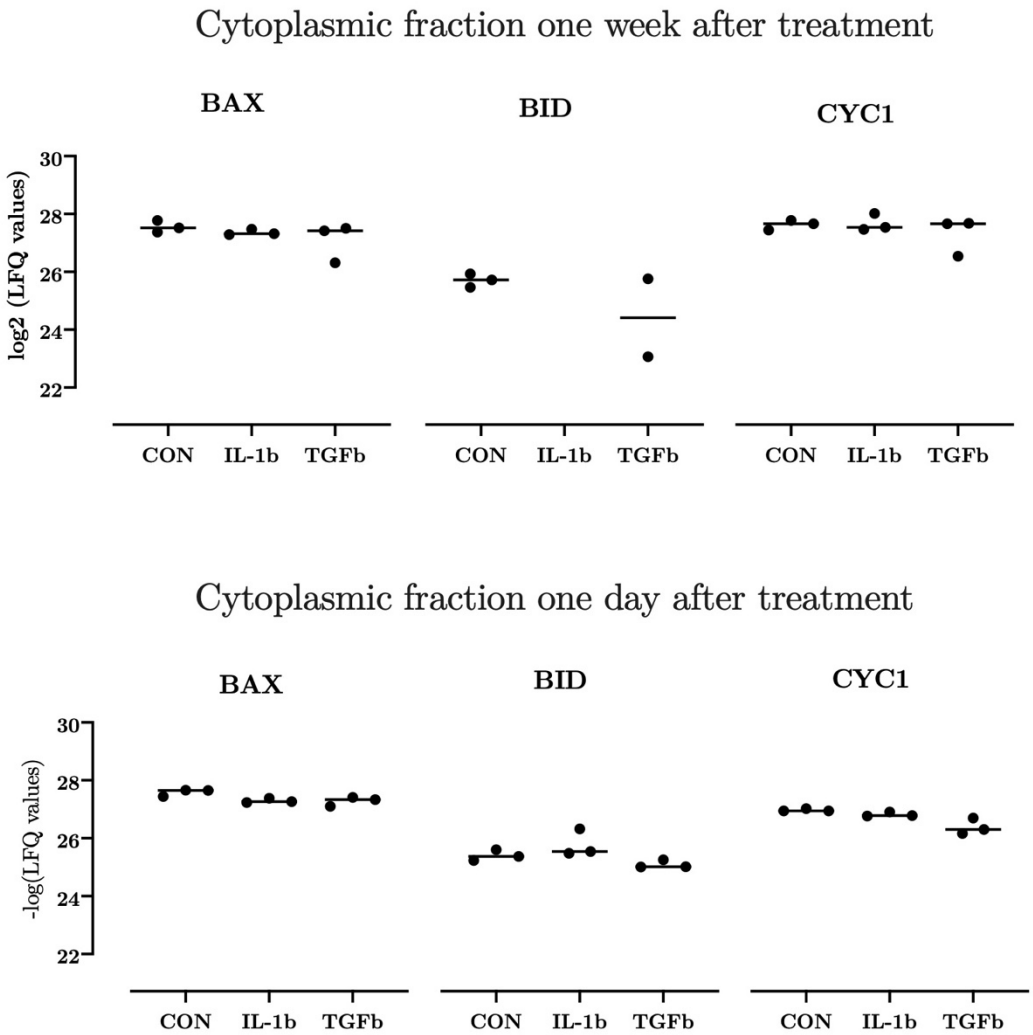

Figure 37 BAX, BID and CYC1 levels in the cytoplasmic fractions of IL-1b treated cells one day and one week post treatment

as apoptotic inhibitors (*e.g.* BCL2) is crucial.[127] BID levels in the supernatants one day post treatment are consistent throughout the different treatment conditions. **NDUFA12** levels are decreased in the cytoplasmic fractions of cells that had previously been treated with TGF-β one week after treatment. NDUFA12 levels are inconsistent throughout the cytoplasmic fractions one day post treatment. NDUFA12 is a NADH dehydrogenase and part of the mitochondrial membrane respiratory chain complex 1, involved in oxidative phosphorylation. Deletion of NDUFA12 has been shown to reduce complex 1 activity in HEK293T cells [128].

4.6.2.2. CCD-18Co secretome changes

The most notable secretome changes are to be observed in IL-1β treated cells, one day after IL-1β treatment (Figure 38). TGF-β treated cells show no significant alterations in their secretome profiles one day after treatment. As problems occurred during the sample preparation of supernatant samples of TGF-β treated cells one week post treatment, only two replicates were included in this analysis.

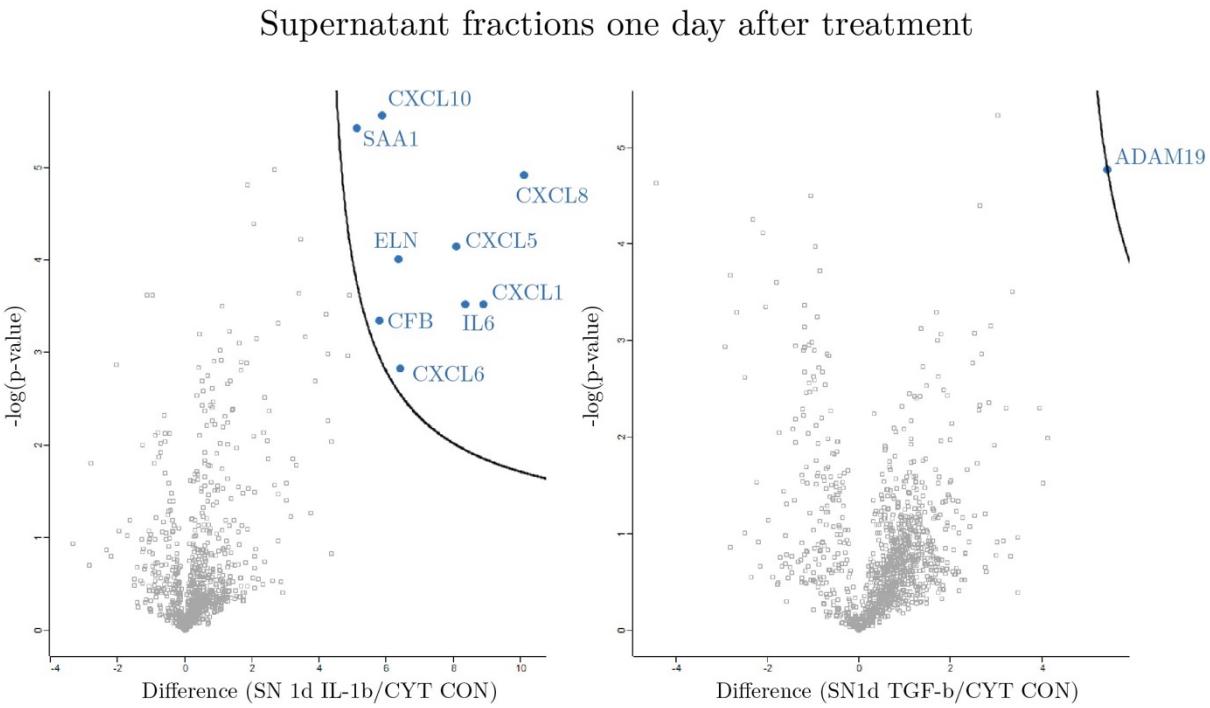

Figure 38 Secretome changes one day post IL-1b and TGF-b treatment; FDR=0.01, S_0=2

Secretome changes one day post IL-1β treatment

IL-1β treatment of CCD-18Co cells induces significant changes in the secretome of these cells. The colonic fibroblasts/myofibroblasts show a strong neutrophil-chemotactic response to IL-1β treatment shortly after the stimulus (Table 6).

Table 6 List of differentially regulated proteins in the secretome of IL-1b treated cells one day post treatment

Gene names	p-value	Difference	Protein names
CXCL8	$0{,}01*10^{-3}$	10.11	Interleukin-8
CXCL1	$0{,}30*10^{-3}$	8.90	Growth-regulated alpha protein
IL6	$0{,}30*10^{-3}$	8.36	Interleukin-6
CXCL5	$0{,}07*10^{-3}$	8.08	C-X-C motif chemokine 5
CXCL6	$1{,}47*10^{-3}$	6.43	C-X-C motif chemokine 6
ELN	$0{,}10*10^{-3}$	6.38	Elastin
CXCL10	$0{,}03*10^{-4}$	5.88	C-X-C motif chemokine 10
CFB	$0{,}45*10^{-3}$	5.80	Complement factor B
SAA1;SAA2	$0{,}04*10^{-4}$	5.12	Serum amyloid A-1 protein;Amyloid protein A

CXCL8 was identified in the cytoplasmic fraction of IL-1β treated cells one day post treatment, as well as in the supernatant of these cells. The protein was also found in one out of three control samples one week after treatment, in one out of three supernatants of the TGF-β treated cells one day post treatment and in one out of three replicates of the supernatants one week post IL-1β treatment. CXCL8 – also known as interleukin-8 – is one of the strongest chemoattractants for neutrophils, involved in leading neutrophils to sites of injury is known to be upregulated during inflammation [129]. **CXCL1** was identified in both, the supernatant of TGF-β treated and IL-1β treated cells, as well as in two out of three supernatants of control cells. The levels of CXCL1 were the highest in IL-1β treated cells. CXCL1 was also identified in two out of three supernatants of control samples one week after treatment and all of the supernatants of IL-1β and TGF-β treated cells one week post treatment. The chemokine CXCL1 is an important part of the immune response, as it aids in the recruitment, as well as the activation of neutrophils.[130] **IL6** was identified in all

supernatants of TGF-β and IL-1β treated cells one week and one day post treatment, as well as in one out the three control supernatants one week post treatment. It was not identified in any of the cytoplasmic fractions. IL6 has previously been shown to induce alpha-smooth muscle actin in fibroblasts, hereby inducing the differentiation of myofibroblasts from fibroblasts, which is a crucial process for wound healing.[131] **CXCL5** was only identified in the supernatant of IL-1β treated cells one day post treatment. CXCL5 is a protein, involved in CXCR2 mediated neutrophil trafficking, suggested to be involved in the neutrophil homeostasis, as CXCL5 deficient mice have shown to accumulate neutrophils in their bone marrow [132]. **CXCL6** could only be identified in secretome samples. The protein was identified in all supernatants of IL-1β treated cells one day post treatment, as well as in one out of the three replicates of TGF-β treated cell-supernatants. One week post treatment it was only identified in one out of the three supernatants of IL-1β treated cells. **CXCL6** is – similar to other C-X-C motif proteins – involved in neutrophil activation and possesses bactericidal properties [133]. Elastin (**ELN**) was only detected in supernatants of IL-1β and TGF-β treated cells, one day post treatment, with the highest levels being secreted by IL-1β treated cells. The protein is important for connective tissue homeostasis [134], our data suggest that the production is stimulus dependent as it was not to be identified in any supernatants one week post treatment. **CXCL10**, a chemokine involved in the direction of activated T cells to areas of inflammation [135], was only present in the supernatants of IL-1β treated cells, one day after treatment and in one out of two supernatants one week post TGF-β treatment. **CFB** was only identified in supernatants of IL-1β and TGF-β treated cells one day post treatment and one out of three supernatants of IL-1β treated cells one week after treatment. The secretion of CFB has been shown to be stimulus, as well as dose and time-dependent [136]. Complement factor B (CFB) is part of the complement system, which consists of different proteins, crucial for the innate immune response [137]. **SAA1/SAA2** was

detected in supernatants of cells previously being treated with IL-1β one day after treatment, as well as in one out of three control supernatants, one out of three supernatants of IL-1β treated cells and both supernatants of TGF-β treated cells one week after treatment. As only one unique peptide was detected for this protein, it could not be determined whether SAA1 or SAA2 was present. Both proteins are acute phase proteins, considered as marker proteins for inflammation and infection. SAA proteins act as chemoattractants for neutrophils and T-cells [138].

Secretome changes one day post TGF-β treatment

One of the most differentially regulated proteins to be identified in supernatants of TGF-β treated cells one day after treatment was **ADAM19**. ADAM19 was found in all supernatants one day post treatment with the lowest levels having been measured in control samples and the highest in supernatants of TGF-β treated cells. The protein was also identified in one out of three control-supernatants one week after treatment. ADAM19 is important for cell and tissue development [139] and has also been reported to be implicated in the development of mesenchymal cells.

4.6.3. Comparison of CCD-18Co one day and one week post treatment

4.6.3.1. Cytoplasmic fractions

In general, significant changes were noticeable when comparing cells one day and one week post treatment (Figure 39). Interestingly, also in control samples drastic changes were noticed. In total, 789 out of 3,735 proteins identified in the cytoplasmic fractions of control samples were differentially regulated, 819/3,735 proteins were differentially regulated in IL-1β treated and 724/3,735 in TGF-β treated samples. 591/819 of differentially regulated proteins after IL-1β treatment were shared with the differentially regulated proteins in control samples and 529/724 were shared between

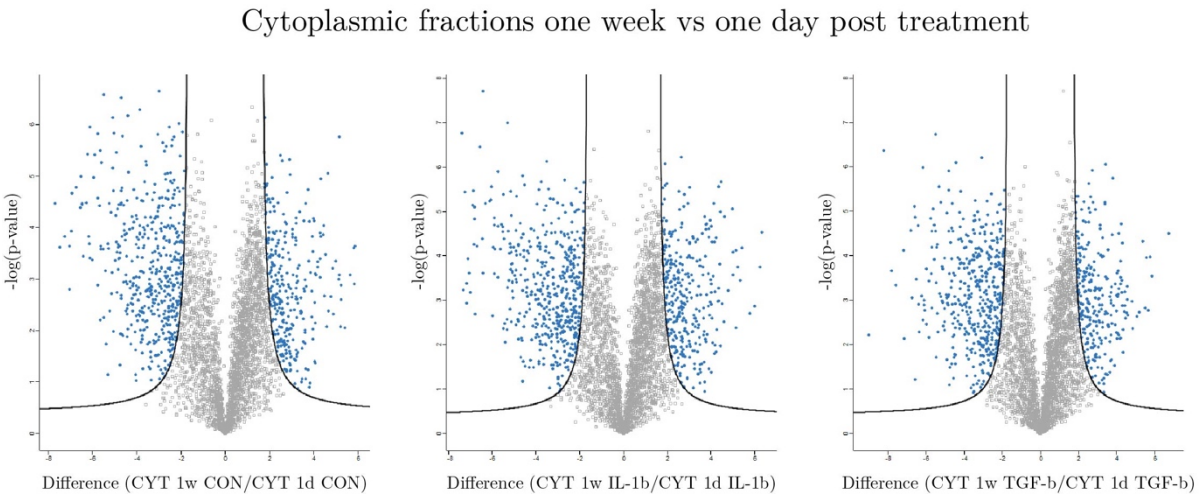

Figure 39 Volcano plots showing differentially regulated cytoplasmic proteins between one day and one week post treatment; FDR=0.01, S_0=2

the TGF-β treated cells and the control samples. A total of 156 proteins for IL-1β treated cells and 63 for TGF-β treated cells were unique. Gene ontology term (biological process) based network analyses revealed that downregulated proteins in control samples are involved in metabolic processes, protein localization, membrane organization and also macromolecule catabolic processes (Figure 40). Upregulated proteins in the cytoplasmic fractions of control samples are involved in intracellular transport, metabolic and biosynthetic processes, involving organonitrogen compounds, vesicle mediated transport, cellular component organization and other processes (Figure 41).

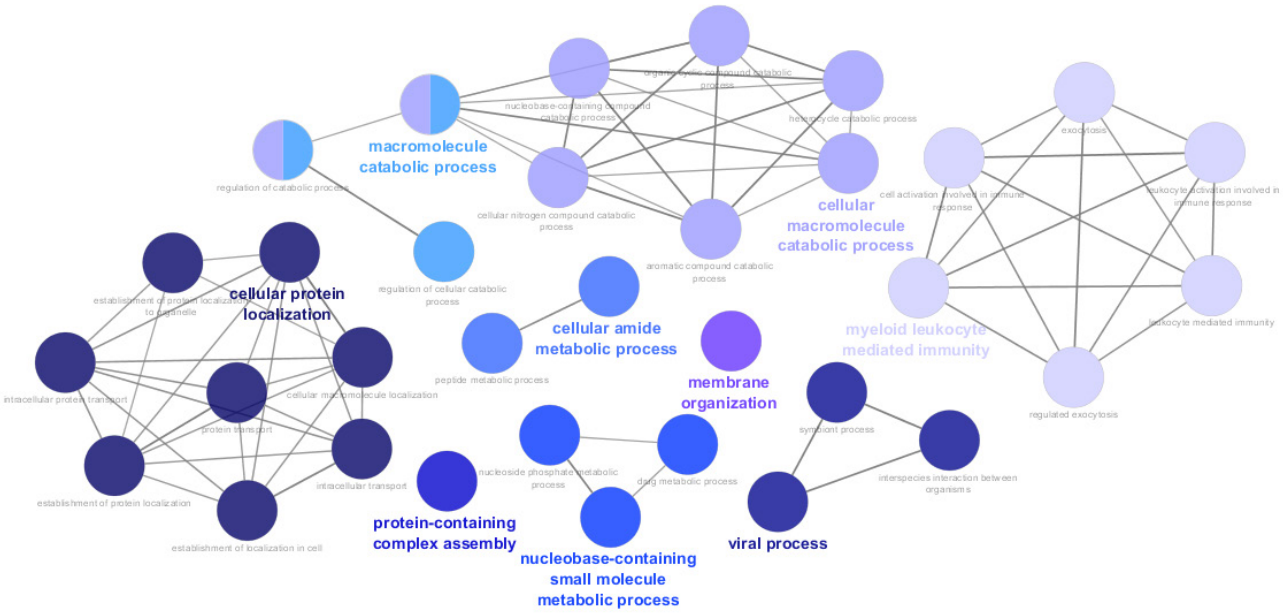

Figure 40 Biological processes downregulated in control samples one week after treatment in comparison to one day after treatment

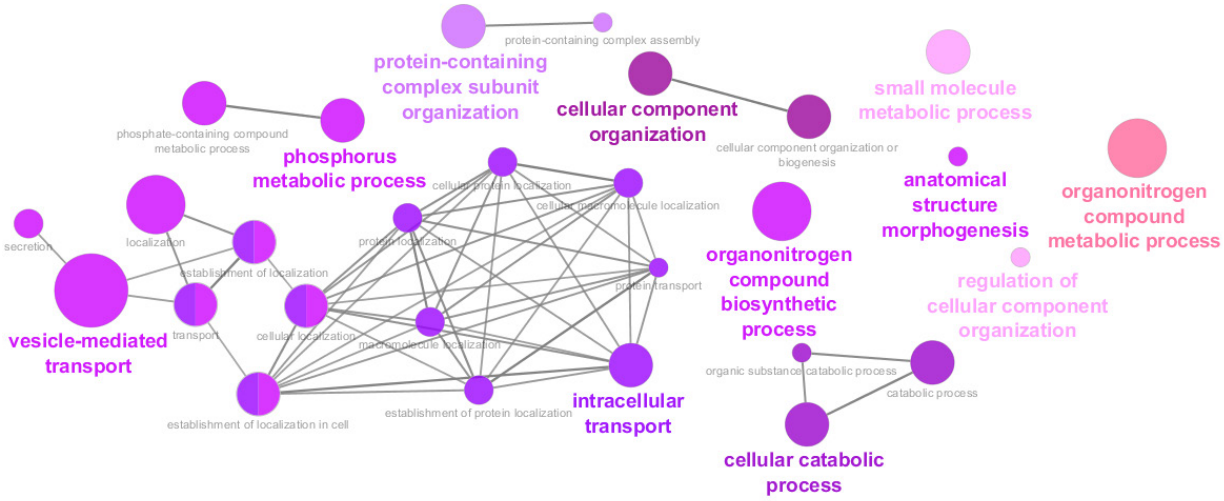

Figure 41 Biological processes upregulated in control samples one week after treatment in comparison to one day after treatment

The analysis of up- and downregulated proteins when comparing cytoplasmic fractions of cells one day and one week post IL-1β treatment yielded similar results, which was expected, taking into account that 72% of differentially regulated proteins are shared between the control and the IL-1β treated cells. Downregulated processes involved the intracellular transport, as well as cytokine mediated signaling pathways,

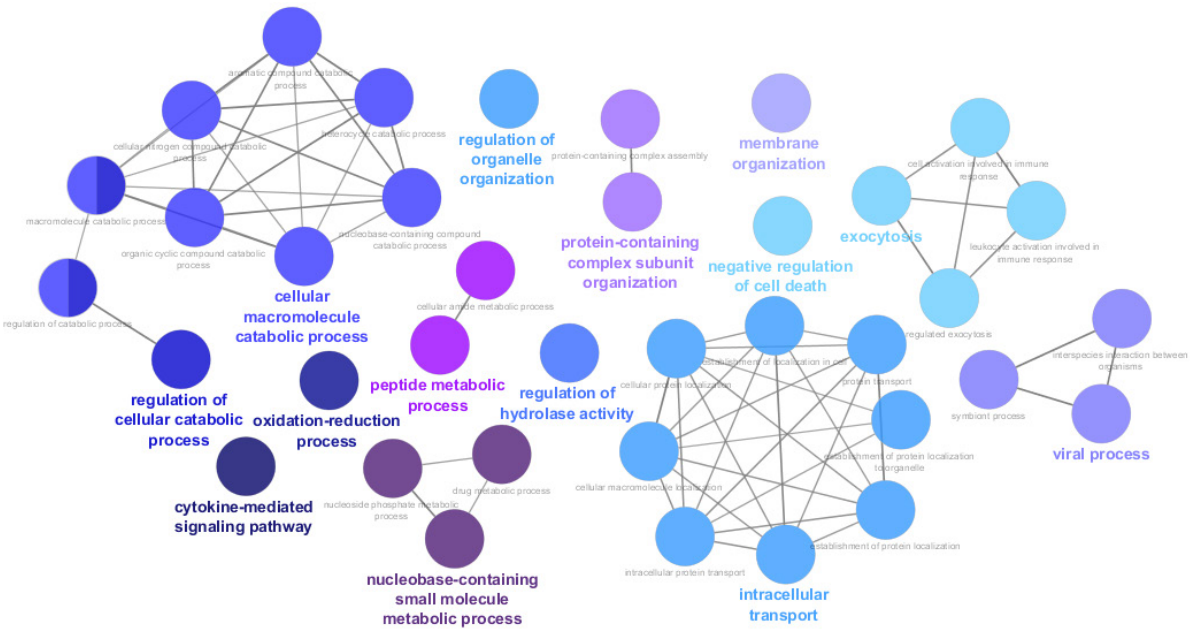

Figure 42 Biological processes downregulated in IL-1b treated samples one week after treatment in comparison to one day after treatment

peptide metabolic processes, regulation of organelle organization, membrane organization, exocytosis, negative regulation of cell death and others (Figure 42).

The analysis of upregulated proteins showed their involvement in intracellular transport, organonitrogen compound biosynthetic and metabolic processes, small molecule metabolic processes, cellular response to chemical stimulus, anatomical structure morphogenesis and other processes (Figure 43).

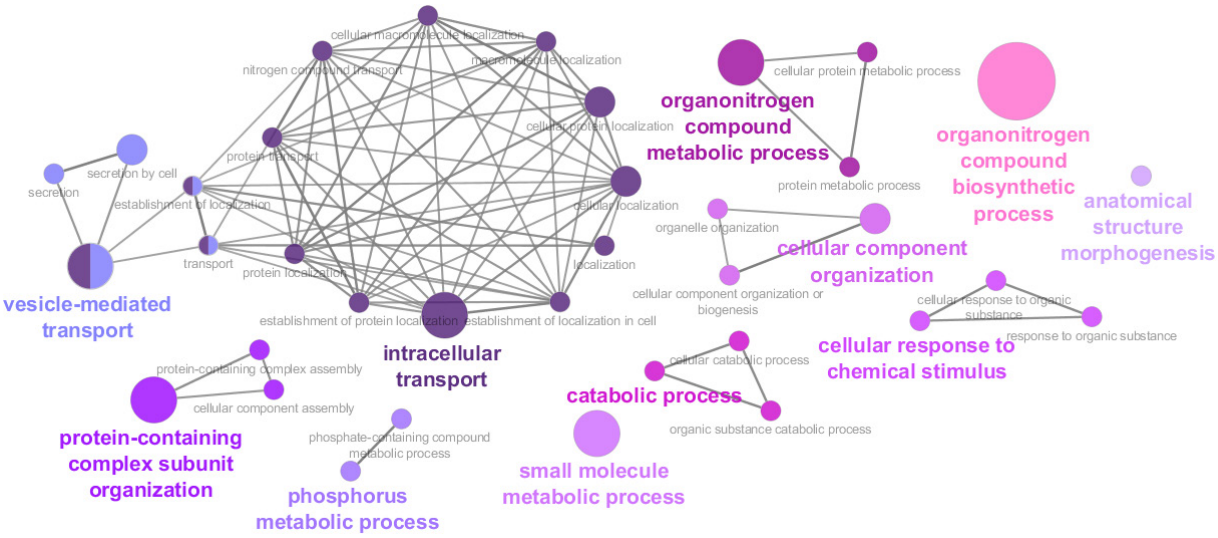

Figure 43 Biological processes upregulated in IL-1b treated samples one week after treatment in comparison to one day after treatment

GO term analysis of the downregulated proteins in TGF-β treated cells showed their involvement in regulated exocytosis, positive regulation of cell death, peptide metabolic processes, membrane organization, regulation of cellular localization, intracellular transport and others (Figure 44). For this analysis, 454 downregulated proteins were used. The analysis of upregulated proteins revealed the upregulation of intracellular transport, as well as small molecule metabolic processes, vesicle mediated transport, organonitrogen compound biosynthetic processes and others (Figure 45).

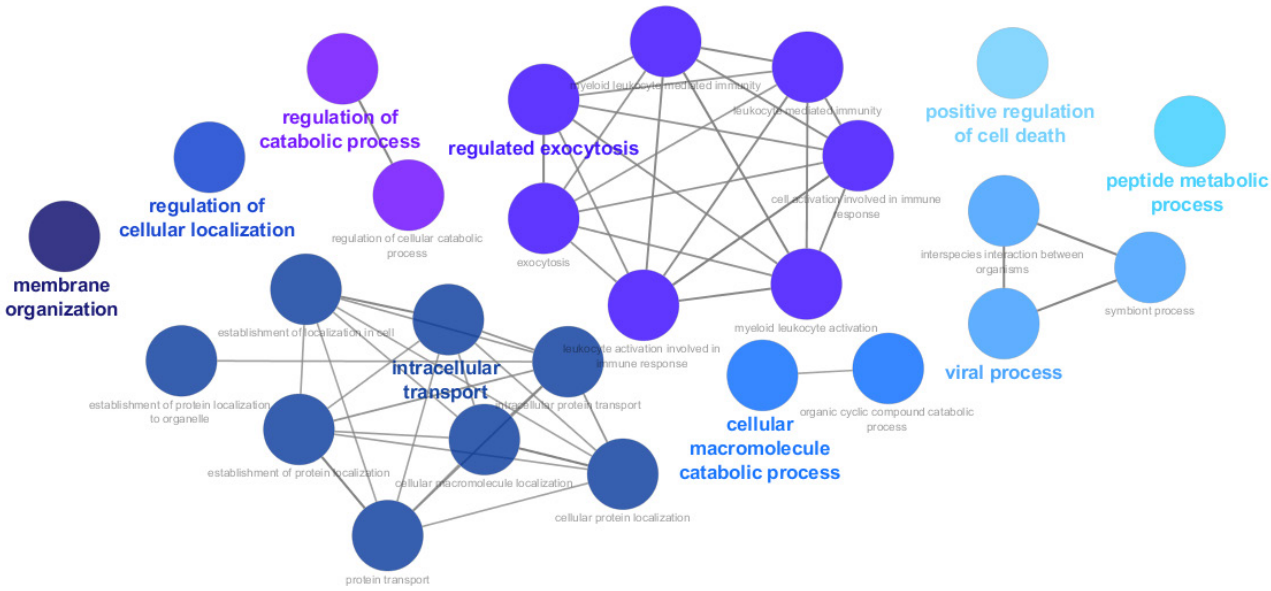

Figure 44 Biological processes downregulated in TGF-b treated samples one week after treatment in comparison to one day after treatment

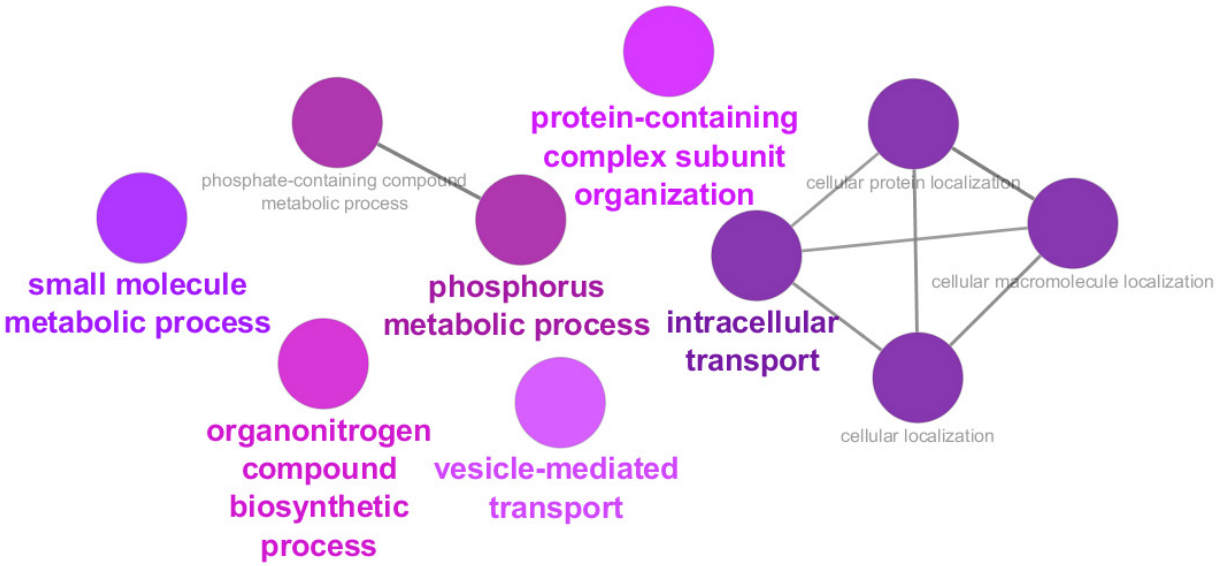

Figure 45 Biological processes upregulated in TGF-b treated samples one week after treatment in comparison to one day after treatment

As many of the abovementioned processes down- or upregulated over the course of one week post treatment were shared among the IL-1β, TGF-β as well as control cells, a more detailed analysis showing only process which were not regulated in control cells was performed as well.

The analysis of proteins downregulated in IL-1β treated cells and not in control cells showed that these proteins are involved in organonitrogen compound metabolic processes, negative regulation of biological processes, cellular processes and response to stimulus, among others (Figure 46). Upregulated processes involved organonitrogen compound metabolic processes, regulation of biological processes, cellular component organization and others (Figure 47).

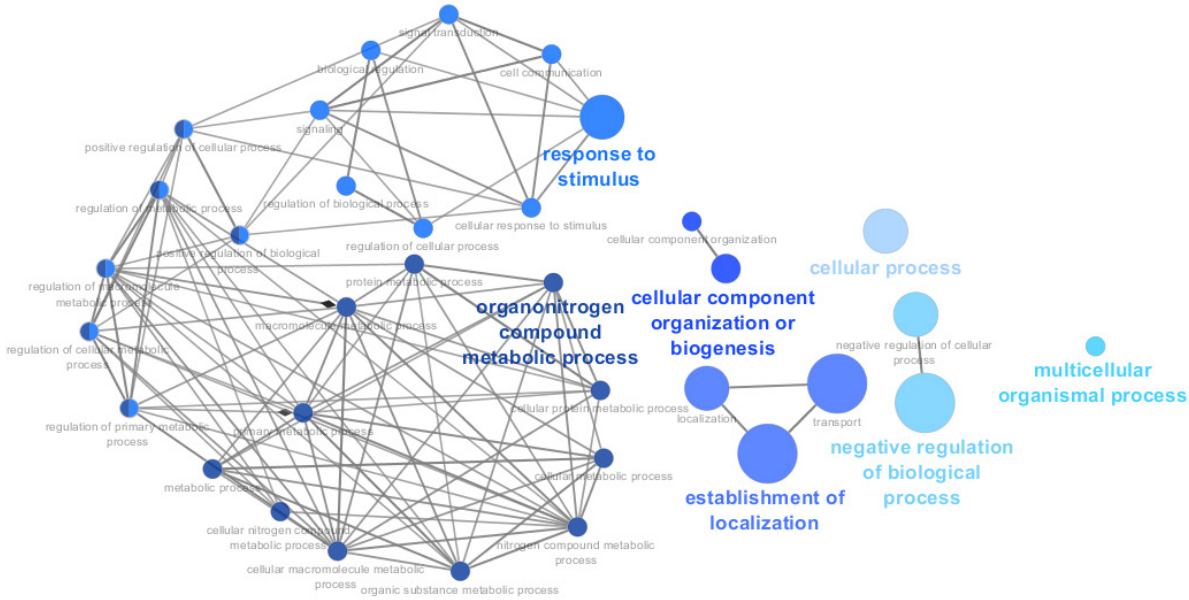

Figure 46 Biological processes downregulated in IL-1b treated cells; not shared with upregulated processes in control samples

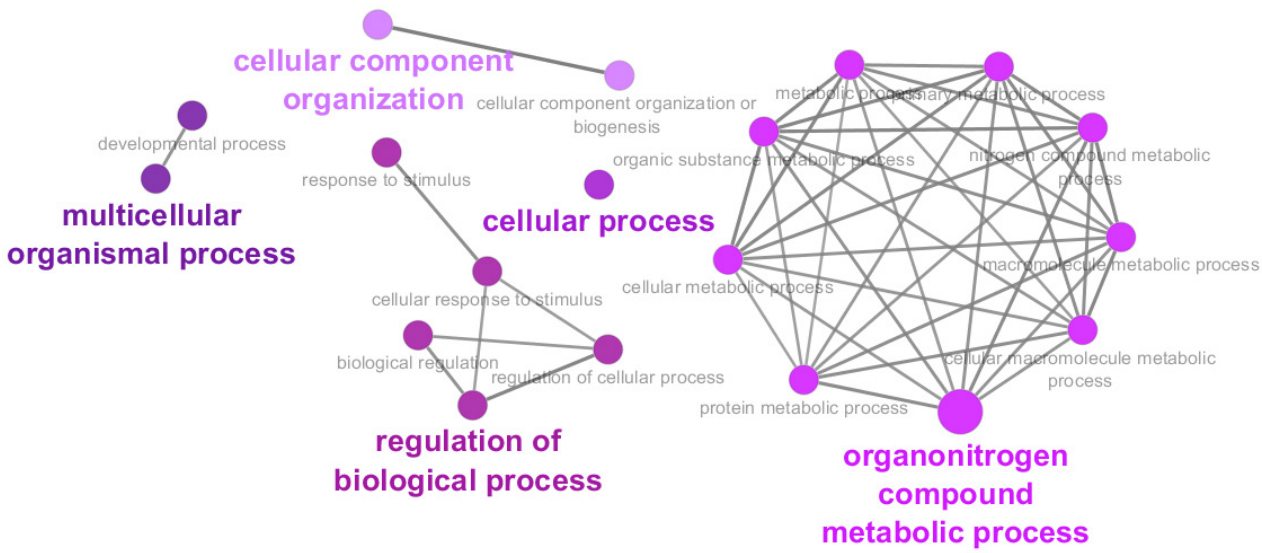

Figure 47 Biological processes upregulated in IL-1b treated cells; not shared with downregulated processes in control samples

Processes downregulated only in the cytoplasmic fractions of TGF-β treated cells, not in the control cells, involved the positive regulation of cellular and biological processes, localization, developmental processes and the cellular component organization and biogenesis, among others (Figure 48). Upregulated processes included organic substance metabolic processes, regulation of cellular processes and cellular processes (Figure 49).

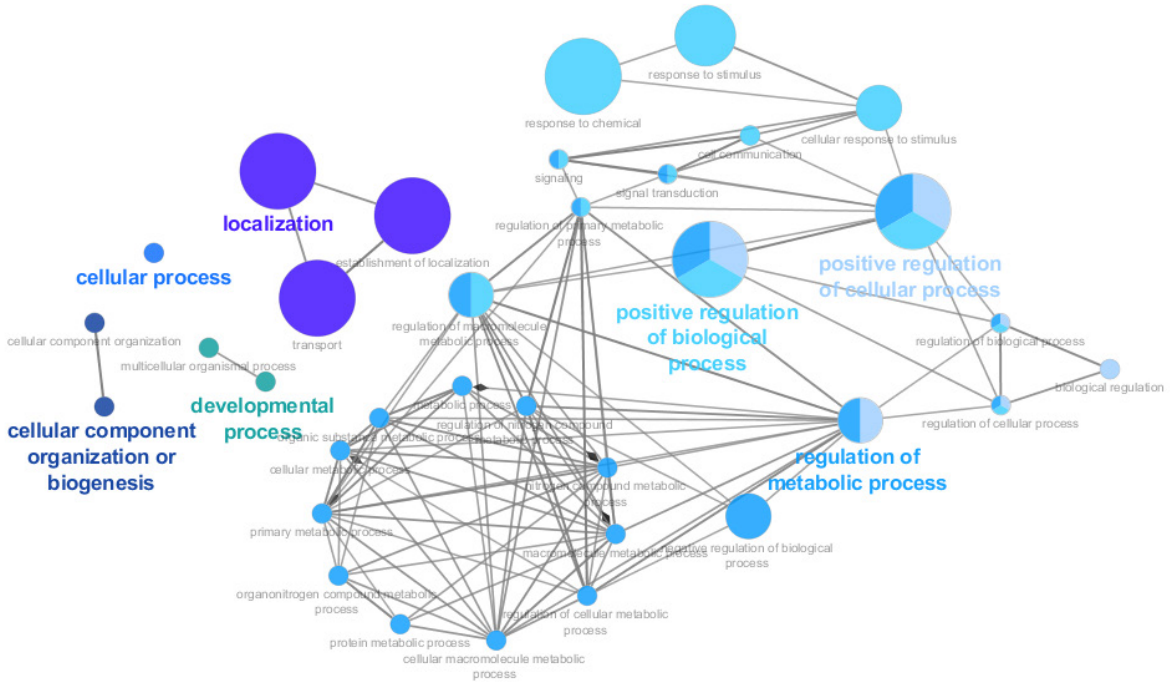

Figure 48 Biological processes downregulated in TGF-b treated cells; not shared with downregulated processes in control samples

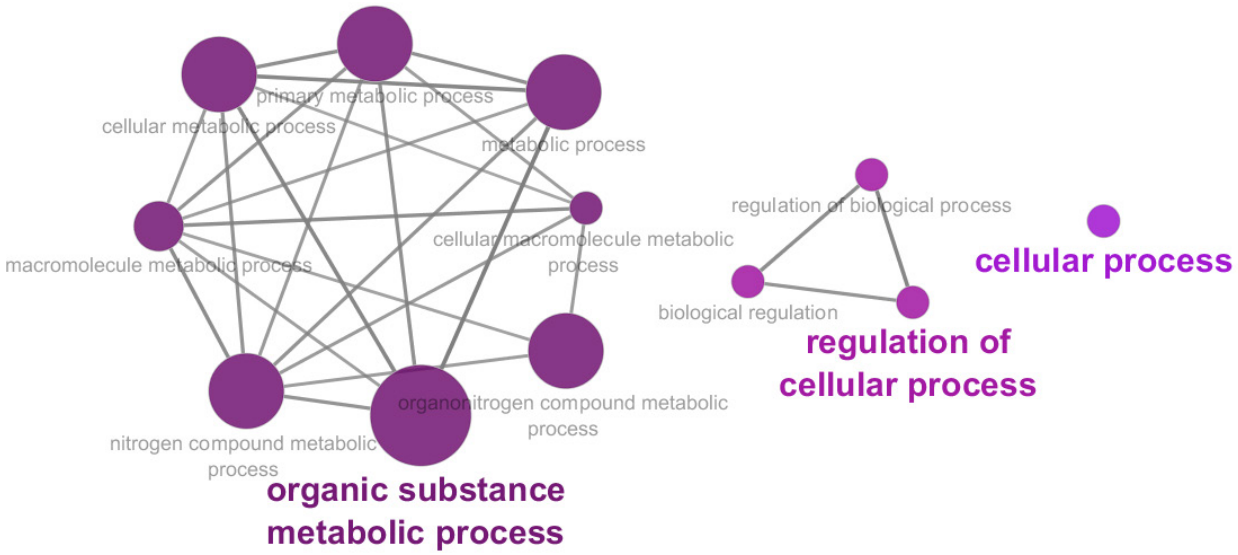

Figure 49 Biological processes upregulated in TGF-b treated cells; not shared with upregulated processes in control samples

4.6.3.2. Supernatant fractions

All three comparisons reveal significant changes in the secreted proteome of control samples, IL-1β treated samples and TGF-β treated samples when comparing these samples with their counterpart samples one day post treatment (Figure 50). Proteins, changing in abundance when comparing the IL-1β treated, as well as TGF-β treated samples are often involved in the response to stimuli, which indicates, that IL-1β, as well as TGF-β treatment induces acute proteome alterations that do not persist when the stimulus arrests. Some of the protein regulations are shared among the different groups, such as the downregulation of APOC3, TMSB10, CDH2, BASP1 and the upregulation of RPL18A, HSPA9, LIMCH1, COL6A2, LAMB4 and PCSK6. **APOC3** (Apolipoprotein C-III) was not identified in any cell fractions one day post treatment and was absent in nearly all fractions one week post treatment, except for the supernatant of one of the IL-1β treated cells. **TMSB10** (Thymosin beta-10) was only found in the supernatant fractions one day post treatment, as well as in one of the supernatants of TGF-β treated cells one week post treatment. TMSB10 is associated with growth and proliferation processes [140]. **CDH2** was identified in all supernatant fractions one day post treatment, however, only in one of the supernatants of TGF-β treated samples one week post treatment. CDH11 was exclusively identified in two out of three supernatants of the control samples one week post treatment. The downregulation and concurrent upregulation of CDH11 is a process, which is critical for adaption of a pro-fibrotic phenotype in myofibroblasts [141]. **RPL18A** (60S ribosomal protein L18a) was only identified in the supernatant fractions one week post treatment. The protein was also present in all cytoplasmic fractions, with slightly higher abundance in all fractions one week after treatment. **HSPA9** (Stress-70 protein, mitochondrial; mortalin) was present in all supernatant fractions, showed higher abundance, however, in the supernatant fractions one week post treatment. The protein was also present in all cytoplasmic fractions with reverse abundance ratios: its

abundance was higher one day post treatment when compared to one week post treatment. Mortalin is a protein involved in the cellular response to stress and its upregulation has been reported to have protective and anti-apoptotic functions [142]. **LIMCH1** (LIM and calponin homology domains-containing protein 1) was identified in all cytoplasmic fractions with higher expression levels one week post treatment. In the supernatant fractions, the protein was only identified one week after treatment and was present in all different treatment conditions. LIMCH1 is involved in the formation of actin stress fibers, which regulate cell migration and morphology [143]. **LAMB4 (**Laminin subunit beta-4) was identified in all 3 control sample supernatants, one out of three supernatants of IL-1β treated cells and one out of three supernatants of TGF-β treated cells one day post treatment. It was identified in all supernatants one week post treatment. LAMB4 was not found in any of the cytoplasmic fractions. **PCSK6** (Proprotein convertase subtilisin/kexin type 6) was exclusively identified in supernatants one week post treatment.

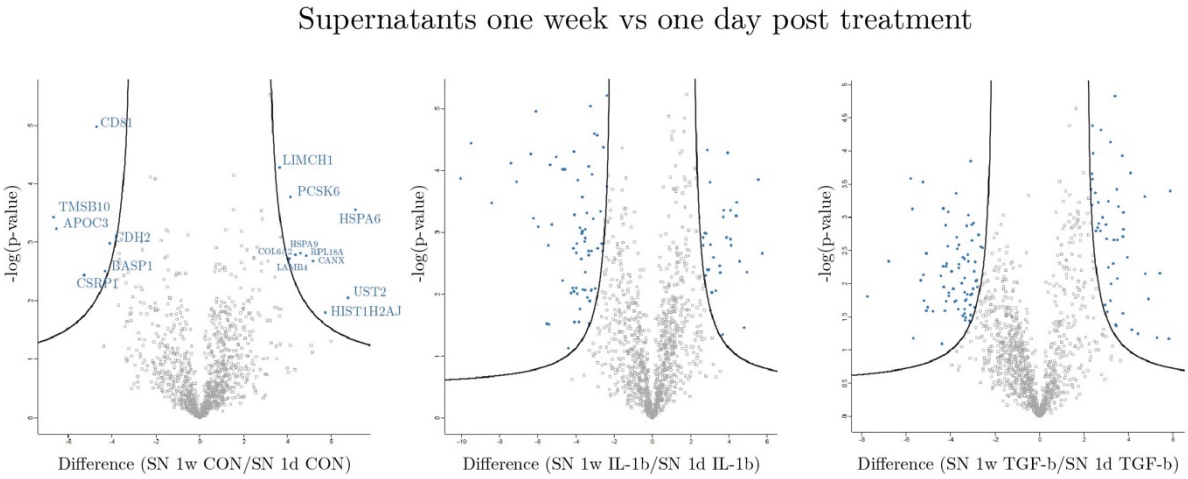

Figure 50 Volcano plots showing differentially regulated secreted proteins between one day and one week post treatment, FDR=0.01, S_0=2

Downregulated processes of the secreted proteins one week post IL-1β treatment in comparison to secreted proteins one day post IL-1β treatment are involved in the negative regulation of biological processes, as well as the regulation of biological processes, cellular processes, cellular compartment organization, establishment of localization, among others (Figure 51). Upregulated proteins are involved in the regulation of biological processes, cellular processes, response to stimuli and organonitrogen compound metabolic processes (Figure 52).

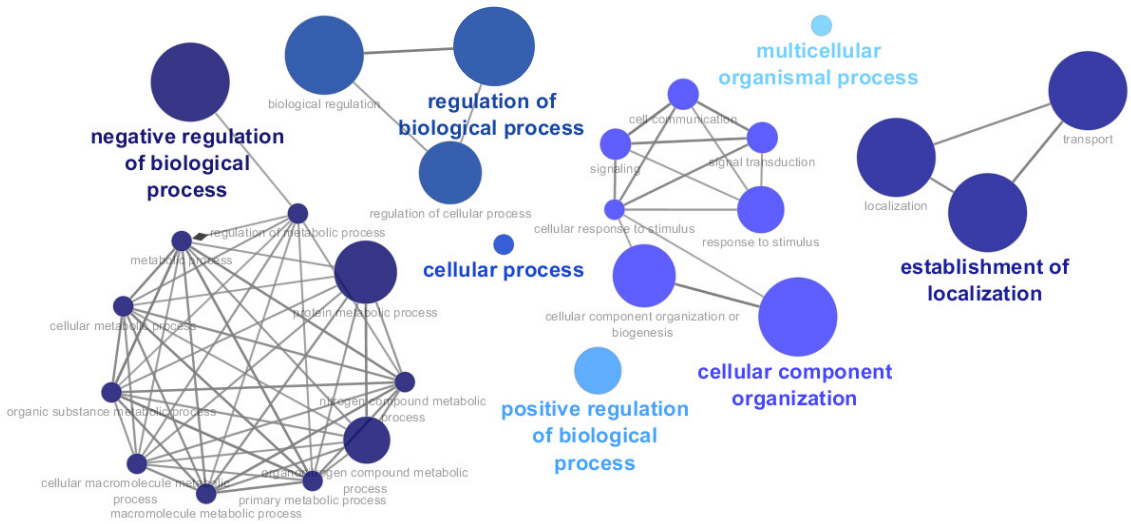

Figure 51 Biological processes in which downregulated proteins of the secretome fractions between one week and one day after IL-1b treatment are involved in

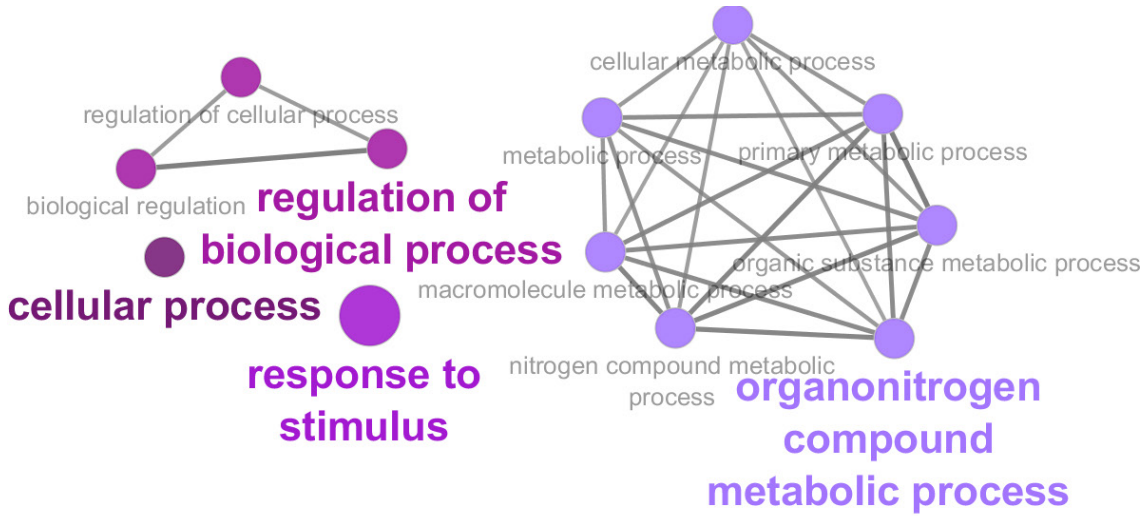

Figure 52 Biological processes in which upregulated proteins of the secretome fractions between one week and one day after IL-1b treatment are involved in

Secreted proteins which decreased in abundance one week after TGF-β stimulation in comparison to one day after stimulation are involved in cellular component organization or biogenesis, establishment of localization, biological regulation, primary metabolic processes, response to stimulus and cellular processes (Figure 53). Secreted proteins which increased in abundance one week after treatment are involved in protein metabolic processes, response to stimulus, cellular processes, localization, negative regulation of biological processes, as well as multicellular organismal processes (Figure 54).

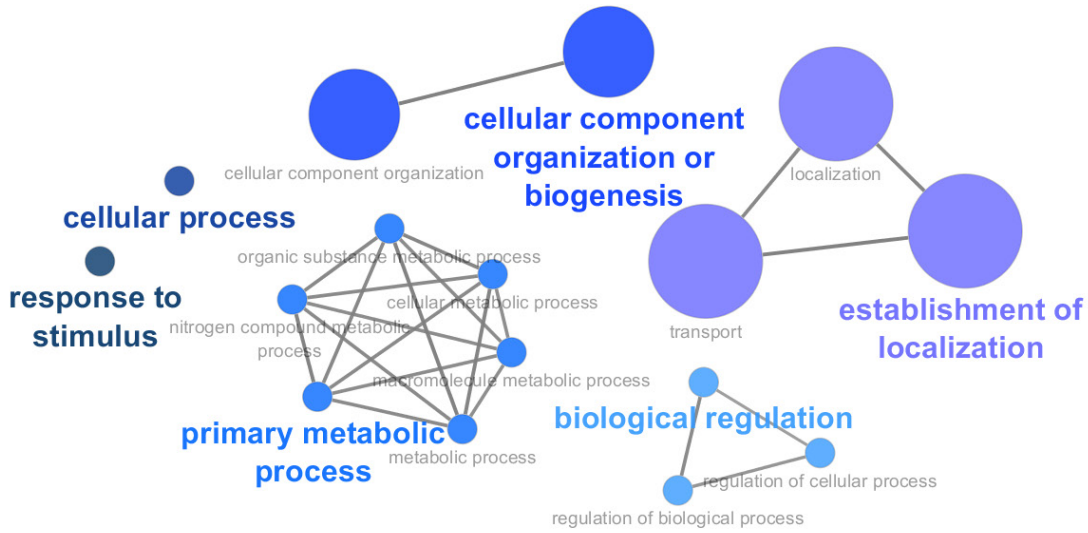

Figure 53 Biological processes in which downregulated proteins of the secretome fractions between one week and one day after TGF-b treatment are involved in

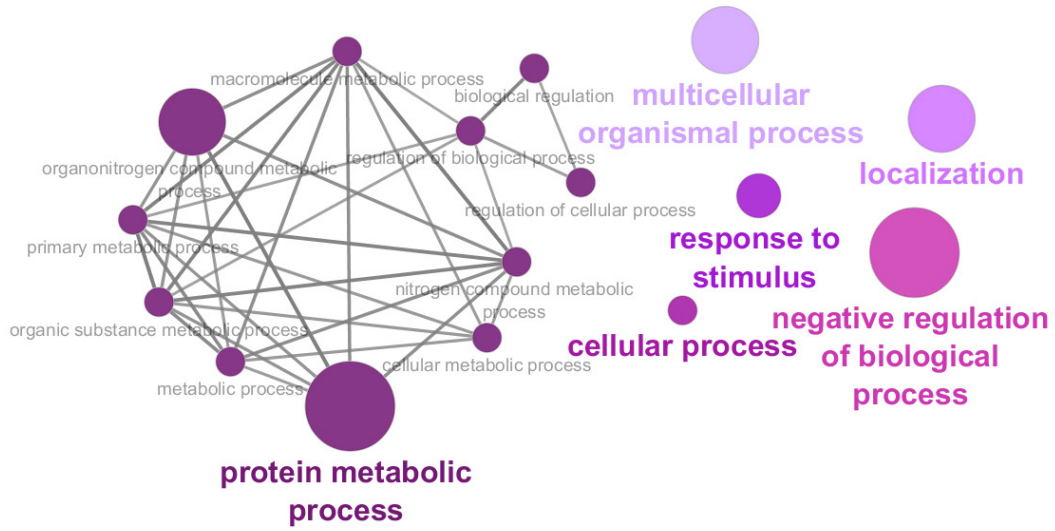

Figure 54 Biological processes in which upregulated proteins of the secretome fractions between one week and one day after TGF-b treatment are involved in

5. Conclusions and outlook

The analysis of proteomic alterations in patients with active ulcerative colitis showed that a plethora of processes is altered during inflammation. Overall, the mucus layer and hence the intestinal barrier function is impaired, leading to a deprotected epithelium and the facilitation of the entering of bacteria and bacterial products which are able to attack the cells present in the epithelium. Together with an increased population of sulfate reducing bacteria which has been proposed to occur in the rectum itself and even more so in patients with active UC this leads to further destruction of the protective layers above the epithelium. Our data also suggests an impaired H_2S metabolism during inflammation, which deteriorates the patients' ability to cope with increased H_2S levels. Entry of bacterial products induces an immune response in the host, leading to recruitment of neutrophils and other cells of the immune system as a defense mechanism against these bacteria. Neutrophils are known to generate reactive oxygen species as well as secrete IL-1β which has been shown in the *in vitro* study performed on CCD-18Co myofibroblasts/fibroblasts to induce the secretion of

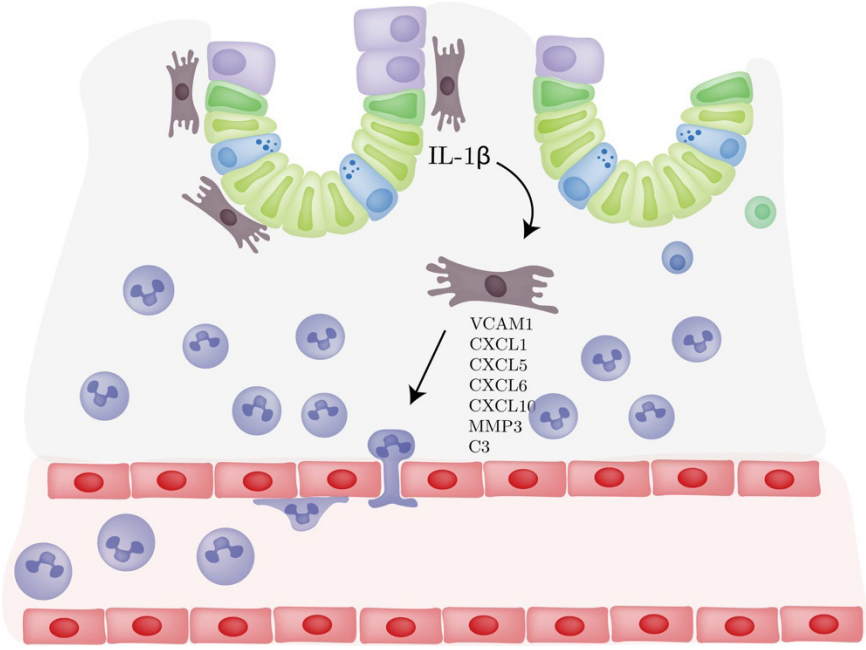

Figure 55 Neutrophil recruitment by fibroblasts/myofibroblasts

neutrophil-chemoattractive as well as neutrophil-chemotactic proteins that lead to the recruitment of more neutrophils to the site of inflammation. Together with the increased secretion of extracellular matrix degrading proteins the migration of neutrophils into the lamina propria and crypt region becomes facilitated. The recruitment of more neutrophils leads to the production of even more ROS and, therefore, to further tissue and cell disruption, altogether ending in a feedback-loop and uncontrolled, as well as excessive recruitment of neutrophils. Overall, the combination of the *in vitro* analysis of inflammatorily stimulated CCD-18Co cells, as well as the analysis of colonic biopsy specimen could suggest that myfibroblasts/fibroblasts would contribute to the disease progression and possibly also to the prolonged persistence of inflammation in patients with active ulcerative colitis. Their response to IL-1β which is a common inflammatory protein leads to a very obvious neutrophil chemoattractive response, which could explain in part the phenotype of ulcerative colitis.

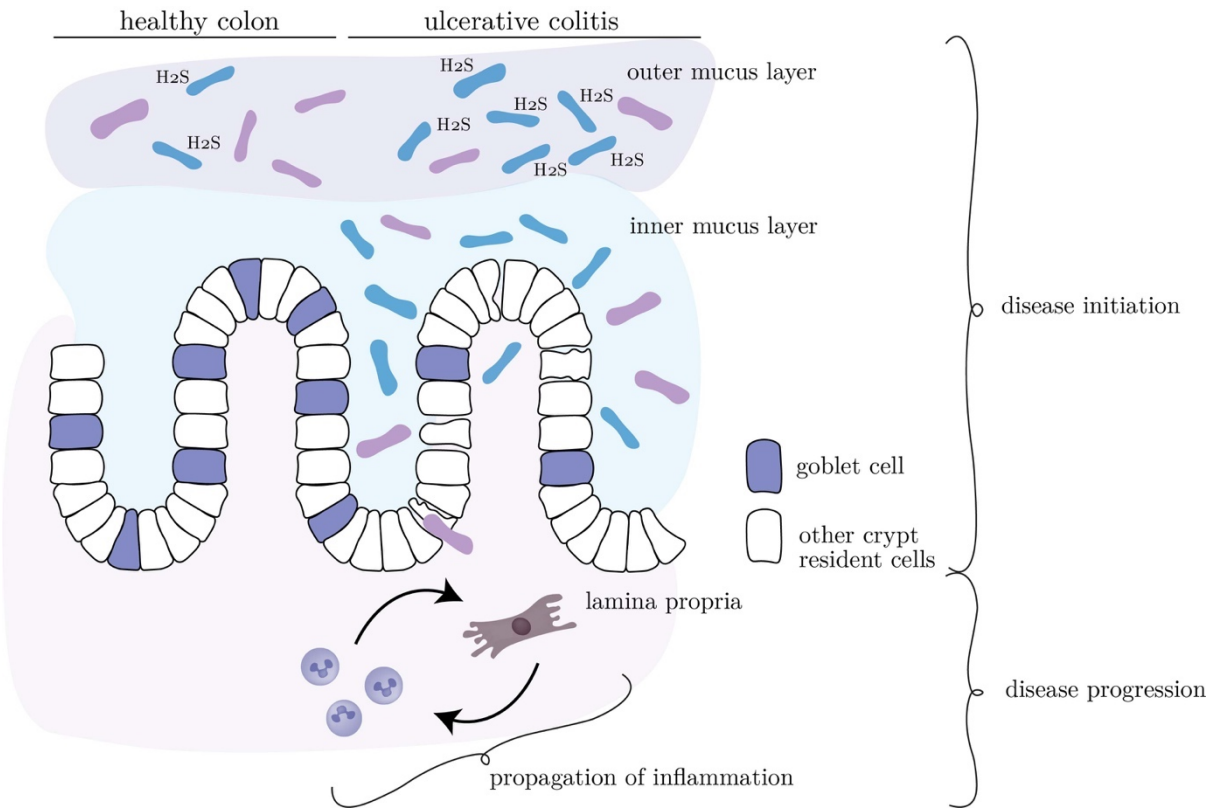

Figure 56 Hypothesis of the contribution of fibroblasts/myofibroblasts to the disease phenotype and progression of ulcerative colitis

The plasma proteome and eicosanoid analyses led to heterogenous results, possibly due to the fact that plasma is a systemic acting substance in the body, not always indicative of processes restricted to a single part of the human body sometimes concentrated to only a very small area of said body part. Local analyses of eicosanoids in biopsy specimen could lead to more concrete results. Further studies, including more patients as well as primary cultures of fibroblasts/myofibroblasts from patients suffering from the disease and additional treatment with IL-1β would be helpful for the validations of the findings of this project. Also, IL-1β levels would have to be assessed to confirm the proposed hypothesis.

6. Supplementary information

6.1. Patient medication and CRP levels

Table 7 Patient medication, CRP and calprotectin levels, dates of blood, stool and biopsy sampling; calprotectin levels not correlating with inflammation severity due to date of stool sampling are highlighted in orange

Pat Nr.	Medication	Date of biopsy excision	Date of blood sampling	CRP Blood [mg/L]	Date of stool sampling	Fecal calprotectin [µg/g]
4	12,5 mg Prednisolone	12.12.18	12.12.18	63.2	17.12.18	815
1	Mezavant 500 mg, Inflectra (100 mg, 27.11.18)	06.12.18	06.12.18	8.9	05.12.18	757
0	Urbason 6 mg, Entyvio (300 mg, 15.11.18)	29.11.18	29.11.18	4.9	17.01.19	1071
7	Mesagran 1000 mg, Cortiment 9 mg, Femoston conti, Furadantin retard	21.03.19	21.03.19	0.3	04.04.19	50
3	Mezavant 2400 mg	06.12.18	06.12.18	1.2	10.12.18	482
6	Cortiment 9 mg	21.03.19	21.03.19	1	11.01.19	403

6.2. Results of histo-pathological evaluation of colonic biopsies

P0

Colon ascendens - normal, goblet cells regular
Colon transversum (proximal) colon mucosa with slightly altered crypt architecture, crypts dissociated, regular goblet cell distribution, lamina propria slightly fibrotic and broadened, inflammatory infiltration visible, no crypt abscesses, ulcers or epithelioid cell granuloma
Colon transversum (distal) – similar to proximal transversum, a little more inflammatory infiltration, more eosinophil granulocytes
Colon descendens – altered crypt architecture, crypts dissociated, reduced goblet cell count, lamina propria broadened, more granulocytes, small crypt abscess, leukocyte extravasation

Colon sigmoideum – partly regular crypt architecture, partly dissociated, in some parts low goblet cell count, in some regular count, lamina propria partly with intensive inflammatory infiltration, leukocyte extravasation
Rectum - Colon mucosa with altered crypt architecture, crypts dissociated, reactive alterations in crypt and surface epithelium, leukocyte extravasation in many crypts, lamina propria inflammatorily infiltrated by different cells

P1

Colon dscendens, transversum – intact surface epithelium, crypt architecture distorted, edema in lamina propria, inflammatory infiltration, no leukocyte extravasation, fibrotic
*Colon descendens, colon sigmoideum, rectu*m – rudimentary colonic mucosa, crypts irregular; epithelium: increased mitosis, reactive nucleus alterations; lamina propria partly scarred, leukocyte infiltration, crypt abscesses, necrotic parts of ulcers, regeneration of epithelium noticeable

P3

Colon ascendens, transversum – slightly distorted crypt architecture, in part shortened and elongated, in part branched, lamina propria broadened, dense cell population (lymphocytes and plasma cells, some granulocytes), leukocyte extravasation, lymphocytic aggregates
Colon descendens, sigmoideum – slightly distorted crypt architecture, mucosal edema, lamina propria shows chronic inflammatory cell infiltration (eosinophils, granulocytes – invading surface epithelium via basal membrane)
Rectum – slightly distorted crypt architecture, scarred lamina propria with inflammatory infiltration

P4

Colon ascendens, transversum – regular crypt architecture, regular goblet cell distribution, subepithelial basement membrane and lamina propria without inflammatory infiltration
Colon descendens, colon sigmideum, rectum – some surface erosions and ulcers, slightly distorted crypt architecture, crypts abnormally elongated, some crypts lateral to colon lumen, lamina propria with very dense cell population (lymphocytes, plasma cells, inflammatory cells), inflammatory cells infiltrate crypt epithelium, some crypt abscesses, leukocyte extravasation

P6

Colon ascendens, transversum, descendens, sigmoideum – slightly altered crypt architecture, Paneth cell metaplasia in some crypt bases, some crypts elongated, lamina propria edema, loosened, in part dense inflammatory cell population, many eosinophil granulocytes, small lymphoid cell aggregations, no epithelial distortion, epithelium in part infiltrated by lymphocytes, epithelial very slightly inflammatorily altered, no neutrophils visible
Rectum – altered crypt architecture, crypts irregularly altered, many Paneth cells, lamina propria edematous, infiltrated by neutrophils and eosinophils, epithelium inflammatory state, lymphoid cell aggregates in stroma

P7

Colon ascendens, transversum, descendens, sigmoideum – regular crypt architecture, no epithelial alterations, basement membrane normal, small edema in lamina propria
Rectum – erosions, plasmacytosis, reparative alterations, crypt architecture distorted, eosinophils and neutrophils, surface epithelium altered

6.3. Eicosanoids without significant abundance differences

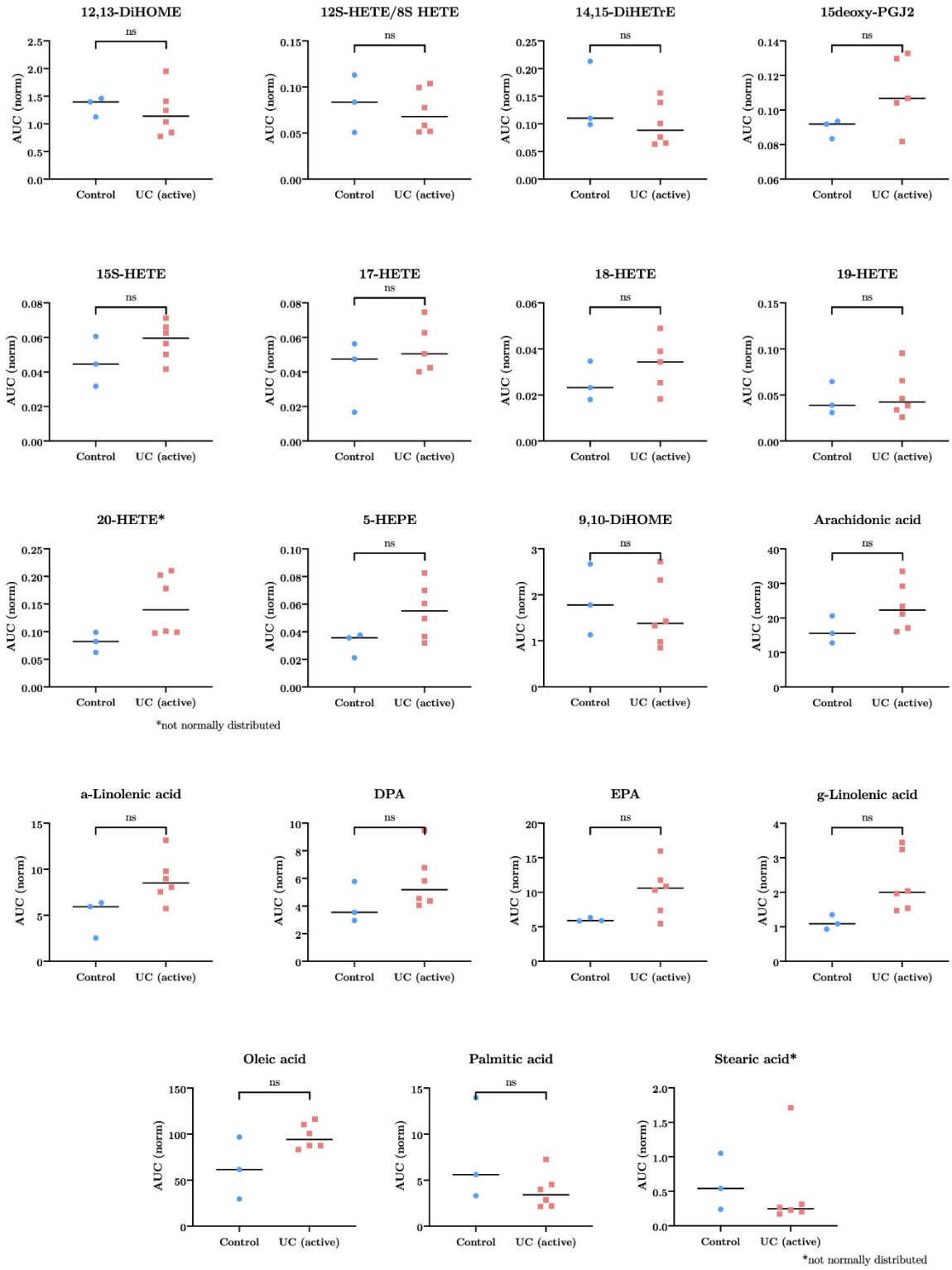

Figure 57 Plasma eicosanoids not showing significant abundance changes

6.4. Eicosanoids QQ-Plots

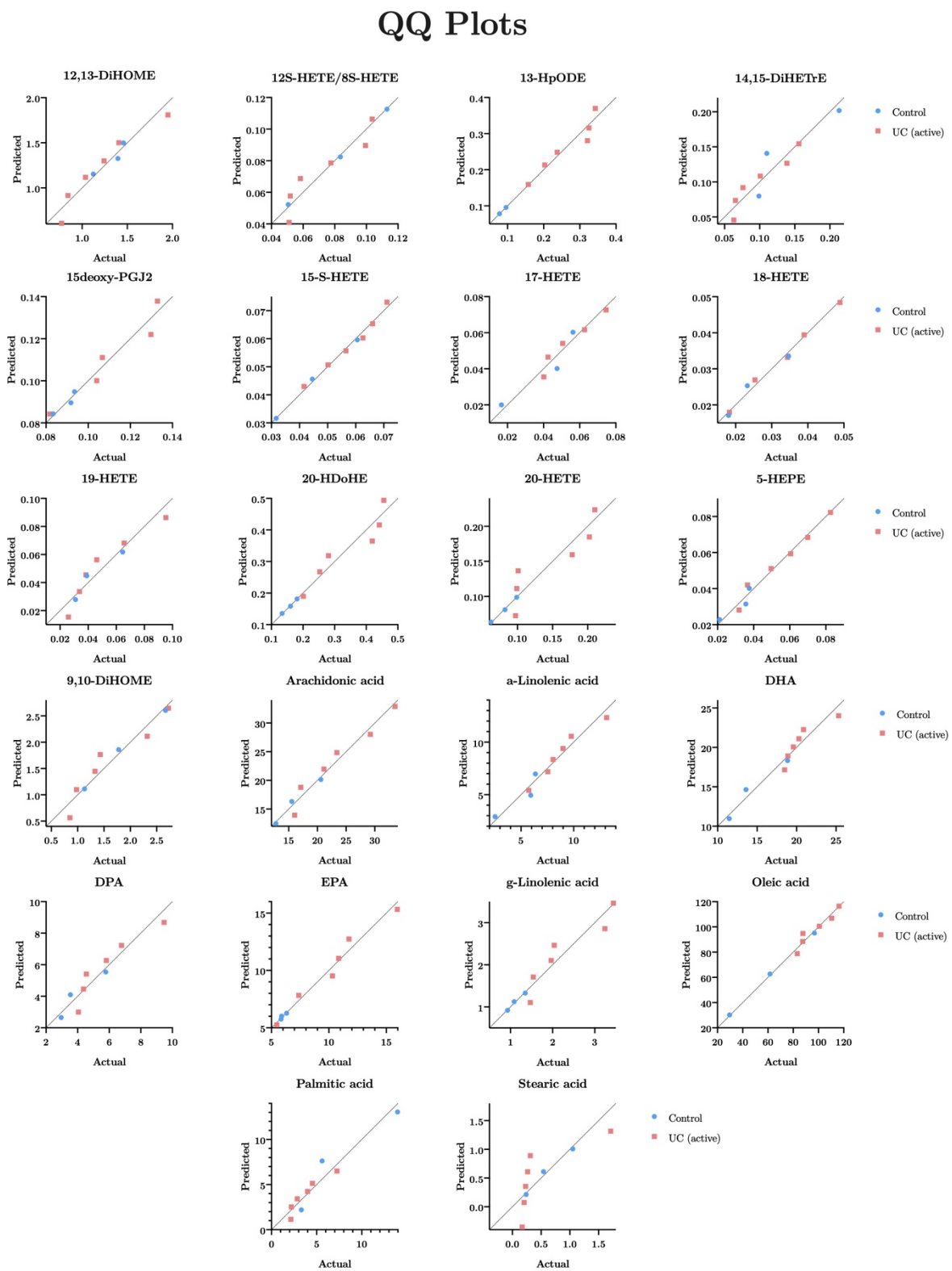

Figure 58 QQ Plots indicative of normal distribution of eicosanoid levels in patient and control samples

Acknowledgement

First of all, I would like to express my sincere gratitude to both of my supervisors Univ.-Prof. Dr. Christopher Gerner and Dr. Astrid Slany for giving me the opportunity to perform research on a topic which lies very close to my heart. I truly appreciate all the fruitful discussions, as well as the unconditional support I received from both of them and I am very thankful for the time spent and the experiences gained while working on this interdisciplinary project.

Subsequently, I would like to thank Lukas Janker for his friendly ear, active support and assistance which I received during the year. Overall, I owe having a great time during the work for my master's thesis in large part to him.

Furthermore, I would like to thank Laura Niederstätter for her help and advice in the analysis of eicosanoids, which was a great part of this master's thesis.

Generally, I would like to thank all members of the Gerner group for their friendly and open-minded nature.

I would also like to thank our collaboration partners at the Rudolfstiftung hostpital as this project would not have been possible without them and their vigorous efforts.

Stefanie Rubenzucker should not go unmentioned in this section of my master's thesis. Stefanie grew to be a great friend on whom I can always count on, as well as come to for support in all sorts of concerns. I am very grateful for having gained her as a friend of mine over the course of my master's project.

My dearest appreciation and gratefulness is dedicated to my boyfriend, who has always supported me unconditionally in each and every one of my projects. Without him having my back at all times I would not be where I am today, and I am sincerely thankful for having him in my life.

Last but not least I want to thank my parents and grandparents who have always been there for me and have helped me overcome every hurdle life has faced me with thus far. Their encouragement and affirmation contributed in large part to my personal, as well as professional growth and development.

References

1. Ng, S.C., et al., *Worldwide incidence and prevalence of inflammatory bowel disease in the 21st century: a systematic review of population-based studies.* The Lancet, 2017. **390**(10114): p. 2769-2778.
2. Molodecky, N.A., et al., *Increasing incidence and prevalence of the inflammatory bowel diseases with time, based on systematic review.* Gastroenterology, 2012. **142**(1): p. 46-54 e42; quiz e30.
3. Kelsen, J. and R.N. Baldassano, *Inflammatory bowel disease: the difference between children and adults.* Inflamm Bowel Dis, 2008. **14 Suppl 2**: p. S9-11.
4. Cosnes, J., et al., *Epidemiology and natural history of inflammatory bowel diseases.* Gastroenterology, 2011. **140**(6): p. 1785-94.
5. Khor, B., A. Gardet, and R.J. Xavier, *Genetics and pathogenesis of inflammatory bowel disease.* Nature, 2011. **474**(7351): p. 307-17.
6. Leena Halme, P.P.-S., Ulla Turunen, Maarit Lappalainen, Martti Färkkilä, Kimmo Kontula, *Family and twin studies in inflammatory bowel disease.* World J Gastroenterol, 2006. **12**(23): p. 3668-3672.
7. de Lange, K.M. and J.C. Barrett, *Understanding inflammatory bowel disease via immunogenetics.* J Autoimmun, 2015. **64**: p. 91-100.
8. Sartor, R.B., *The influence of normal microbial flora on the development of chronic mucosal inflammation.* Research in Immunology, 1997. **148**(8-9): p. 467-476.
9. Cong, Y., et al., *CD4+ T Cells Reactive to Enteric Bacterial Antigens in Spontaneously Colitic C3H/HeJBir Mice: Increased T Helper Cell Type 1 Response and Ability to Transfer Disease.* Journal of Experimental Medicine, 1998. **187**(6): p. 855-864.
10. Tromm, A., May, B., *Entzündliche Darmerkrankungen Endoskopische Diagnostik.* 2015: Falk Foundation e.V.
11. Ungaro, R., et al., *Ulcerative colitis.* The Lancet, 2017. **389**(10080): p. 1756-1770.
12. Vavricka, S.R., et al., *Extraintestinal Manifestations of Inflammatory Bowel Disease.* Inflamm Bowel Dis, 2015. **21**(8): p. 1982-92.
13. Autenrieth, D.M., Baumgart, D. C., *Toxic megacolon.* Inflamm Bowel Dis, 2012. **18**(3): p. 584-91.
14. Lakatos, P.L., Lakatos, L., *Risk for colorectal cancer in ulcerative colitis: Changes, causes and managment strategies.* World J Gastroenerol, 2008. **14**(25): p. 3937-3947.

15. Rogler, G., L. Biedermann, and M. Scharl, *New insights into the pathophysiology of inflammatory bowel disease: microbiota, epigenetics and common signalling pathways.* Swiss Med Wkly, 2018. **148**: p. w14599.
16. Dubuquoy, L., et al., *Impaired expression of peroxisome proliferator-activated receptor γ in ulcerative colitis.* Gastroenterology, 2003. **124**(5): p. 1265-1276.
17. Cario, E., Podolsky, D.K., *Differential alteration in intestinal epithelial cell expression of toll-like receptor 3 (TLR3) and TLR4 in inflammatory bowel disease.* Infect Immun, 2000. **68**(12): p. 7010-7.
18. Chapman, M.A., Grahn, M.F., Boyle, M.A., Hutton, M., Rogers, J., Williams, N.S., *Butyrate oxidation is impaired in the colonic mucosa of sufferers of quiescent ulcerative colitis.* Gut, 1994. **35**(1): p. 73-6.
19. De Preter, V., et al., *Impaired butyrate oxidation in ulcerative colitis is due to decreased butyrate uptake and a defect in the oxidation pathway.* Inflamm Bowel Dis, 2012. **18**(6): p. 1127-36.
20. Nepelska, M., et al., *Commensal gut bacteria modulate phosphorylation-dependent PPARgamma transcriptional activity in human intestinal epithelial cells.* Sci Rep, 2017. **7**: p. 43199.
21. Gartner, L., Hiatt, J., , *Color Textbook of Histology* 3ed. 2006.
22. DeRoche, T.C., Xiao, S.Y., Liu, X., , *Histological evaluation in ulcerative colitis.* Gastroenterology Report, 2014. **2**(3): p. 178-192.
23. Alberts, B., Johnson, A., Lewis, J., Morgan, D., Raff, M., Roberts, K., Walter, P., , *Molekularbiologie der Zelle.* 6 ed. 2017: Wiley-VCH.
24. Atuma, C., Strugala, V., Allen, A., Holm, L., , *The adherent gastrointestinal mucus gel layer: thickness and physical state in vivo.* American Journal of Physiology, 2001. **280**(5): p. G922-G929.
25. Johansson, M.E., Phillipson, M., Petersson, J., Velcich, A., Holm, L., Hansson, G.C., *The inner of the two Muc2 mucin-dependent mucus layers in colon is devoid of bacteria.* Proc Natl Acad Sci U S A, 2008. **105**(39): p. 15064-15069.
26. Marchesi, J.R., Adams, D.H., Fava, F., et al., , *The gut microbiota and host health: a new clinical fronier.* Gut, 2016. **65**(2): p. 330-339.
27. Hold, G.L., Pryde S. E., Russell, V. J., Furrie, E., Flint, H. U., , *Assessment of microbial diversity in human colonic samples by 16S rDNA sequence analysis.* FEMS Microbiol Ecol, 2002. **39**(1): p. 33-39.
28. Consortium, H.M.P., *Structure, function and diversity of the healthy human microbiome.* Nature, 2012. **486**(7402): p. 207-214.
29. Frank, D.N., St. Amand, A. L., Feldman, R. A., Boedeker, E. C., Harpaz, N., Pace, N. R., , *Molecular-phylogenic characterization of microbial community imbalances in human inflammatory bowel diseases.* Proc Natl Acad Sci U S A, 2007. **104**(34): p. 13780-13785.

30. Halfvarson, J., et al., *Dynamics of the human gut microbiome in inflammatory bowel disease.* Nat Microbiol, 2017. **2**: p. 17004.
31. Gophna, U., Sommerfeld, K., Gophna, S., Doolittle, W. F., Veldhuyzen van Zanten, S. J. O., *Differences between Tissue-Associated Intestinal Mircofloras of Patients with Crohn's Disease and Ulcerative Colitis.* J Clin Microbiol, 2006. **44**(11): p. 4136-4141.
32. Pitcher, M.C.L., Cummings, J. H., *Hydrogen sulphide: a bacterial toxin in ulcerative colitis?* Gut, 1996. **39**(1): p. 1-4.
33. Guo, F.F., Yu, T. C., Hong, J., Fang, J. Y., , *Emerging Roles of Hydrogen Sulfide in Inflammatory and Neoplastic Colonic Diseases.* Front Physiol, 2016. **7**: p. 156.
34. Macfarlane, G.T., Gibson G. R., Cummings, J. H., *Comparison of fermentation reactions in different regions of the human colon.* J Appl Bacteriol, 1992. **72**(1): p. 57-64.
35. Teigen, L.M., Geng, Z., Sadowsky, M. J., Vaughn, B. P., Hamilton, M. J., Khoruts, A., *Dietary Factors in Sulfur Metabolism and Pathogenesis of Ulcerative COlitis.* Nutrients, 2019. **11**(4): p. 931.
36. Pitcher, M.C.L., Beatty, E. R., Cummings, J. H., , *The contribution of sulphate reducing bacteria and 5-aminosalicylic acid to feacal sulphide in patients with ulcerative colitis.* Gut, 2000. **46**: p. 65-72.
37. Roediger, W.E., Duncan, A., Kapaniris, O., Millard, S., , *Reducing sulfur compounds of the colon impair colonocyte nutrition: implications for ulcerative colitis.* Gastroenterology, 1993. **104**(3): p. 802-809.
38. Ijssennagger, N., R. van der Meer, and S.W.C. van Mil, *Sulfide as a Mucus Barrier-Breaker in Inflammatory Bowel Disease?* Trends Mol Med, 2016. **22**(3): p. 190-199.
39. Mosli M., B., M. A., Al-Judaibi, B., Al-Ameel, T., Saleem, A., Bessissow, T., Ghosh, S., Almadi, M., *Advances in the Diagnosis and Management of Inflammatory Bowel Disease: Challenges and Uncertainties.* Saudi J Gastroenterol, 2014. **20**(2): p. 81-101.
40. Marshall, J.B., *Tuberculosis of the gastrointestinal tracht and peritoneum.* Am J Gastroenterol, 1993. **88**: p. 989-99.
41. Gecse, K.B., Vermeire, S., *Differential diagnosis of inflammatory bowel disease: limitations and complications.* The Lancet Gastroenterology and Hepatology, 2018. **3**(9): p. 644-653.
42. Cioffi, M., De Rosa, A., Serao, Rosalba, Picone, I., Vietri, M. T., , *Laboratory markers in ulcerative colitis: Current insights and future advances.* World J Gastroenerol, 2015. **6**(1): p. 13-22.
43. Mumolo, M.G., Bertani, L., Ceccarelli, L., Laino, G., Di Fluri, G., Albano, E., Tapete, G., Costa, F., *From bench to bedside: Fecal calprotectin in*

inflammatory bowel diseases clinical setting. World J Gastroenerol, 2018. **24**(33): p. 3681-3694.

44. Sipponen, T., Kolho, K. L., *Fecal calprotectin in diagnosis and clinical assessment of inflammatory bowel disease.* Scandinavian Journal of Gastroenterology, 2014. **50**(1): p. 74-80.
45. Mooiweer, E., Severs, M., Schipper, M. E., Fidder, H. H., Siersema, P. D., Laheij, R. J., Oldenburg, B., *Low fecal calprotecitn predicts sustained clinical remission in inflammatory bowel disease patients: a plea for deep remission.* J Crohns Colitis, 2015. **9**(1): p. 50-5.
46. Ordás, I., Eckmann, L., Talamini, M., Baumgart, D. C., Sandborn, W. J., *Ulcerative colitis.* Lancet, 2012. **380**(9853): p. 1606-19.
47. Erben, U., Loddenkemper, C., Doerfel, K., Spieckermann, S., Haller, D., Heimesaat, M. M., Zeitz, M., Siegmund, B., Kühl, A. A., *A guide to histomorphological evaluation of intestinal inflammation in mouse models.* Int J Clin Exp Pathol, 2014. **7**(8): p. 4557-4576.
48. Lewis, J.D., Chuai, S., Nessel, L., Lichtenstein, G. R., Aberra, F. N., Ellenberg, J. H., , *Use of the Noninvasive Components of the Mayo Score to Assess Clinical Response in Ulcerative Colitis.* Inflamm Bowel Dis, 2018. **14**: p. 1660-1666.
49. Panés, J., Alfaro, I., , *New treatment strategies for ulcerative colitis.* Expert Review of Clinical Immunology, 2017. **13**(10): p. 963-973.
50. Kornbluth, A., Sachar, D. B., The Practice Parameters Committee of the American College of Gastroenterology, *Ulcerative Colitis Practice Guidelines in Adults: American College of Gastroenterology, Practice Parameters Committee.* The American Journal of Gastroenterology, 2010. **105**(3): p. 501-523.
51. Marshall, J.K., Thabane, M., Steinhart, A. H., et al., *Rectal 5-aminosalicylic acid for induction of remission in ulcerative colitis* Cochrane Database Syst Rev., 2010.
52. Lynch, R.W., Lowe, D., Protheroe, A., et al., *Outcomes of rescue therapie in acute severe ulcerative colitis: data from the United Kingdom inflammatory bowel disease audit.* Aliment Pharmacol Ther, 2013. **38**: p. 935-945.
53. Chebli, L.A., Chaves, L. D., Pimentel, F. F., Guerra, D. M., Barros, R. M., Gaburri, P. D., Zanini, A., Chebli, J. M., *Azathioprine maintains long-term steroid-free remission through 3 years in patients with steroid-dependent ulcerative colitis.* Inflamm Bowel Dis, 2010. **16**(4): p. 613-9.
54. Mocciaro, F., Renna, S., Orlando, A., Rizzuto, G., Sinagra, E., Orlando, E., Cottone, M., , *Cyclosporine or infliximab as recue therapy in severe refractory ulcerative colitis: Early and long-term data from a retrospective observational study.* Journal of Crohn's and Colitis, 2012. **6**(6): p. 681-686.

55. Panaciccione, R., Ghosh, S., Middleton, S., Márquez, J. R., Scott, B. B., Flint, L., van Hoogstraten, H. J., Chen, A. C., Zheng, H., Danese, S., Rutgeerts, P., *Combination therapy with infliximab and azathioprine is superior to monotherapy with either agent in ulcerative colitis.* Gastroenterology, 2014. **146**(2): p. 392-400.
56. Rawla, P., Sunkara, T., Jeffrey, P. R., *Role of biologics and biosimilars in inflammatory bowel disease: current trends and future perspectives.* J Inflamm Res, 2018. **11**: p. 215-226.
57. Tripathi, K., Feuerstein, J. D., , *New developments in ulcerative colitis: latest evidence on management, treatment and maintenance.* Drugs Context, 2019. **8**: p. 212572.
58. Editorial, *A current view on inflammation.* Nature Immunology, 2017. **18**(8): p. 825.
59. Guo, H., Callaway, J. B., Ting, J. P. Y., *Inflammasomes: mechanism of action, role in disease, and therapeutics.* Nature Medicine, 2015. **21**(7): p. 677-687.
60. Zhen, Y., Zhang, H., *NLRP3 Inflammasome and Inflammatory Bowel Disease.* Front Immunol, 2019. **10**: p. 276.
61. Dionne, S., D'Agata, I. D., Hiscott, J., Vanounou, T., Seidman, E. G., *Colonic explant production if IL-1 and its receptor antagonist is imbalanced in inflammatory bowel disease (IBD).* Clin Exp Immunol, 1998. **112**(3): p. 435-42.
62. Zaki, M.H., Boyd, K. L., Vogel, P., et al., , *The NLRP3 inflammasome protects against loss of epithelial integrity and mortality in experimental colitis.* Immunity, 2010. **32**: p. 379-391.
63. Perera, A.P., Fernando, R., Shinde, T., Gundamaraju, R., Southam, B., Sohal, S. S., Robertson, A. A. B., Schroder, K., Kunde, D., Eri, R., *MCC950, a specific small molecule inhibitor of NLRP3 inflammasome attenuates colonic inflammation in spontaneous colitis mice.* Scientific Reports, 2018. **8**.
64. Ranson, N., Veldhuis, M., Mitchell, B., Fanning, S., Cook, A., Kunde, D., Eri, R., *NLRP3-Dependent and -Independent Processing of Interleukin (IL)-1β in Active Ulcerative Colitis.* Int J Mol Sci, 2019. **20**(1): p. 57.
65. Netea, M.G., van de Veerdonk, F. L., van der Meer, J. W. M., Dinarello, C. A., Josten, L. A. B., *Inflammasome-Independent Regulation of IL-1 Familiy Cytokines.* Annual Review of Immunology, 2015. **33**(1): p. 49-77.
66. Joosten, L.A., Netea, M.G., Koenders, M. I., Helsen, M. M., Sparrer, H., Pham, C. T., van der Meer, J. W., Dinarello, C.A. van den Berg, W. B., , *Inflammatory arthritis in caspase 1 gene-deficient mice: contribution of proteinase 3 to caspase 1-independent production of bioactive interleukin-1beta.* Arthritis Rheum, 2009. **60**(12): p. 3651-62.
67. Lukens, J.R., Gross, J. M., Calabrese, C., Iwakura, Y., Lamkanfi, M., Vogel, P., Kanneganti, T. D., *Critical role for inflammasome-independent IL-1b*

production in osteomyelitis. Proc Natl Acad Sci U S A, 2014. **111**(3): p. 1066-1071.

68. Bennike, T.B., et al., *Neutrophil Extracellular Traps in Ulcerative Colitis: A Proteome Analysis of Intestinal Biopsies.* Inflamm Bowel Dis, 2015. **21**(9): p. 2052-67.
69. de Oliveira, S., Rosowski, E. E., Huttenlocher, A., *Neutrophil migration in infection and wound repair: going forward in reverse.* Nat Rev Immunol, 2016. **16**(6): p. 378-391.
70. Caielli, S., Banchereau, J., Pascual, V., *Neutrophils come of age in chronic inflammation.* Curr Opin Immunol, 2012. **24**(6): p. 671-7.
71. Nourshargh, S., Alon, R., *Leukocyte Migration into Inflamed Tissues.* Immunity, 2014. **41**(5): p. 694-707.
72. Ley, K., Laudanna, C., Cybulsky, M. I., Nourshargh, S., *Getting to the site of inflammation: the leukocyte adhesion cascade updated.* Nature Reviews Immunology, 2007. **7**(9): p. 678-689.
73. Bressenot, A., Salleron, J., Bastien, C., Danese, S., Boulagnon-Rombi, C., Peyrin-Biroulet, L., *Comparing histological activity indexes in UC.* Gut, 2014. **64**(9): p. 1412-1418.
74. Wéra, O., Lancellotti, P., Oury, C., *The Dual Role of Neutrophils in Inflammatory Bowel Diseases.* Journal of Clinical Medicine, 2016. **5**(12): p. 118.
75. Roulis, M., Flavell, R. A., , *Fibroblasts and myofibroblasts of the intestinal lamina propria in physiology and disease.* Differentiation, 2016. **92**(3): p. 116-131.
76. Bagalad, B.S., Kumar, K. P. M., Puneeth, H. K., *Myofibroblasts: Master of disguise.* J Oral Maxillofac Path, 2017. **21**(3): p. 462-463.
77. van Beurden, H.E., Von den Hoff, J. W., Torensma, R., Maltha, J. C., Kujpers-Jagtman, A. M., *Myofibroblasts in palatal wound healing: prospects for the reduction of wound contraction after cleft palate repair.* J Dent Res, 2005. **84**(10): p. 871-80.
78. Thannickal, V.J., Lee, D. Y., White, E. S., Cui, Z., Larios, J. M., Chacon, R., Horowitz, J. C., Day, R. M., Thomas, P. E., *Myofibroblast differentiation by transforming growth factor-beta1 is dependent on cell adhesion and integrin signaling via focal adhesion kinase.* J Biol Chem, 2003. **278**(14): p. 12384-9.
79. Toullec, A., et al., *Oxidative stress promotes myofibroblast differentiation and tumour spreading.* EMBO Mol Med, 2010. **2**(6): p. 211-30.
80. Gregory, A.D., Kliment, C. R, Metz, H. E., Kim, K. H., Kargl, J., Agostini, B. A., Crum, L T., Oczypok, E. A., Oury, T. A., Houghton, A. M., *Neutrophil elastase promotes myofibroblast differentiation in lung fibrosis.* J Leukoc Biol, 2015. **98**(2): p. 143-52.

81. Masur, S.K., Dewal, H. S., Dinh, T. T., Erenburg, I. Petridou, S., *Myfibroblasts differentiate from fibroblasts when plated at low density.* Proc Natl Acad Sci U S A, 1996. **93**(9): p. 4219-4223.
82. Slany, A., et al., *Contribution of Human Fibroblasts and Endothelial Cells to the Hallmarks of Inflammation as Determined by Proteome Profiling.* Mol Cell Proteomics, 2016. **15**(6): p. 1982-97.
83. Tahir, A., Bileck, A., Muqaku, B., Niederstaetter, L., Kreutz, D., Mayer, R. L., Wolrad, D., Meier, S. M., Slany, A., Gerner, C., *Combined Proteome and Eicosanoid Profiling Approach for Revealing Implications of Humab Fibroblasts in Chronic Inflammation.* Anal Chem, 2017. **89**(3): p. 1945-1954.
84. Andoh, A., Fujino, S., Okuno, T., Fujiyama, Y., Bamba, T., *Intestinal subepithelial myofibroblasts in inflammatory bowel diseases.* J Gastroenterol, 2002. **37**: p. 33-37.
85. Shores, D.R., Binion, D. G., Freeman, B. A., Baker, P. R. S., *New Insights into the Role of Fatty Acids in the Pathogenesis and Resolution of Inflammatory Bowel Disease.* Inflamm Bowel Dis, 2011. **17**(10): p. 2192-2204.
86. Funk, C.D., *Prostaglandins and leukotrienes: advances in eicosanoid biology.* Science, 2001. **294**: p. 1871-1875.
87. Martin, C.R., *Lipids and Fatty Acids in the Preterm Infant, Part 1: Basic Mechanisms of Delivery, Hydrolysis, and Bioavailability.* NeoReviews, 2015. **16**(3).
88. Yu, K., Bayona, W., Kallen, C. B., Harding, H. P., Ravera, C. P., McMahon, G., Brown, M., Lazar, M. A., *Differential activation of peroxisome proliferator-activated receptors by eicosanoids.* J Biol Chem, 1995. **270**(41): p. 23975-83.
89. Esteve-Comas, M., Ramírez, M., Fernández-Bañares, F., Abad-Lacruz, A., Gil, A., Cabré, E., Gonzáles-Huix, F., Moreno, J., Humbert, P., Guilera, M., Boix, J., Gassul, M. A., , *Plasma polyunsaturated fatty acid pattern in active inflammatory bowel disease.* Gut, 1995. **33**: p. 1365-1369.
90. Esteve-Comas, M., Núñez, M. C., Fernández-Bañares, F., Abad-Lacruz, A., Gil, A., Cabré, E., González-Huix, F., Bertrán, X., Gassul, M. A., *Abnormal plasma polyunsaturated fatty acid pattern in non-active inflammatory bowel disease.* Gut, 1993. **34**: p. 1370-1373.
91. Masoodi, M., et al., *Altered colonic mucosal Polyunsaturated Fatty Acid (PUFA) derived lipid mediators in ulcerative colitis: new insight into relationship with disease activity and pathophysiology.* PLoS One, 2013. **8**(10): p. e76532.
92. Wiese, D.M., Horst, S. N., Brown, C. T., Allaman, M. M., Hodges, M. E., Slaughter, J. C., Druce, J. P., Beaulieu, D. B., Schwartz, D. A., Wilson, K. T., Coburn, L. A., , *Serum Fatty Acids Are Correlated with Inflammatory Cytokines in Ulcerative Colitis.* PLoS One, 2016. **11**(5).

93. Wasinger, V.C., Cordwell, S. J., Cerpa-Poljak, A., Yan, J. X., Gooley, A. A., Wilkins, M. R., Duncan, M. W., Harris, R., Williams, K. L., Humphery-Smith, I., *Progress with gene-product mapping of the Mollicutes: Mycoplasma genitalium.* Electrophoresis, 1995. **16**: p. 1090-1094.
94. Yates, J.R., *The Revolution and Evolution of Shotgun Proteomics for Large-Scale Proteome Analysis.* Journal of American Chemical Society, 2013. **135**(5): p. 1629-1640.
95. *Shotgun Proteomics.* Methods in Molecular Biology, ed. J.M. Walker. 2014: Springer Protocols.
96. Fenn, J.B., Mann, M., Meng, C. K., Wong, S. F., Whitehouse, C. M., *Electrospray Ionization for Mass Spectrometry of Large Biomolecules.* Science, 1989. **246**(4926): p. 64-71.
97. Edman, P., *A method for the determination of amino acid sequence in peptides.* Arch Biochem, 1949. **22**(3): p. 475.
98. Mann, M., Hørjup, P., Roepstoff, P., , *Use of mass spectrometric molecular weight information to identify proteins in sequence databases.* Biol Mass Spectrom, 1993. **22**(6): p. 338-45.
99. Banerjee, S., Mazumdar, S., *Electrospray Ionization Mass Spectrometry: A Technique to Access the Information beyond the Molecular Weight of the Analyte.* International Journal of Analytical Chemistry, 2011. **2012**.
100. Juraschek, R., Dülcks, T., Karas, M., *Nanoelectrospray - More Than Just a Minimized-Flow Electrospray Ionization Source.* Journal of the American Society for Mass Spectrometry, 1999. **10**(4): p. 300-308.
101. Giffiths, W.J., *Nanospray mass spectrometry in protein and peptide chemistry*, in *Proteomics in Functional Genomics*, P. Jollès, Jörnvall, H., Editor. 2000. p. 69-79.
102. *Exactive Series, Exactive Plus, Exactive Plus EMR, Q Exactive, Q Exactive Focus, Q Exactive Plus, Q Exactive HF and Q Exactive HF-X Operating Manual*, T. Scientific, Editor. 2017.
103. Michalski, A., Damoc, E., Hauschild, J. P., Lange, O., Wieghaus, A., Makarov, A., Nagaraj, N., Cox, J., Mann, M., Horning, S., *Mass Spectrometry-based Proteomics Using Q Exactive, a High-performance Benchtop Quadrupole Orbitrap Mass Spectrometer.* Mol Cell Proteomics, 2011. **10**(9).
104. Bradford, M.M., *A rapid and sensitive method for the quantitation of microgram quantities of protein utilizing the principle of protein-dye binding.* Anal Biochem, 1976. **72**: p. 248-254.
105. Smith, P.K., et al., *Measurement of protein using bicinchoninic acid.* Anal Biochem, 1985. **150**(1): p. 76-85.

106. Cox, J., Mann, M., *MaxQuant enables high peptide identification rates, individualized p.p.b.-range accuracies and proteome-wide quantification.* Nat Biotechnol, 2008. **26**: p. 1367-72.
107. Tyanova, S., Temu, T., Sinitcyn, P., Carlson, A., Hein, M., Geiger, T., Mann, M., Cox, J., *The Perseus computational platform for comprehensive analysis of (prote)omics data.* Nature Methods, 2016. **9**: p. 731-40.
108. Coskun, M., *Intestinal Epithelium in Inflammatory Bowel Disease.* Front Med, 2014. **1**(24).
109. Ardi, V.C., Kupriyanova, T. A., Deryugina, E. I., Quigley, J. P., *Human neutrophils uniquely release TIMP- free MMP-9 to provide a protent catalytic stimulator of angiogenesis.* Proc Natl Acad Sci U S A, 2007. **104**(51): p. 20262-20267.
110. Jakubowska, K., Pryczynicz, A., Iwanowicz, P., Niewinski, A., Maciorkowska, E., Hapanowicz, J., Jagodzinska, D., Kemona, A., Guzinska-Ustymowicz, K., *Expressions of Matrix Metalloproteinases (MMP-2, MMP-7, and MMP-9) and Their Inhibitors (TIMP-1, TIMP-2) in Inflammatory Bowel Diseases.* Gastroenterol Res Pract, 2016.
111. Faderl, M., Noti, M., Corazza, N., Mueller, C., *Keeping bugs in check: The mucus layer as a critical component in maintaining intestinal homeostasis.* IUBMB Life, 2015. **67**(4): p. 275-285.
112. Klapproth S., M.F.A., Zeller M., Ruppeert R., Breithaupt U., Mueller S., Haas R., Mann M., Sperandio M., Fässler R., Moser M., *Minimal amounts of kindlin-3 suffice for basal platelet and leukocyte functions in mice* Blood, 2015. **126**(24): p. 2592-600.
113. Judd T. A., D.A.S., Lemberg D. A., Turner D., Leach S. T., *Update of fecal markers of inflammation in inflammatory bowel disease.* Journal of Gastroenterology and Hepatology, 2011. **26**: p. 1493-1499.
114. Yürüker B., N.V., *Alpha-actinin and vinculin in human neutrophils: reorganization during adhesion and relation to the actin network.* J Cell Sci, 1992. **101**(Pt 2): p. 403-14.
115. Pennington K.L., C.T.Y., Torres M.P., Andersen J.L., *The dynamic and stress-adaptive signaling hub of 14-3-3: emerging mechanisms of regulation and context-dependent protein-protein interactions.* Oncogene, 2018. **37**: p. 5587-5604.
116. Serada S., F.M., Terabe F., Iijima H., Shinzaki S., Matsuzaki S., Ohkawara T., Nezu, R., Nakajiama, S., Kobayashi T., Plevy S.E., Takehara T., Naka T., *Serum Leucine-rich Alpha-2 Glycoprotein Is a Disease Activity Biomarker in Ulcerative Colitis.* Inflammatory Bowel Diseases, 2012. **18**(11): p. 2169-2179.
117. Matsumoto T., U.M., Ide H., Ishihara M., Hamada-Ode K., Shimamura Y., Ogata K., Inoue K., Taniguchi Y., Taguchi T., Horino T., Fujimoto S., Terada

Y., *Small Heat Shock Protein Beta-1 (HSPB1) Is Upregulated and Regulates Autophagy and Apoptosis of Renal Tubular Cells in Acute Kidney Injury.* PLoS One, 2015. **10**(5).

118. Bogdan D., F.J., Kanjiya M.P., Park S.H., Carbonetti G., Studholme K., Gomez M., Lu Y., Elmes M.W., Smietalo N., Yan S., Ojima I., Puopolo M., Kaczocha M., *Fatty acid-binding protein 5 controls microsomal prostaglandin E synthase 1 (mPGES-1) induction during inflammation.* J Biol Chem, 2018. **293**(14): p. 5295-5306.
119. Jumeau C., A.F., Assrawi E., Cobret L., Duquesoy P., Giurgea I., Valeyre D., Grateu G., Amselem S., Bernaudin J.F., Karabina S.A., *Expression of SAA1, SAA2 and SAA4 genes in human primary monocytes and monocyte-derived macrophages.* PLoS One, 2019. **14**(5).
120. L.M., S., *Symposium review: Oxylipids and the regulation of bovine mammary inflammatory responses.* Journal of Dairy Science, 2018. **101**(6): p. 5629-5641.
121. Tabbaa M., G.M., Roizen M.F., Bernstein A.M., *Docosahexaenoic Acid, Inflammation, and Bacterial Dysbiosis in Relation to Peridontal Disease, Inflammatory Bowel Disease, and the Metabolic Syndrome.* Nutrients, 2013. **5**(8): p. 3299-3310.
122. Simmons, J.G., Pucilowska, J. B., Keku, T. O., Lund, P. K., *IGF-I and TGF-b1 have distinct effects on phenotype and proliferation of intestinal fibroblasts.* Journal of Physiology-Gastrointestinal and Liver Physiology, 2002. **283**(3).
123. Baum, J., Duffy, H. S., *Fibroblasts and Myofibroblasts: What are we talking about?* J Cardiovasc Pharmacol, 2012. **57**(4): p. 376-379.
124. Rangaraj, A., Ye, L., Sanders, A. J., Price, P. E., Harding, K. G., Jiang, W. G., , *Molecular and cellular impact of Psoriasin (S100A7) on the healing of human wounds.* Exp Ther Med, 2017. **13**(5): p. 2151-2160.
125. Arijs, I., De Herthog, G., Lemaire, K., Quintens, R., Van Lommel, L., Van Steen, K., Leemans, P., Cleynen, I., Van Assche, G., Vermeire, S., Geboes, K., Schuit, F., Rutgeerts, P., *Mucosal Gene Expression of Antimicrobial Peptides in Inflammatory Bowel Disease Before and After First Infliximab Treatment.* PLoS One, 2009. **4**(11).
126. Hellmann, J., Tang, Y., Zhang, M.J., Hai, T., Bhatnagar, A., Srivastava, S., Spite, M., , *Atf3 negatively regulates Ptgs3/Cox2 expression during acute inflammation.* Prostaglandins Other Lipid Mediat, 2016.
127. van Caam, A., Vonk, M., van den Hoogen, F., van Lent, P., van der Kraan, P., *Unravelling SSc Pathophysiology; The Myofibroblast.* Front Immunol, 2018. **9**.
128. Stroud, D.A., Surgenor, E. E., Formosa, L. E., Reljic, B., Frazier, A. E., Dibley, M. G., Osellame, L. D., Stait, T., Beilharz, T. H., Thornburn, D. R., Salim, A., Ryan, M. T., , *Accessory subunits are integral for assembly and function of human mitochondrial complex I.* Nature, 2016. **538**(7623): p. 123-126.

129. de Oliviera, S., Reyes-Aldarsoro, C. C., Candel, S., Renshaw, S. A., Mulero, V., Calado, A., *Cxcl8 (IL-8) mediates neutrophil recruitment and behavior in the zebrafish inflammatory response.* J Immunol, 2013. **190**(8): p. 4349-59.
130. Sawant, K.V., Poluri, K. M., Dutta, A. K., Sepuru, K. M., Troshinka, A., Garofalo, R., Rajarathnam, K., *Chemokine CXCL1 mediated neutrophil recruitment: Role of glycosaminoglycan interactions.* Scientific reports, 2016. **6**.
131. Gallucci, R.M., Lee, E. G., Tomasek, J. J., *IL-6 Modulates Alpha-Smooth Muscle Actin Expression in Dermal Fibroblasts from IL-6-Deficient Mice.* Journal of Investigative Dermatology, 2006. **126**(3): p. 561-568.
132. Levy, O., *Neutrophils: Balancing the books.* Nature Reviews Immunology, 2012. **12**(3): p. 155.
133. Jovic, S., Linge, H. M., Shikhagaie, M. M., Olin, A. I., Erjefält, J. S., Mörgelin, M., Egesten, A., , *The neutrophil-recruiting chemokine GCP-2/CXCL6 is expressed in cystic fibrosis airways and retains its functional properties after binding to extracellular DNA.* Mucosal Immunology, 2016. **9**: p. 112-123.
134. Klingberg, F., Hinz, B., White, E.S., *The myofibroblast matrix: implications for tissue repair and fibrosis.* J Pathol, 2013. **229**(2): p. 298-309.
135. Smit, M.J., Verdijk, P., van der Raaij-Helmer, E. M., Navis, M., Hensbergen, P. J., Leurs, R., Tensen, C. P., , *CXCR3-mediated chemotaxis of human T cells is regulated by a Gi- and phospholipase C-dependent pathway and not via activation of MEK/p44/p42 MAPK nor Akt/PI-3 activation.* Blood, 2003. **102**(6): p. 1959-65.
136. Zhao, Y.X., Andoh, A., Shimada, M., Takaya, H., Hata, K., Fujiyama, Y., Bamda, T., *Secretion of complement components of the alternative pathway (C3 and factor B) by the human alveolar type II epithelial cell line A549.* International Journal of Molecular Medicine, 2000.
137. Nesargikar, P.N., Spiller, B., Chavez, R., *The complement system: history, pathways, cascade and inhibitors.* Eur J Microbiol Immunol, 2012. **2**(2): p. 103-111.
138. De Buck, M., Gouwy, M., Wang, J. W., Van Snick, J., Opndakker, G., Struyf, S., Van Damme, J., *Structure and Expression of Different Serum Amyloid A (SAA) Variants and their Concentration-Dependent Functions During Host Insults.* Curr Med Chem, 2016. **23**(17): p. 1725-1755.
139. Klein, T., Bischoff, R., *Active Metalloproteases of the A Disintegrin And Metalloprotease (ADAM) Family: Biological Funtion and Structure.* Journal of Proteome Research, 2010. **10**(1): p. 17-33.
140. Santelli, G., Califano, D., Chiappetta, G., Vento, M. T., Bartoli, P. C., Zullo, F., Trapasso, F., Viglietto, G., Fusco, A., , *Thymosin b-10 Gene Overexpression Is a General Event in Human Carcinogenesis.* Am J Pathol, 1999. **155**(3): p. 799-804.

141. Black, M., Milewski, D., Le, T., Ren, X., Xu, Y., Kalinichenko, V. V., Kalin, T. V., , *FOXF1 Inhibits Pulmonary Fibrosis by Preventing CDH2-CDH11 Cadherin Swith in Myofibroblasts.* Cell Rep, 2018. **23**(2): p. 442-458.
142. Londono, C., Osorio, C., Gama, V., Alzate, O., *Mortalin, Apoptosis, and Neurodegeneration.* Biomolecules, 2012. **2**(1): p. 143-164.
143. Lin, Y.H., Zhen, Y. Y., Chien, K. Y., Lee, I. C., Lin, W. C., Chen, M. Y., Pai, L. M., *LIMCH1 regulates nonmuscle myosin-II activity and suppresses cell migration* Mol Cell Biol, 2017. **28**(8): p. 1054-1065.

List of figures

Figure 1 Colonic regions affected by ulcerative colitis 10
Figure 2 Colonic membrane structure 12
Figure 3 Colonic crypt structure and cellular composition in ulcerative colitis 13
Figure 4 Mucus structures acting as a physical barrier and protection for the colonic epithelium 14
Figure 5 Ulcerative colitis treatment scheme, modified after Panés et al. (2017) 18
Figure 6 Different steps of the neutrophil extravasation cascade, modified after Ley et al. (2007) 20
Figure 7 Fatty acid and eicosanoid metabolism and synthesis pathways; modified from Martin C.R. (2015) 23
Figure 8 Q Exactive™ mass spectrometer and ESI-process leading to ion generation, modified after Exactive Series, Operating Manual 26
Figure 9 Master's thesis workflow; including the proteomic analyses of colon tissue specimen, plasma samples, inflammatorily stimulated (myo-)fibroblasts, as well as eicosanoid analyses of plasma samples 29
Figure 10 Digestion protocol optimization using colon tissue 34
Figure 11 SDS-PAGE for the assessment of tissue intactness 49
Figure 12 Method comparison results showing the numbers of identified peptides for each digestion protocol 50
Figure 13 H&E stained cross sections of colonic crypts showing signs of acute inflammation; **A**: Patient 0, colon sigmoideum; **B**: Patient 1, rectum; **C**: Patient 1, colon descendens; **D**: Patient 3, colon sigmoideum 53
Figure 14 Principal component analysis of proteomic analysis of colonic biopsy samples 54
Figure 15 Volcano plot showing alterations in relative protein abundance between inflamed and non-inflamed colonic areas; FDR=0.01, S0=0.5 55
Figure 16 Biological processes downregulated during UC induced inflammation 55
Figure 17 Biological processes upregulated during UC induced inflammation 55
Figure 18 Structure and components of the intestinal epithelial layer 56
Figure 19 Heatmaps showing the relative abundance of proteins involved in the epithelial membrane integrity during inflammation 57
Figure 20 Role of matrix metalloproteinases in the degradation of the extracellular matrix 58
Figure 21 Heatmap showing the relative abundance of proteins involved in the degradation of the extracellular matrix during inflammation 58
Figure 22 Intestinal barrier and protein secretion by epithelial cells, goblet cells and Paneth cells 59
Figure 23 Heatmaps showing the relative abundance of goblet cell derived proteins (left) and antimicrobial proteins/peptides (right) 59
Figure 24 Schematic of the process of neutrophil extravasation 60
Figure 25 Heatmaps showing the relative abundance of neutrophil-derived proteins in inflamed and non-inflamed areas 60
Figure 26 Schematic of the mitochondrial H_2S metabolism 61
Figure 27 Heatmaps showing relative abundances of proteins involved in the H_2S metabolism 61

Figure 28 Heatmap showing the relative abundance of myofibroblast-/fibroblast-derived proteins in inflamed and non-inflamed regions 62
Figure 29 Principal component analysis of CU patient and control plasma samples - component 1 and 2 63
Figure 30 Principal component analysis of patient and control plasma samples - component 1 and 3 63
Figure 31 Volcano plot showing differentially regulated proteins between plasma of P4 and control samples; FDR=0.01, S0=2 64
Figure 32 Principal component analysis of eicosanoids in patient and control plasma samples 67
Figure 33 Significantly regulated eicosanoids between patient and control plasma samples; eicosanoids labelled with " * " showed significant differences in their abundance (p-value<0.05) 68
Figure 34 Protein expression of vimentin, fibronectin and laminin subunit beta-2 in CCD-18Co cells 70
Figure 35 S100A7 abundance comparison in the different cellular fractions and treatment conditions 71
Figure 36 Volcano plots showing differentially regulated proteins in the cytoplasmic fractions one day and one week post treatment with IL-1b and TGF-b; FDR=0.01, S_0=2 72
Figure 37 BAX, BID and CYC1 levels in the cytoplasmic fractions of IL-1b treated cells one day and one week post treatment 73
Figure 38 Secretome changes one day post IL-1b and TGF-b treatment; FDR=0.01, S_0=2 .. 74
Figure 39 Volcano plots showing differentially regulated cytoplasmic proteins between one day and one week post treatment; FDR=0.01, S_0=2 78
Figure 40 Biological processes downregulated in control samples one week after treatment in comparison to one day after treatment 78
Figure 41 Biological processes upregulated in control samples one week after treatment in comparison to one day after treatment 79
Figure 42 Biological processes downregulated in IL-1b treated samples one week after treatment in comparison to one day after treatment 79
Figure 43 Biological processes upregulated in IL-1b treated samples one week after treatment in comparison to one day after treatment 80
Figure 44 Biological processes downregulated in TGF-b treated samples one week after treatment in comparison to one day after treatment 81
Figure 45 Biological processes upregulated in TGF-b treated samples one week after treatment in comparison to one day after treatment 81
Figure 46 Biological processes downregulated in IL-1b treated cells; not shared with upregulated processes in control samples 82
Figure 47 Biological processes upregulated in IL-1b treated cells; not shared with downregulated processes in control samples 82
Figure 48 Biological processes downregulated in TGF-b treated cells; not shared with downregulated processes in control samples 83
Figure 49 Biological processes upregulated in TGF-b treated cells; not shared with upregulated processes in control samples 83
Figure 50 Volcano plots showing differentially regulated secreted proteins between one day and one week post treatment, FDR=0.01, S_0=2 85
Figure 51 Biological processes in which downregulated proteins of the secretome fractions between one week and one day after IL-1b treatment are involved in 86

Figure 52 Biological processes in which upregulated proteins of the secretome fractions between one week and one day after IL-1b treatment are involved in 86
Figure 53 Biological processes in which downregulated proteins of the secretome fractions between one week and one day after TGF-b treatment are involved in 87
Figure 54 Biological processes in which upregulated proteins of the secretome fractions between one week and one day after TGF-b treatment are involved in 87
Figure 55 Neutrophil recruitment by fibroblasts/myofibroblasts 88
Figure 56 Hypothesis of the contribution of fibroblasts/myofibroblasts to the disease phenotype and progression of ulcerative colitis 89
Figure 57 Plasma eicosanoids not showing significant abundance changes 94
Figure 58 QQ Plots indicative of normal distribution of eicosanoid levels in patient and control samples 95

List of tables

Table 1 Mayo-score components and disease severity grading 17
Table 2 Mass spectrometric parameters used for the analysis of proteins 43
Table 3 Mass spectrometric parameters used for the analysis of eicosanoids 47
Table 4 Patient data sorted by highest Mayo-score, areas of most severe inflammation are highlighted in orange 51
Table 5 List of differentially regulated proteins between P4 and control cohort 66
Table 6 List of differentially regulated proteins in the secretome of IL-1b treated cells one day post treatment 75
Table 7 Patient medication, CRP and calprotectin levels, dates of blood, stool and biopsy sampling; calprotectin levels not correlating with inflammation severity due to date of stool sampling are highlighted in orange 91